Examination of Aggregation Prone Proteins and their Higher Order Interactions by Ion Mobility-Mass Spectrometry

by

Molly Therese Soper

A dissertation submitted in partial fulfillment
of the requirements for the degree of
Doctor of Philosophy
(Chemistry)
in the University of Michigan
2015

Doctoral Committee:

Assistant Professor Brandon T. Ruotolo, Chair
Professor Philip C. Andrews
Professor Ayyalusamy Ramamoorthy
Assistant Professor Bing Ye

Dedication

Dedicated to the memory of John A. Ensley. Pippi, you have inspired me to pick up the fight against Alzheimer's.

Acknowledgements

I would first like to thank my advisor Brandon T. Ruotolo. Without his guidance this dissertation would not be possible. Over the past years he has imparted wisdom going beyond day to day activities in the lab, and provided an example of persistence, attention to detail, and passion as a scientist. I have been truly blessed to work under his influence.

Additionally, I would like to thank my committee members, current and former, Professor Philip Andrews, Professor A. Rams. Ramamoorthy, Assistant Professor Bing Ye, and Professor Mi Hee Lim for serving as my committee members and providing valuable insight during my candidacy exam, data meeting and throughout my time at the University of Michigan. Thank you for challenging my insight, increasing the understanding of my research, and teaching me to become a better scientist.

In my time as a student in the Ruotolo lab, I have had the great pleasure of working with a wonderful group of fellow students and post-doctoral researchers. Firstly, I would like to thank Dr. Suk-Joon Hyung without whom I would have been lost in the field of Amyoid β. Drs. Yueyang Zhong, Linjie Han, and Russel Bornschein have guided, trained, encouraged my early years in the lab. I could not have asked for better examples to follow in the footsteps of. Shuai Niu, for experiencing the struggles and milestones in the life of a graduate student with me. Joseph Eschweiler, for assistance in many things computational. Sugyan Mani Dixit and Daniel Polasky for brining fresh eyes and enthusiasm into the lab. Alexander Brown and Stephanie Godden, for being great students to mentor and your dedicated work to projects which were never easy. You have taught me as much as I taught you. Dr. Richard Kerr, for your assistance with all things amyloid, commiseration included. Dr. Billy Samulak for lending a hand whenever needed. And lastly, Jessica Rabuck-Gibbons, for your constant enthusiasm, scientific input and friendship. I will forever remember our networking opportunities.

In addition to my coworkers, I would like to thank my collaborators. Professor Mi Hee Lim and her students Dr. Alaina DeToma, Amit Pithadia, Dr. Akiko Kochi, Dr. Masha Savelieff, for all

their help with amyoid related projects, broadening my knowledge of the field and exposing me to structural biology. Dr. Magdalena Ivanova for preparing samples of Ubiquilin2 and exposing me to another area of protein aggregation, in addition to always helpful advice.

And lastly, this work would not have been possible without the support of my friends and family. To my friends at the University of Michigan, Dr. Wendi Hale and Dr. Sabrina Peczonczyk, you are such strong women and a constant inspiration. Our coffee dates were always a welcome break in the day. Dr. Jeanne Hankett, the year we lived together was one of my favorite living in Ann Arbor. To Jordan Clark, for intellectual and nonsense conversations alike. A true lifelong pander-friend. Additionally, Amy Smith and Katie Brandt even if you didn't always know what I was talking about I know I always have your support. Shawn Clark, for challenging traditional ways of thinking and teaching me the meaning of *Res ipsa loquitur.*

To my fiancé and my parents, thank you for your unwavering support in the good times and bads. For challenging me to be better, encouraging me to never give up, and standing by me through it all.

Table of Contents

List of Figures

List of Tables

List of Appendices

Abstract

Amyloid forming peptides and proteins present an extreme challenge for modern analytical measurement techniques. When natively-folded biomolecules partition into misfolded forms, they produce a myriad of inherently unstable conformations that eventually lead to the presumed cytotoxic species linked to disease. Most often, these cytotoxic states take the form of small oligomeric species that exist within a complex mixture of other oligomers that may, or may not, be related to a disease etiology. In addition, these dynamically-generated oligomers are present in small amounts, within a complex mixture of other biomolecules, small molecules, and metal ions that may also influence the ensemble of states being measured. Ion mobility separation, coupled to mass spectrometry, has recently become a key technology for the analysis of amyloid-forming peptides and proteins due to its ability to analyze low concentrations of complex mixtures. Described here is the application of IM-MS to study protein interactions with small molecules, dipeptides, and neuropeptides. This combine information furthers the knowledge base of neurodegenerative diseases from a structural standpoint.

First, the interaction of amyloid beta: leucine enkephalin was discovered in a screen of many neuropeptides. This interaction was characterized using IM-MS through collision cross section and K_d measurements. Multiple copies of leucine enkephalin are found to bind with amyloid beta, each with an approximate binding strength of 60 micromolar. Modeling suggests binding near the structured core region of amyloid beta. Following these initial studies, site directed amino acid substitution of leucine enkephalin reveals that the hydrophobic C-terminal residues phenylalanine and leucine are critical for binding to occur. Alanine substitutions of amyloid beta residues, selected based on simulated annealing results, indicate residues Y10 and Q15 to be most critical for the interaction of amyloid beta with the dipeptide FL. Molecular dynamics models were filtered using IM-MS experimental results, and structures representative of the interaction are shown. Additionally, workflow to study amyloid beta has been applied to the oligomerization of ubiquitin monomer and linear tri-ubiqutin in the presence of copper ions, measuring an increase in the number of dimeric species. Stability measurements using collision induced unfolding, and aggregation propensity of Ubiquilin2 are also studied.

Chapter 1.

Introduction

Amyloid forming peptides and proteins present an extreme challenge for modern analytical measurement techniques. When natively-folded biomolecules partition into misfolded forms, they produce a myriad of inherently unstable conformations that eventually lead to the presumed cytotoxic species linked to diseases such as Alzheimer's and Parkinson's Disease. Most often, these cytotoxic states take the form of small oligomeric species that exist within a complex mixture of other oligomers that may, or may not, be related to a disease etiology. In addition, these dynamically-generated oligomers are present in small amounts, within a complex mixture of other biolmolecules, small molecules, and metal ions that may also influence the ensemble of states being measured. All of these factors conspire to create an exceedingly complex mixture, within which the conformational, oligomeric, and molecular composition of a single targeted, disease-associated species is typically sought. As such, separative tools, capable of portioning such a complex mixture in the context of both molecular shape and identity, are required to completely evaluate the molecular mechanisms involved in biomolecular amyloid formation.

Ion mobility (IM) separation, coupled to mass spectrometry (MS), has recently become a key technology for the analysis of amyloid-forming peptides and proteins. The general concept of IM involves the measurement of gas phase ion migration rate or trajectory in the presence of both an electric field and a drag force to analytes such that larger ions possess longer migration times, or altered trajectories, compared to smaller ions of equal molecular mass. Additionally, ions possessing greater charge can be separated from those with lower levels through the same combination of forces. By virtue of the charging mechanisms operative in electrospray ionization (ESI), protein oligomers often have mass -to- charge (m/z) values identical to protein monomers, making the size and charge separation afforded by IM essential in analyzing MS data acquired for amyloidogenic systems. Described here is the detail of IM-MS methodology as applied to disease associated protein aggregation systems.

1.1. Amyloid in Human Disease

Proteins which are unable to remain correctly folded, or which do not fold correctly lead to biological malfunction and many diseases[1]. These misfolded proteins can aggregate and interact with cellular components, potentially causing cell death. Amyloidoses are a specific group of protein folding disease, where specific proteins misfold and aggregate leading to extracellular amyloid deposits, made up of highly organized β-sheets[2]. Diseases in this class include, but are not limited to Alzheimer's, Huntington's, systemic amyloidosis, type II diabetes and Parkinson's[3, 4].Aggregation can occur when a protein never folds to the correct structure or it is unable to maintain the fold. This may be due to a mutation in protein sequence, interaction with metals, changes in pH or temperature, and even chemical modification[5, 6]. Figure 1.1 below

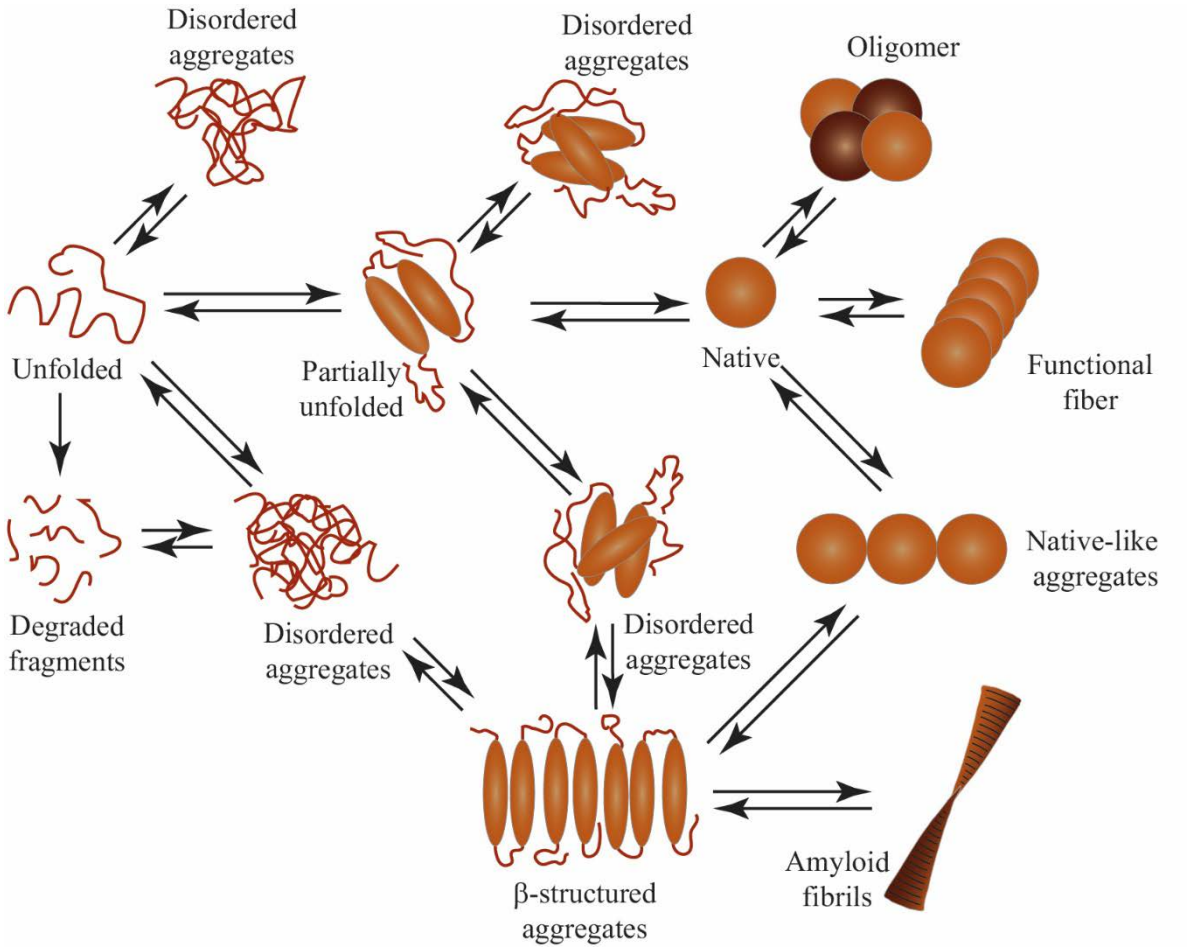

Figure 1.1. Overview of the possible states accessed by a protein which leaves its native fold. This includes degradation of the unstructured protein, or disordered aggregate formation which may or may not be on disease pathway. Some disordered aggregates form an equilibrium with β-structured aggregates which go on to form amyloid fibrils.

highlights the pathways available to a protein which leaves its native fold. The when the equilibrium shifts between the native fold and a partially unfolded form, cellular processes should assist in the degradation of the unfolded protein. However if the abundance achieves a certain threshold the protein moves towards nucleation of β-structured aggregates which grow into fibrils.

The amyloid hypothesis suggests a causative link between protein deposits and pathological symptoms of disease[3, 4, 7] and has been widely accepted. However, experimental data now suggests the most toxic species to the cell is actually pre-fibrillar aggregates. This has been demonstrated with Amyloid β (Aβ), α synuclein and transthyretin[8-13]. It is thought that the misfolding of the protein allows hydrophobic residues, which would be buried in the native state, to interact with membranes or cellular components[14], causing toxicity. Additionally, the channel hypothesis has been proposed [131]. This suggests that aggregates in a pore structure may interact and insert into lipid membranes with cytotoxic results[5, 15, 16].

1.1.1. Alzheimer's Disease and Amyloid β

Of all forms of dementia, it is thought that 50-60% of all cases are Alzheimer's Disease (AD)[17, 18]. AD symptoms include memory loss, cognitive decline, and is the sixth leading cause of death in the US[19-21]. Three are currently three hypotheses on the pathogenesis of AD 1) the metal ion hypothesis[22-26], 2) the amyloid cascade hypothesis[19, 20, 27] and 3) the oxidative stress hypothesis[28-30]. The metal ion hypothesis suggests AD is caused through impaired metal ion homeostasis (Zn, Cu and Fe) with the end result being Aβ imbalance[24, 25]. By the oxidative stress hypothesis, age, genetics, or environment enhances oxidative stress, causing gene defects and mitochondrial function to decline[28, 31, 32]. As the target of this thesis, the amyloid cascade hypothesis is briefly summarized below.

A non-amyloidogenic cleavage of the amyloid precursor protein (APP) occurs at residue 687 with α-Secretase. This happens within the Aβ formation region and thus prevents its formation. Pathogenic Aβ is formed from β-secretase and γ-secretase cleavage of APP at residues 672 and 710-714 respectively, and so, is traditionally 39-43 residues long[33, 34]. The most abundant from of Aβ is 40 amino acids while the most pathogenic form is 42[33, 35, 36]. Once formed Aβ can produce soluble oligomers, protofibrils, or extracellular aggregates. As discussed previously it is thought that the extracellular aggregates are not directly toxic, but rather the soluble oligomers

and protofibrils cause cell death[37-39]. It is thought that $A\beta_{1-42}$ is more toxic than $A\beta_{1-40}$ because the two additional hydrophobic amino acids[36, 40, 41]. Pathogenicity is theorized to occur in one of several ways. The first is that Aβ oligomers directly damage the neurons and cause cell death[42, 43]. Second, formation of membrane-soluble channels destroy electrochemical signaling[44-46]. Lastly it is possible Aβ disrupts the respiratory chain within the mitochondria causing oxidative stress[34, 47, 48].

1.2. Ion Mobility Mass Spectrometry for Protein Aggregation Determination

IM is a gas phase separation technique that shares a similar operation principle with the solid and solution phase electrophoresis methods typically applied by biochemists. The combination of IM and MS instrumentation provides additional advantages realized in the analysis of oligomeric mixtures. Such experiments typically begin with ESI, which charges protein oligomer ions according to their overall surface area. In this context, all protein ion populations occupy a range

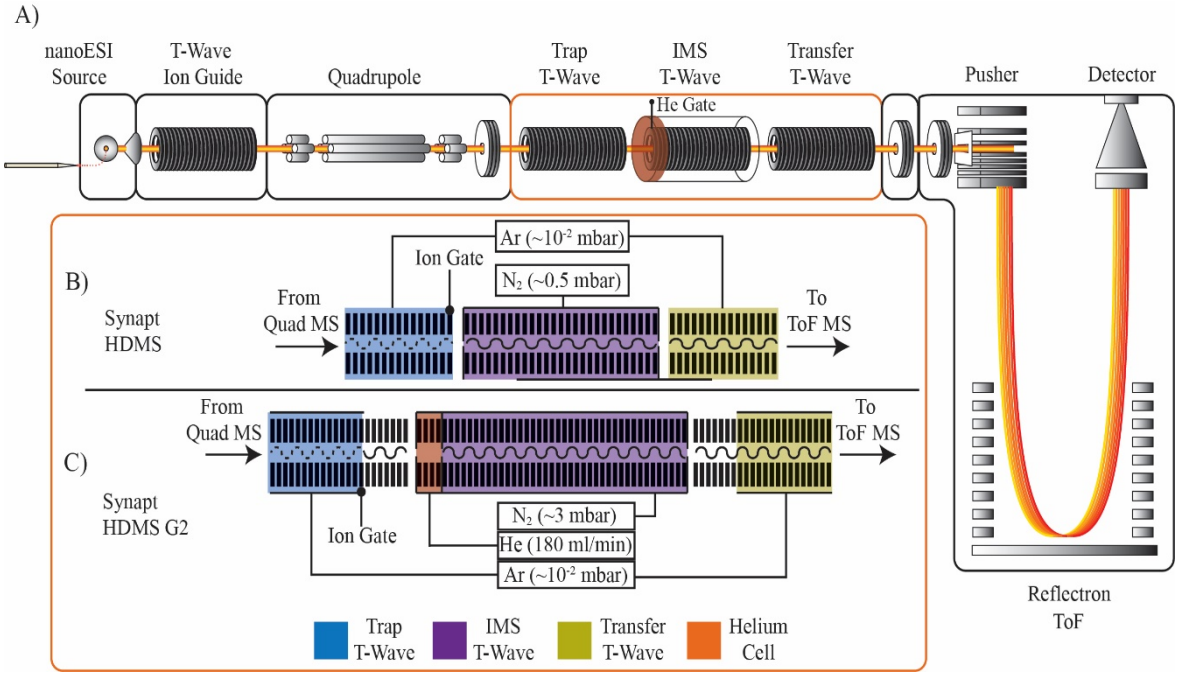

Figure 1.2 – General Schematic of the Synapt HDSM quadrupole-ion mobility-time-of-flight mass spectrometry instruments used here. A) Complete instrument diagrams shown with the four main regions of the instrument: ion generation with nESI source, ion selection in the quadrupole mass analyzer (capable of selecting up to 8,000 m/z in the Synapt HDMS, and modified to select up to 32,000 m/z in the Synapt HDMS G2), ion mobility separation (detailed in B and C), and ion mass analysis using a time of flight mass analyzer. B) Detailed ion mobility separation, tri-wave region, of the Syanpt HDMS and C) tri-wave region of the Synapt HDMS G2. The tri-wave region includes three T-wave ion guides the ion trap (blue), ion mobility cell (purple), and transfer (yellow-green) regions. The HDMS G2 is additionally equipped with a He cell (orange) to assist with transition across the pressure gradient with minimal ion activation. Typical pressures associated with the regions are indicated.

of charge states, and those generated for the monomer will inherently overlap with the dimer, creating some m/z signals that are a composite of multiple oligomer states. IM separates ions based on their CCS (CCS, a rotationally averaged size measurement), and charge. For monomers and oligomers possessing an overlapping m/z ratio, these properties will differ. As such IM is a critical tool to decouple the influence of oligomers which could not be separated based on MS alone[49, 50]. Work presented in this thesis was completed on one of two IM-MS platforms by Waters (Milford, MA): the Synapt HDMS or the Synapt G2 HDMS. The platforms are both equipped in a similar fashion, as diagramed below (Figure 1.2), with a nanoelectrospray (nESI) ionization source, a quadrupole mass analyzer, travelling-wave ion mobility separator (IMS), and Time of Flight (TOF) mass analyzer. Variation between platforms includes a high m/z quadrupole and a helium gate at the entrance to the IMS on the Synapt G2, in addition to different detectors. The high mass quadrupole allows for the selection of larger proteins and their oligomers, while the helium gate lowers the center of mass energy of collisions for injection into the IM separator. The lower energy means more labile structures will survive the injection.

1.2.1. Ion Generation

To analyze samples using IM-MS, one must first transition sample into the gas phase while simultaneously charging the analyte. Two ion sources common in biological MS experiments have been used to analyze the content and composition of amyloidogenic peptides and proteins. The most common of the two being electrospray ionization or its nano form. This technology directly converts solution-phase protein at low micromolar concentrations into gas-phase ions by aerosolizing the sample into micrometer-nanometer scale droplets, desolvating those droplets to reveal naked protein ions, and charging these proteins in a manner highly correlated with their solvent accessible surface areas[51]. nESI can generate a desolvated structure on the nanosecond time scale with concomitant cooling from the loss of water[52]. The speed and cooling effects of ESI allow for the capture of solution phase equilibria with regards to oligomeric and structural populations in aggregating systems. The mechanisms of ESI are described below. In contrast Matrix-Assisted Laser Desorption Ionization (MALDI), provides more circuitous routes between the native state and gas-phase ions, such as requirement of a matrix, and the ions are typically singly charged. The matrix is added in solution, and the water allowed to evaporate forming a

solid around the protein ion, which may alter solution phase structure. For these reasons therefore not generally preferred over ESI[53, 54].

Two models for ion formation using electrospray ionization have been proposed. The first, the charged residue mechanism, proposes ion generation through evaporation and Coulombic fission[55-57] and is mostly widely accepted for the ionization of large molecules. After emission from the electrostatically charged capillary tip (1-4kV)[58] droplets undergo evaporation, and the droplet diameter decreases until charges within become too crowded. At this point, the "Rayleigh limit", Coulombic repulsion breaks surface tension of the droplet and fission occurs. The process is repeated until the analyte has become completely desolvated, "naked", leaving the charges deposited on the surface of the protein, or protein complex. (Figure 1.3). In a similar, but distinctly different mechanism, the Ion Evaporation Model[59], before the protein has become

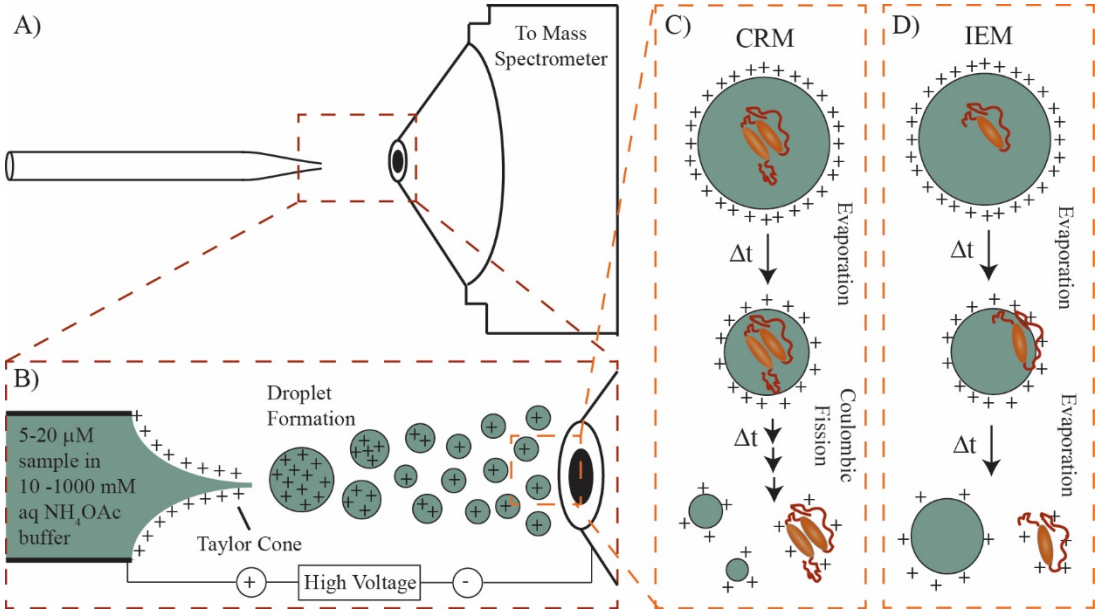

Figure 1.3 – Diagram of the mechanism of electrospray ionization (ESI) where A) diagrams the relative position of the conductive capillary needle with analyte solution near the entrance of the mass spectrometer. B) When high voltage is applied to the capillary and entrance, a Taylor cone is formed generating highly charged droplets which experience evaporation reducing their diameter. Protein molecules are charged primarily through the CRM in C) where droplets undergo evaporation followed by a series of droplet fission events until only charged protein remains. Alternatively, smaller proteins may undergo IEM shown in D) where, as the droplet evaporates the electric field increases, forcing the analyte to the surface where it evaporates off, taking charge from the droplet as it leaves.

completely desolvated, the charges of the protein and the other charges in the droplet cause ejection of the analyte into the gas phase. This mechanism is more accepted for small molecules.

Likely a combination of the two is in effect[60], especially when analyzing a complex mixture of proteins and/or peptides with small molecules.

1.2.2. Protein Transmission, Mass Analysis and Detection

The hybridization of a quadrupole mass filter and orthogonal ToF analyzer has allowed for an in depth analysis of intact macromolecular complexes not accessible by other technologies. These macromolecular complexes however, come with an increased challenge. To more easily transmit large ions two parameters can be manipulated. First, pressures may be adjusted by adding collision gas or reduce pumping in various places through the flight path of the ions[61] . Second, one can use a flow restricting sleeve to increase the pressure of the first ion guide[62]. This 'collisionally cools' the trajectories of the ions by dampening their radial velocity and better guides them to the detector[62]. While collisional cooling of most protein aggregating systems is not necessary due to their small monomer size, to see large oligomers or to conduct studies on disordered proteins of a larger size, this method may be of advantage.

A quadrupole mass analyzer, is built from four parallel rods which are positioned equidistantly from the center-axis of the instrument[63, 64]. Paired rods are placed opposite one another. One pair is applied with a direct current (DC) and the other radio frequency (RF) voltages. In the first pair, the DC voltage is the same for each rod. For the other pair RF voltage oscillates at the same frequency, but opposite magnitude. Due to the field created, ions with a single m/z are transmitted through to the detector. Operation can be performed in single ion monitoring mode, or in a scanning mode with both DC and RF voltages applied. Turning the quadrupole to RF-only mode (DC voltage = 0) operates the devices as an ion guide and allows a wide range of m/z ions to pass through the field making the technique optimal for continuous ion sources.

In contrast to the four rod geometry of the quadruople, ToF mass spectrometers[65, 66] are made up of three regions: an ion pusher, a flight tube, and a detector. By nature of the ion pusher, ToF is a pulsed technique and can be suitably coupled to fast separations. A packet of ions are pushed into the flight tube with specific kinetic energy. Ions with equivalent charge have equivalent energy, and ions of higher charge have higher energy. Once in the flight tube, ions that are more massive or lower charged will travel through the flight tube at a slower velocity while lighter or higher charged ions will travel faster, due to kinetic energy being directly proportional both mass

and velocity. The time it takes ions to travel the flight tube and be recorded by the detector can then be converted into m/z, giving this mass analyzer an unlimited m/z range.

1.2.3. IM Separation

The theoretical basis for measuring the mobility of ions in the gas phase was first described by Langevin in 1903[67].Work presented by Bradbury in 1931[68] applied this theoretical work to measure the mobility of ions in the gas phase. By modifying previously established methods[69, 70] of introducing pulsed packets of ions, Bradbury was able to compare the mobility of both negatively, and positively charged ions. Although this early work lacked the sensitivity to measure minor differences in mobility, it would lay the corner stone for modern instruments with resolutions capable of distinguishing smaller changes in ion size.

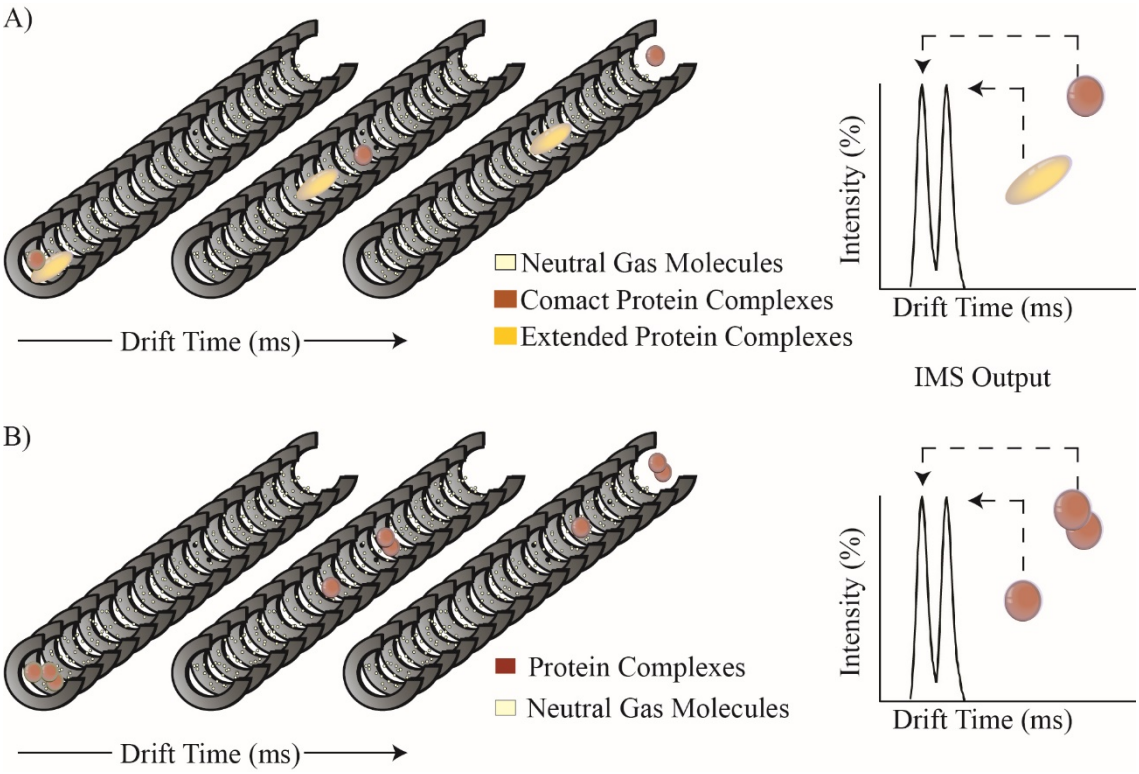

Figure 1.4 – Drift Cell Ion Mobility Separation. Ions are introduced into the mobility separator at a defined start time. Ions traverse the drift cell under the influence of a uniform weak electric field. Separation then occurs under the influence of a constant number density of a neutral backing gas (*e.g.*, He or N_2). A) Given two proteins with same relative charge, the small compact protein will traverse the cell unimpeded and exit rapidly, larger ions due to their extended conformational state will interact with the backing gas more often and therefore exit later. B) When separating ions of the same m/z (*i.e.*, monomer^{n+} and dimer^{2n+}), ions with the increased level of charge will traverse the cell faster due to the increased influence of the static field on higher charge states.

Arguably the simplest form of IM instrumentation is the drift tube. This equipment separates ions, within a pulsed packet, according to their mobility through a pressurized (1-1000 mBar) drift cell in the presence of an axial electric field[71]. All ions experience the same electric field, and the time to traverse the drift cell is measured. Ion drift times can be easily converted to CCS, defined as a rotationally averaged ion-neutral interaction potential[72, 73]. The velocity of an ion, under the influence of the superimposed electric field is also proportional to its charge[72, 74], therefore, any ion with a lower CCS (Figure 1.4A), or higher absolute charge (Figure 1.4B)[71, 75], will exit the drift cell before a large, lower-charged ion. Ion CCS is also weakly correlated to molecular mass, resulting in apparent 'trend-lines' on a plot of IM drift time versus m/z for different molecular classes that display similar packing densities in the gas-phase. For example, peptide ions typically have a higher packing density than lipids of equivalent molecular mass, but do not typically create ions of greater gas-phase densities than nucleotides (*i.e.*, Lipid CCS > Peptide CCS > Nucleotide CCS). Within a given molecular class, detailed CCS measurements can provide further anti-correlations with respect to molecular mass, further weakening the general correlation discussed above and providing increased orthogonality between IM and mass spectrometry (MS) measurements[76-80]. By measuring the drift time of a defined ion population iteratively over many different axial electric field strengths, drift tube IM instruments can record the mobility of an ion, and thus its CCS, to a high degree of precision and accuracy if the experimental conditions are known[81]. The experimental conditions accounted for in such a calculation include: the mass and density of the buffer gas, the operating temperature and pressure of the drift cell, as well as an accurate calculation of the ion's mass and charge[49, 74, 82]. To accurately assess the analyte mass and charge required to complete the CCS calculations, the drift cell is most often coupled to a MS analyzer (Figure 1.5). The first example of combined IM-MS instrumentation, capable of both drift time and m/z measurements, was described in 1962[83]. This instrumentation was used for the study of ion-molecule reaction kinetics, and it was not until 1989 that such equipment was applied to obtain ion geometry and reactivity information[84, 85]. In addition to the IM drift cell previously described, two further variations on the mobility separator have been applied to the study of amyloidogenic proteins and protein complexes. These are the travelling wave, and high field

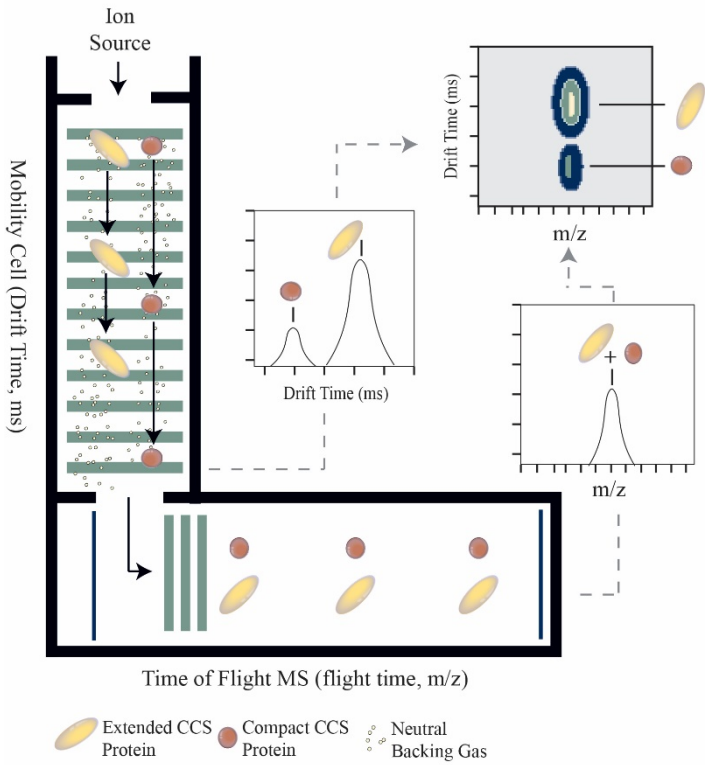

Figure 1.5 – IM separation combined with ToF MS to create a multi-dimensional separation and analysis tool. Within the IM component ions are initially separated according to their CCS and charge on the millisecond time scale. Following is mass analysis within the ToF mass analyzer, occurring on the microsecond time scale allowing for the rapid deconvolution of mass spectra, by separating conformational and oligomeric families with overlapping m/z values.

asymmetric ion mobility separators[86-88]. The travelling wave technique, extensively used in this work, is expanded upon below.

The travelling wave ion guide, or T-wave, separates ions based on their differential mobilities under the influence of a direct current (DC) voltage wave originating within a stacked ring ion guide. This non-uniform voltage traverses the stacked-ring ion guide through the sequential application of a DC voltage to neighboring electrodes, forming a voltage wave along the axial plane of the device. As this travelling voltage wave traverses the guide, analyte ions are propelled by the wave, and collide with a neutral gas during transit through the device. Ions with larger CCS exhibit an increased number of collisions, slowing their migration when compared to more compact ions with the same molecular mass. Due to this increased collision frequency, large CCS ions are more likely to pass over the crest of multiple wave fronts during their transit

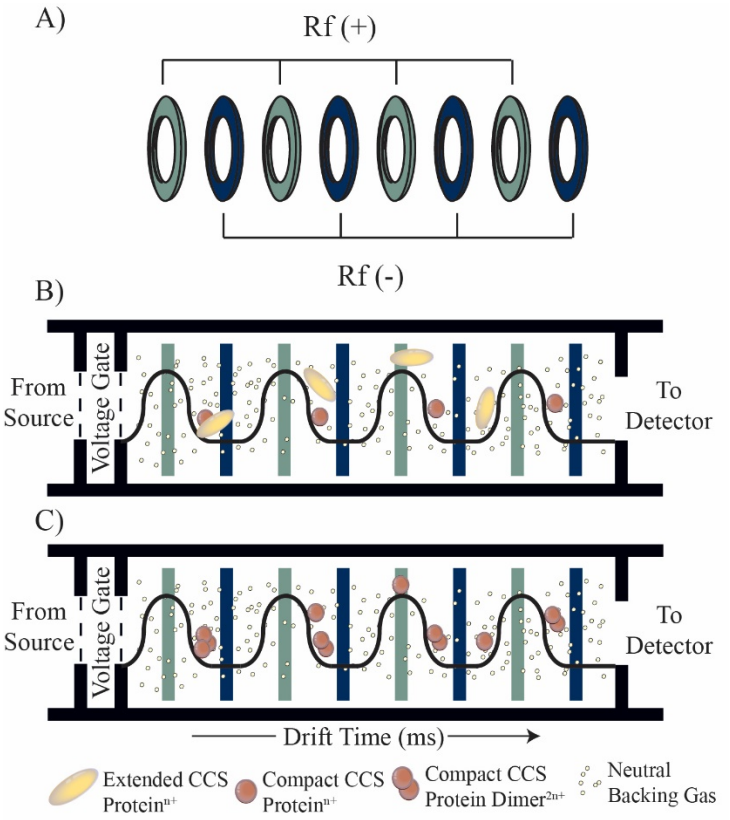

Figure 1.6 – Travelling Wave Ion Mobility Separator. The T-wave mobility separator differs from the drift cell by A) using a non-uniform voltage distribution across the length of the cell to separate ions as a result of a DC voltage applied to individual electrodes of alternating the alternating Rf stacked ring ion guide. Voltage is applied to sequential electrode producing a 'travelling wave'. Repulsion between the polarity differences of the wave and analyte, propels ions through the mobility separator. As ions ride the crest of the DC wave more conformationally extend B) and lower charged C) ions undergo increased interactions with the backing gas and are more likely to pass over the crest, exiting the T-wave later.

through the device. As with the drift tube device described above, the absolute charge adopted by an ion also represents a key factor in T-wave IM separation, with ions of increased charge repelled by the voltage wave more strongly and will therefore exhibit decreased migration times[89, 90].

Compared to drift tube IM, the T-wave exhibits a more complex relationship between measured drift time and CCS. While drift tube IM possess a direct relationship between drift time and CCS, the T-wave exhibits an exponential relationship between these two values, which varies between 0.2 and 0.8 under typical experimental conditions. This exponential relationship results in a T-wave CCS axis that is elongated and expanded relative to the migration times measured in the device. In addition, because the functional form of the relationship between IM migration time and ion size varies substantially in T-wave separators, data acquired using this method are typically calibrated in order to generate accurate CCS values for unknown ions. In contrast, these calibrations are not required in drift tube IM if all the relevant experimental variables are known. Additionally, peak resolution ($t/\Delta t$) in drift tube IM depends only upon the voltage differential applied to the device and the temperature of the experiment, whereas T-wave IM resolution is influenced by the properties of the waves used to propel the

ions (*e.g.* frequency) and exhibits a direct correlation to the mobility of the ions analyzed[73, 75, 91, 92].

Calibration of T-wave drift time data requires strict control over the travelling wave parameters used to separate ions. Calibration of travelling wave data uses known CCS values for a series of calibrant ions, measured originally on drift tube IM analyzers[50, 92-103]. Using the exponential formalism described briefly above, under controlled instrument conditions, a calibration curve can be constructed to generate T-wave CCS values for a broad range of biomolecular ions[73, 104, 105]. The calibrants selected for this procedure should have drift times that bracket those of the unknown, to reduce errors that result from extrapolation of the data points[91, 92, 94, 104]. Using these calibration techniques, a high level of reproducibility, precision and accuracy in T-wave CCS values can be achieved[106]. Most T-wave CCS values are normalized to drift tube CCS values recorded in helium in order to enable detailed computational analyses; however, T-wave drift times are typically recorded in nitrogen to maximize resolving power and T-wave instrument performance. While such conversions impart negligible errors for large protein ion CCS values, these errors become increasingly significant for small molecule and peptide T-wave CCS values[92, 93].

1.2.4. Collision Induced Unfolding

Beyond the measurement of CCS, IM-MS can measure protein structure transitions in the gas-phase through collision induced unfolding (CIU)[107-109]. In a typical CIU experiment ions of a single charge state are first selected in the quadrupole mass filter. Upon entry into the trap t-wave the ion population is activated via collisions with argon. Voltages in the trap region are raised to increase the energy of the collisions (typical range = 20-200 V). Drift time of the ion population is measured at each trap voltage, capturing partially-folded intermediate states which are unique to the gas phase[110]. A plot of the drift times vs voltage, with intensity on the z-axis create a CIU fingerprint[111]. The energy at which the intermediately unfolded conformations appear can be related back to stability of the protein[112, 113].

1.3. Modeling Protein Interactions with Experimental CCS

IM-MS analysis, through the measurement of accurate CCS values for amyloid forming peptides and proteins, enables the production of models that closely estimate the observed gas phase

structural populations. In order for the CCS measurements recorded to be used effectively in the model building process, they must be accurate and precise. In order for the resulting models to be useful for elucidating the biologically-relevant mechanisms of amyloid formation, measurements must have a strong correlation with the solution phase conformations[114]. Recent MS, IM-MS, spectroscopic, and molecular modeling experiments have revealed much regarding the correlated nature of native and gas-phase protein structure. Following protein desolvation on the nano to pico second time scale, hydrogen bond and van der Waals interactions on the protein surface can be destabilized to result in side chain re-arrangements and compactions that are broadly uniform across all protein structural families. For highly-charged proteins, Coulombic repulsion can result in protein remodeling and unfolding, promoting the formation of a range of gas-phase conformers that likely bear little resemblance to those found in solution[52, 114-116]. Protein ions having a sufficiently low charge state do not typically undergo such Coulmbically-mediated distortions and retain compact configurations in the gas-phase that are stable on the millisecond timescale, and can be easily correlated to X-ray and NMR datasets. Such correlations have extended from monomeric proteins to larger hetero-protein complexes, including a range of topologies, architectures, and structures. As IM-MS experiments are run on the millisecond timescale, and since net protein charge is a critical factor in the gas phase stability of ions, exceeding a system-dependent threshold allows the native-like gas-phase state of the protein to unfold[52, 115, 117].

1.3.1. Molecular Dynamics Simulations

Direct comparisons between IM-MS derived CCS values and high-resolution structure data requires computational methods aimed at building and refining models, as well as algorithms designed to simulate IM separation and calculate theoretical CCS values for *in silico* models in order to compare with experimental data. Coarse-grain modeling approaches may assist in the building of multimer models. For example, oligomers of Amyloid β[118] and β2-microglobulin[119] have been analyzed by building spherical models of growth, ranging from globular to linear, then matched to experimental collision cross sections to determine the best fit model[114, 120]. In addition to coarse-grain models, detailed structures of protein misfolding disease systems have been collected using two main kinds of molecular dynamics simulations: simulated annealing and replica exchange molecular dynamics[121-124]. Of the two, simulated annealing is the less

computationally exhaustive, and simpler approach. A protein sequence in the simulation is heated to high temperatures, unfolding the structure within the computational space, followed by a temperature decrease that allows the protein to refold. This temperature oscillation is repeated multiple times, allowing the protein to escape any local energy minima and adopt an energy-minimized structure. Replica exchange molecular dynamics is similar to the simulated annealing method, in that a protein is heated *in silico* to remove it from local minima in the energy landscape. The key difference is that rather than ramping the temperature on one coordinate set at a time, several replicas are run in parallel each starting at different temperature points. Throughout the run, the proteins are exchanged from one temperature level to another. This more effectively samples the energy landscape accessed by molecular dynamics than simulated annealing does, but results in a more computationally-intensive modeling workflow.

1.3.2. Theoretical CCS Calculation Techniques

For IM-MS studies of amyloidogenic proteins, four methods have been applied to convert *in silico* models into theoretical CCS values for comparison with experimental data. These methods are: the trajectory method (TM)[125], projection approximation (PA)[125], exact hard sphere scattering (EHSS)[126], and projection superposition approximation (PSA)[127-130]. These methods all differ according to the level of projected interaction complexity calculated between the backing gas and analyte structure undergoing ion mobility separation, correlating strongly with the computational demands required to perform them. The PA represents the least computationally demanding algorithm, as it calculates only the rotationally averaged CCS[117, 131] using Monte Carlo scoring[127]. This method is known to underestimate the CCS however, which has been supported by experimental observations using the T-wave ion mobility separator[125, 131]. In contrast the TM represents the most accurate method for calculating CCS data from structural models[131], accounting for all the direct and indirect interactions between the analyte and neutral backing gas as well as their collision geometries (*i.e.* angle of deflection)[125]. By accounting for these interactions, the TM represents a computationally intensive method, thereby limiting its application for studying larger complexes.

Compared to the PA, both the EHSS and PSA approaches represent gains in calculated CCS accuracy, while remaining computationally inexpensive compared to the TM. The EHSS improves computational efficiency by removing the long range electrostatic interaction

calculations calculated by the TM, which account for an accuracy difference of only a few percent between the two, but often drastically over-estimates the experimental CCS of proteins and peptides[125, 131, 132]. Comparatively the PSA combines the basics of the PA model, with buffer gas/analyte size and distance dependent collision probabilities that replace the idea of hard interactions between the two[127]. This method has been shown to provide improved agreement between experimental and calculated CCS data, while promoting a tenfold increase in computational speed compared to the TM[129]. Finally, appropriately-scaled versions of PA CCS estimates have also been used to accurately relate X-ray and NMR datasets to IM-MS[120].

1.3.3. Other Experimental Data Used to Refine Models

IM-MS is a dynamic tool, useful in the elucidation of protein mass and size, However, IM-MS data alone is often not enough to generate a complete model of amyloidogenic protein structure. In much of the literature, IM-MS results are presented in combination with other techniques such as NMR, X-ray crystallography, transmission electron microscopy (TEM, described in detail below), and gel electrophoresis. NMR and X-ray crystallography, in contrast to IM-MS, provide higher resolution of the protein structure, however they require more material at a higher purification, and are unable to measure ensembles of structural states and binding stoichiometries. Thus in combination with IM-MS, these technologies allow access to a more complete picture of the structural populations.

In addition, other MS-based tools such as hydrogen/deuterium exchange (HDX), oxidative foot printing, and chemical cross-linking coupled to MS detection can provide structural information. Combined with CCS and other biophysical data, these methods can provide a robust integrated framework from which to filter potential structural models for amyloid-forming peptides and proteins. In general, integrated structural biology workflows allow for an expanded analysis of protein oligomerization and interaction pathways as well as a method to validate nascent functional hypotheses.

In TEM imaging a thin layer of sample is irradiated with an electron beam. This electron beam is focused using electromagnetic lenses and passes through the sample. Electrons are scattered based on sample density. Any unscattered electrons hit a fluorescent screen. This produces an image of the sample, where darker areas represent a higher density due to increased scattering[133]. This tool is highly useful in the study of formed amyloid fibrils[134, 135]. Site directed amino acid

substitution and other chemical modification experiments can also supplement primary IM-MS data to better evaluate hypotheses. Frequently in the context of amyloidogenic peptide and

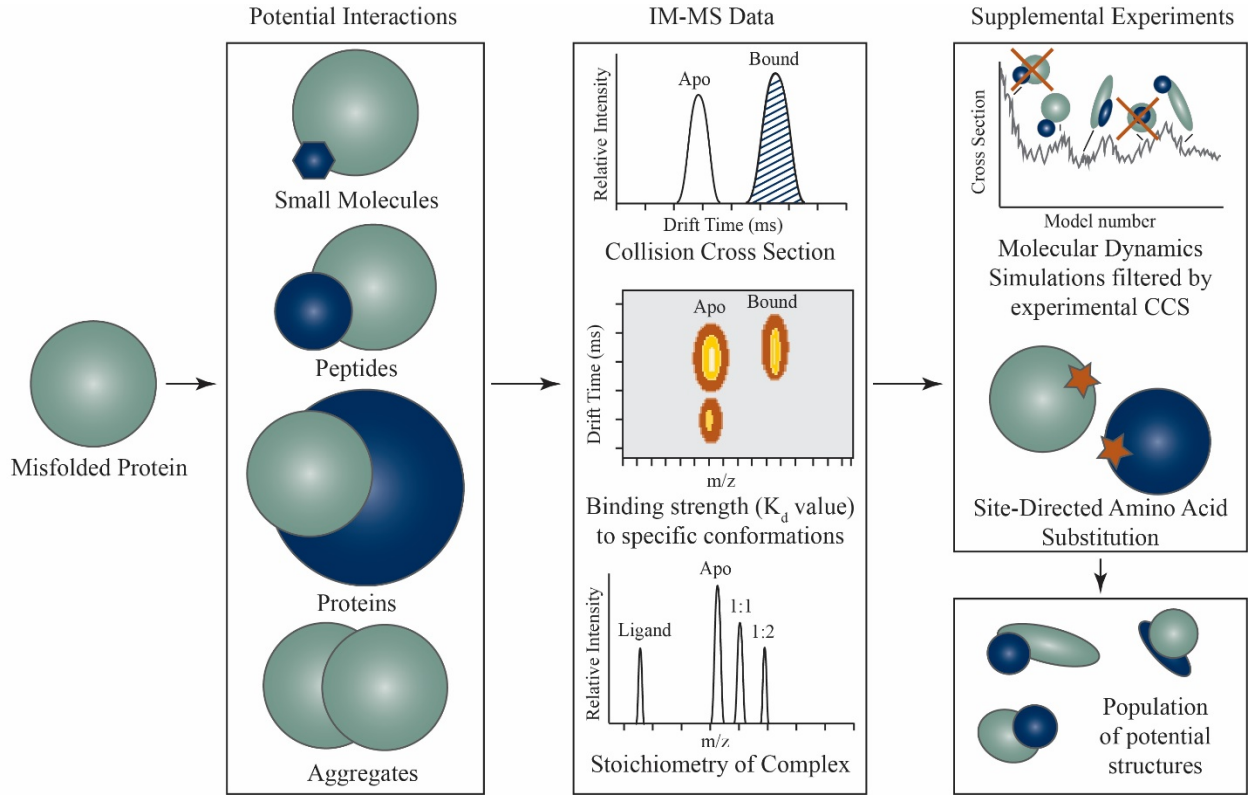

Figure 1.7 – Workflow applying IM-MS to protein misfolding diseases. Interactions of aggregates, protein-protein, protein-peptide, and protein-small molecule can be studied with IM-MS, providing information on CCS and determination of stoichiometries formed. Using a ratio of intensities, binding strength to a specific protein conformation can also be calculated. Following IM-MS experiments, molecular dynamics simulations can be performed and results are filtered by experimental data. Site directed amino acid substitution experiments using IM-MS can also provide further information when compared to WT data. By combining all the data available, the analysis results in both a population of potential structures and putative mechanisms for protein fibrillation.

protein datasets, the biologically relevant mutant forms of the wild type (WT) protein are studied, as in the case of the familial mutations of Amyloid β (Aβ)[136]. Such experiments allow for the assessment of disease relevant complexes relative to similar WT data, analyzing aggregation pathways and structures in both a relative and absolute fashion.

Alternatively, directed amino acid substitutions, targeted to a specific interaction site or region of structural importance suggested by previous IM-MS data, can serve as a control data set in evaluating and filtering available structural models. Such experiments are typically accomplished by altering a residue to prevent the protein from acting in its normal fashion, such as inhibition of random coil to β-sheet fibrils of Aβ by the F19P mutation or oxidation of methionine at residue

35[118, 137]. In addition to altering specific residues within a protein, IM-MS experiments regularly compare sequence variants and isoforms of the same protein to probe for structural information. The most common example of this is the Aβ peptide which encodes 39-42 amino acid residues[118, 138]. It has also been shown with the comparison of aggregation prone human islet amyloid polypeptide (IAPP) with the rat variant, which does not form amyloidogenic fibrils[139], and two structural isoforms of the Syrian hamster prion protein fragment (90-231)[140].

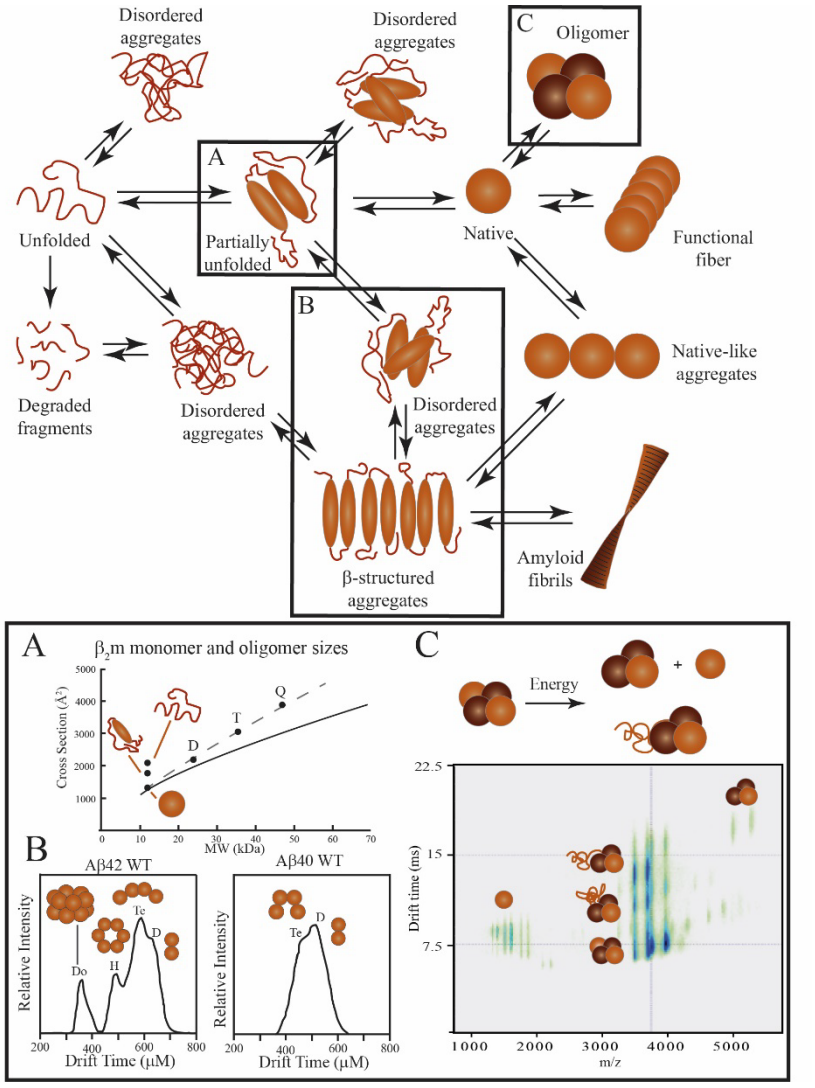

Figure 1.8 – Within the protein misfolding pathway, IM-MS has been applied to partially unfolded proteins, disordered and β-structured aggregates, as well as protein oligomers. A) Three monomeric subunits of β2-microglobulin were studied at varying pH. The solid black line represents a compact growth model for the oligomers. Compared with these compact theoretical structures the experimental data for the dimer, D, trimer, T, and tetramer, Q, have CCS values indicating elongated structures, along the dashed line. B) Drift time data $A\beta_{1\text{-}40}$ and $A\beta_{1\text{-}42}$ at the -5/2 charge state show vastly different populations of oligomer structure as an effect of the two amino acid difference on the c-terminal. C) Upon collisional heating of a protein complex, subunits may dissociate from one another or begin to unfold. In the Transthyretin data shown here, both events are observed at various stages of unfolding and monomeric subunit dissociation. These levels of unfolding and dissociation are strongly correlated to the charge state of the parent ion.

1.4. Relevant Examples and Literature Highlights

IM-MS can be applied in many ways to study the pathway of protein misfolding, oligomerization, and fibril formation[6]. Three major areas of current IM-MS study in this general area are: 1) assessing the conversion of natively-structured monomeric proteins into partially unfolded, disease-associated forms, 2) monitoring the transition between disordered

aggregates and β-structured aggregates, 3) the characterization of larger oligomer populations formed *in vitro* for isolated amyloidogenic peptides and proteins. (Figure 1.8[6, 107, 118, 119]) Examples of amyloidogenic systems where IM-MS has been previously applied over the course of multiple studies include β2-microglobulin (β2m, implicated in haemodialysis related amyloidosis)[119], IAPP (linked to the disease progression in type II diabetes)[124], Aβ peptides and fragments (implicated in or connected to Alzheimer's Disease)[118], α-Synuclein (implicated in Parkinsons's Disease)[141] and Prion protein (associated with Spongiform encephalopathies)[142]. In addition, a Tetrameric Transthyretin (TTR, implicated in familial amyloid neuropathy and senile systemic amyloidosis)[107], ataxin-3 (implicated in Spinocerebellar ataxias)[143], Alpha 1-antitrypsin (implicated in Serpinopathies)[144], and Tau (implicated in Alzheimer's Disease)[145]. While not intended to be comprehensive, the literature overview presented below is designed to highlight relevant papers which have advanced the study of protein misfolding diseases using IM-MS.

1.4.1. Amyloid β

As one of the most studied sequences associated with a protein misfolding disease, Aβ represents an ideal introduction to IM-MS studies in protein aggregation as both the protein interactions with itself, small molecules, and other neuropeptides have been explored. Methods such as modelling, solution phase NMR, X-ray crystallography, and TEM in support of acquired IM-MS data have been employed to answer questions about the Aβ peptide and oligomers.

Drift tube IM-MS data has been reported for many forms of Aβ, and these experiments have revealed much in terms of the structure and olgomerization mechanism for this class of peptides. In addition to studies of the WT Aβ40 and Aβ42 peptides[118, 138, 146], experiments have incorporated the Aβ42 Pro19 alloform[137], Met35(O) of both the Aβ40 and Aβ42[118], in addition to Familial Alzheimer's disease mutations[136] and fragments of Aβ encoding residues 21-30[147, 148] and 39-42[149]. For example, data in 1.7B, shows a drift time distribution comparison of WT Aβ40 and WT Aβ42 labeled as the -5/2 charge state (meaning the -5 charge state of the dimeric form of the peptide or larger charge states for larger, even-numbered oligomers that overlap in m/z)[118]. Identified WT Aβ42 oligomer species include monomers, dimers, tetramers, hexamers, and dodecamers. In contrast WT Aβ40 lacks the hexameric and dodecameric species of the more toxic Aβ42, showing only the dimer and a more compact tetramer. Using a combination of IM and modeling comparisons, data suggests that the two additional C-terminal amino acid residues

found in Aβ42 promotes a conformation difference in lower order oligomers, predominantly within the tetramer. Compared to the Aβ40 species, Aβ42 produces less compact tetramers, and it is these that are suggested to allow the formation of the potentially toxic hexameric paranuclei. These paranuclei are subsequently required to produce the toxic dodecameric oligomer species that allow rapid fibril formation in WT Aβ42. In the absence of these paranuclei, Aβ40 fibril formation is comparatively slower. Mutations that affect the structure of oligomers, can additionally limit the formation of higher order oligomers. Highlighted examples include the mutations F19P Aβ42, as well as Met35(O) in both Aβ40 and 42[118, 137].

While the above work presented evidence of only even number oligomers, additional IM-MS data have identified a trimeric Aβ40 species at a high concentration of 200μM[150]. This work further identified oligomers of masses equal to 16 monomeric subunits in compact as well as extended conformations. The differences between this oligomerization pathway, and the IM-MS data for even-numbered oligomers discussed above is likely promoted by a number of factors common in Aβ research. For example, sample preparation, instrument conditions, ionization sources, and protein concentration all vary substantially between these studies, all potentially leading to altered Aβ oligomerization rate and pathway.

In addition to understanding the mechanisms of isolated Aβ aggregation, IM-MS has begun to emerge as a technique to study the effect of ligand binding on the structure and stabilities of both aggregates and their precursor proteins. On emerging area for study is the interaction between Aβ and other proteins, peptides, and small molecules that might further elucidate the aggregation mechanism of the peptide, and also serve as a foundation for the discovery of new biotherapeutics. For example, several IM-MS datasets have been reported regarding the interactions (-)-epigallocatechin-3-gallate (EGCG), a known small molecule inhibitor of amyloid fibril inhibition, with the Aβ peptides Aβ40, Aβ42, and Aβ(25-35)[121, 151]. Other small molecule inhibitors of Aβ studied using IM-MS include Scyllo-inositol[151], Z-Phe-Ala-diazomethylketone[152], and Diphenylpropynone (appendix III)[153]. In many instances, the small molecules are also studied in conjunction with the presence or absence of metal ions such as zinc and copper[121, 153, 154]. IM-MS data provides information on the altered oligomerization pathway upon binding of one or more of the small molecules, based on the oligomer stoichiometry and size observed.

Beyond the assessment of small molecule-Aβ complexes, IM-MS data has been used to characterize small peptide fragments in terms of their binding site, strength, and structure when in complex with Aβ peptides (see chapter 2). WT Aβ has been shown to interact directly with its C-terminal fragment Aβ(39-42) using IM-MS, and complex formation further leads to an altered aggregation pathway, but not the inhibition of fibril formation[149, 155]. Additionally the Aβ(25-35) fragment has been shown to interact with Tau(273-284), again, reducing fibril formation of Aβ but not abolishing it. However interactions increased the ability for Tau monomers and dimers to aggregate[156].

1.4.2. β2-microgloublin

While many of the studies discussed above focus on the aggregates formed by amyloidogenic peptides such as Aβ, early IM-MS experiments on β2m focused on the structure and dynamics of the monomeric form (Figure 1.8A). High field asymmetric ion mobility spectrometry (FAIMS) and T-wave IM data have been used to analyze the structural forms of β2m that evolve as a function of solution pH, and these data have been linked to solution-phase biophysical measurements under similar conditions[88, 157, 158]. Three different conformer populations were found as a function of pH: the natively folded population at pH 6.0-4.5, a partially folded form at pH 4.5, and a completely unfolded state at pH values less than 3.5. The pH dependence detected in IM-MS data agrees well with data produced with other biophysical studies on isolated β2m folding. In addition to the monomeric population, IM-MS detected β2m oligomers up to and including the tetramer[119]. Subunit exchange within these oligomers was monitored using ^{14}N- and ^{15}N- labelled oligomers to follow the incorporation dynamics of equivalent monomers under equilibrium conditions. Compared to monomers and dimers, the trimer and tetramer exhibited decreases in subunit exchange kinetics, indicating that larger β2m oligomers possess increased stability. IM-MS experiments have also been used to screen β2m interactions with small molecule therapeutics, enabling tests of such compounds to both stabilize protein conformations and oligomers that prevent the formation of cytotoxic species and full-length amyloid. These *in vitro* studies indicated that the mycobacterium-focused antibiotic Rifamycin SV could potentially be repurposed for treatment of haemodialysis related amyloidosis, and acts to bind specific conformers of β2m in solution, although other ansamycin-type antibiotics screened appeared less effective at halting aggregation and amyloid formation[159, 160].

1.4.3. Islet Amyloid Polypeptide/ amylin

IAPP has been studied in depth at the monomeric and dimeric level by IM-MS and replica exchange molecular dynamics simulations[123, 124]. IM-MS has been used, for example, to compare the structures of human IAPP (hIAPP) to the non-amyloidogenic rat IAPP (rIAPP)[139, 161]. In the hIAPP monomer, two conformational families were observed and assigned to a β-hairpin family and a more compact helix-coil family using molecular dynamics simulations. Two pieces of evidence point to the β-hairpin conformation family as the amyloidogenic structure: 1) rIAPP does not adopt this conformational family under the experimental conditions probed, and 2) acidic pH values, which are correlated with increased rate of amyloid fibrillation, promote an increased population of this structure in hIAPP[124]. The dimeric species of hIAPP exhibits a more extended conformation in comparison to rIAPP dimer[123] supporting the notion that β-hairpin monomers are necessary to build β-sheet multimers.

Additional studies analyzed murine amylin using integrated data from TEM, AFM, x-ray diffraction, IM-MS and chemical cross-linking assays to study higher order oligomeric conformations of the peptide[161]. In addition to the monomeric and dimeric species identified previously, more recent studies have identified oligomer sizes up to and including hexamers for both hIAPP and rIAPP *in vitro.* While both peptides exhibited the expected elongated conformations described above, hIAPP appeared to possess increased structural stability when compared with rIAPP analogs[139]. Similar to the screens described above for Aβ and β2m, IM-MS data has identified two small molecule inhibitors of amylin fibril formation, the natural products EGCG and silibinin, that might lead to a deeper understanding of the role hIAPP plays within type II diabetes[139]. With robotically assisted screening, new methods of high throughput inhibitor identification has become possible[162, 163].

1.4.4. α-synuclein

IM-MS data reported for α-synuclein indicate that, although natively unstructured, its ensemble of structural states is dependent upon solution pH[141]. Surprisingly, the protein adopts a more compact structure at pH 2.5 than observed at pH 7. A detailed analysis of these data indicated that this effect relates specifically to the charge the protein carries in the gas-phase, especially when charges are located within its C-terminal region. When the protein possesses eight or less negative charges it adopts a compact structure; when a ninth charge is added the protein

extends[141]. IM-MS has been used to study two disease relevant mutations of α-synuclein: A53T and A30P[164]. Similarly to the WT, A53T IM-MS indicated a compact structure for the -6, -7, and -8 charge states of the protein. In contrast to WT, the A30P only exhibits a compact state while occupying the -6 charge state. Spermine binding to all three variants caused charge reduction and structural compaction and increased aggregation originating from the collapsed monomer populations[164]. Additionally, low concentrations of autoproteolytic fragments were observed by IM-MS between residues 72-140, increasing the propensity of the protein to form aggregates[165].

1.4.5. Prion Protein

Syrian hamster protein protein (SHaPrP) is a model system that has been studied by both drift tube and T-wave IM-MS[140, 142, 166]. Two structural isoforms were analyzed at pH 5.5 and pH 7.0; the α-helical construct, and the β-sheet-rich form of SHaPrP(90-231). Interestingly, at pH 5.5 there was a measureable difference in arrival time distributions recorded for these two prion isoforms, where the α-helical isoform exhibited a smaller CCS than the β-sheet form. At pH 7 however, these differences were not apparent[166]. Other work has applied IM-MS toward CCS measurements of both monomers and higher order PrP(106-126) oligomers in combination with replica exchange molecular dynamics[142]. β-hairpin monomers are suggested to be important in the oligomerization of PrP[142].

1.4.6. Other Amyloidogenic Peptides and Proteins

In addition to the proteins discussed previously, there are a number of proteins associated with protein misfolding disease and aggregation that have been studied by IM-MS, including: TTR[107], Alpha 1-Antitrypsin[144, 167], Insulin[94], Ataxin-3[143], and Tau[145, 156]. For example, in addition to forming misfolded states and large oligomers that are disease-associated, TTR forms a native homo-tetramer, which distinguishes this system from other amyloidogenic proteins studied to date by IM-MS (1.7C). WT and disease associated TTR (L55P) have been tested for their stability while bound to the natural TTR ligand, thyroxin[107]. The stability assay used, based on IM-MS is termed collision induced unfolding (CIU) and uses energetic collisions with background gas to heat protein ions and initiate their unfolding in the gas-phase. While distinct from other MS tools, the methodology utilizes much of the same formalisms discussed in the collision induced dissociation of proteins and multi-protein complexes[168, 169]. In the example of TTR, the variant protein was stabilized to a greater extent by thyroxin binding than the WT TTR

in a manner only observable by the CIU assay[107]. Similar CIU assays are currently being deployed to search for conformationally selective inhibitors and resolve subtle tertiary structure differences that are inaccessible by standard IM-MS technology[81]. As such, CIU will likely be deployed in the future in a broadened way to screen for inhibitors of protein aggregation.

1.5. IM-MS as a Drug Screening Technology

IM-MS cannot currently compete with the speeds of traditional high throughput drug screening methods however, it allows for the analysis of target proteins where binding strength measurements alone are insufficient[81, 162, 163]. Amyolid proteins exist in multiple conformational states, and polydisperse multiprotein ensembles leading to complex mixtures. IM-MS can allow for the detection of small molecules that cause advantageous conformational changes or alter oligomeric states in these complex samples. These changes are ones which may not be observable with traditional fluorescence screening. Current IM-MS technologies is limited to screening hundreds of samples per day due to sample introduction and software available for post-acquisition analysis. The clear trade-off is that of information content, IM-MS while slower is able to assess changes in oligomeric state, binding stoichiometries, conformational and flexibility changes upon ligand binding.

1.6. Summary

While a challenge for many analysis techniques, IM-MS provides advantages in the analysis of amyloid forming peptides and proteins where others might struggle, such as separating and measuring the size of many oligomers in a complex sample. Three IM technologies: drift tube and T-wave (with major impact), and FAIMS (with minor impact) have been utilized in the analysis of amyloidogenic systems. Using IM-MS experimental results as a filtering tool, coarse grain and detailed models of the amyloidogenic systems can be created. Analysis of these models through measurement of CCS can be accomplished through the TM, PA, EHSS, or the PSA methodologies. IM-MS can be combined with other techniques to refine the models of protein aggregation, with these including but not limited to: NMR, X-ray crystallography, TEM, and gel electrophoresis. This is in addition to being compatible with a number of MS-based tools to further assist in refining the models of aggregation, including: HDX, oxidative foot printing, and chemical cross-linking.

IM-MS has been applied to many areas of the protein aggregation pathway, including assessment of the conversion of natively-structured monomeric proteins into partially unfolded, disease-associated forms. Furthermore, IM-MS represents a key tool capable of monitoring the transition between disordered aggregates and β-structured aggregates, as well as characterizing the early steps in the formation of oligomer populations. While the work highlighted here has focused mainly on the disease relevant β2m, IAPP, Aβ, α-Synuclein, and Prion protein systems. Other examples of IM-MS studies into aggregation prone proteins include TTR, Alpha 1-antitrypsin, Insulin, Ataxin-3 and Tau, demonstrating the ever expanding applications of IM-MS. The ability of IM-MS to measure structure, and thus stability while unfolding, gives unique advantage for use as a screening tool for ligands of the protein misfolding diseases discussed, especially in the context of complex mixtures.

In chapter 2, Aβ is screened for interactions with neuropeptides, and the interaction of Aβ with the endogenous opioid neurotransmitter leucine enkephalin is characterized with CCS, K_d, TEM, and simulated annealing. (**Published, Molly T. Soper, Alaina S. DeToma, Suk-Joon Hyung, Mi Hee Lim and Brandon T. Ruotolo (2013) Amyloid-β-neuropeptide interactions assessed by ion mobility-mass spectrometry, *Phys Chem Chem Phys 15,* 8952-8961.)**

In chapter 3, we further characterize the Aβ:LE interaction using site-directed amino acid substitutions of LE. It is discovered that the C-terminal residues phenylalanine and leucine are critical for the interaction. Interactions of Aβ and the dipeptide FL are explored with site-directed amino acid substitutions of Aβ and simulated annealing, discovering Y10 and Q15 to be critical for binding. Hierarchical clustering analysis and detailed structures are used model the interaction. TEM images show FL inhibits downstream fibril formation.

In chapter 4, the methodology to study Aβ developed in chapters 2 and 3 is applied to two larger protein systems: ubiquitin and the ubiquitin-like ubiquilin2. The aggregation propensity of ubiquitin and linear polyubiquitins is studied in the presence of copper. With a 1:1 ratio of copper (with respect to number of ubiquitin domains), dimerization occurs with both mono and liner tri-ubiquitin. We follow these studies with analysis of ubiquilin2 through comparison of WT and P506T variant forms using CIU and measurement of the dimer present.

1.7 References

[1] Radford, S. E., and Dobson, C. M. (1999) From computer simulations to human disease: emerging themes in protein folding, *Cell 97*, 291-298.

[2] Jimenez, J. L., Guijarro, J. I., Orlova, E., Zurdo, J., Dobson, C. M., Sunde, M., and Saibil, H. R. (1999) Cryo-electron microscopy structure of an SH3 amyloid fibril and model of the molecular packing, *The EMBO journal 18*, 815-821.

[3] Kelly, J. W. (1998) The alternative conformations of amyloidogenic proteins and their multi-step assembly pathways, *Current opinion in structural biology 8*, 101-106.

[4] Dobson, C. M. (2001) The structural basis of protein folding and its links with human disease, *Philosophical Transactions of the Royal Society of London B: Biological Sciences 356*, 133-145.

[5] Stefani, M., and Dobson, C. M. (2003) Protein aggregation and aggregate toxicity: new insights into protein folding, misfolding diseases and biological evolution, *Journal of molecular medicine 81*, 678-699.

[6] Chiti, F., and Dobson, C. M. (2006) Protein misfolding, functional amyloid, and human disease, *Annu. Rev. Biochem. 75*, 333-366.

[7] Reilly, M. M. (1997) Genetically determined neuropathies, *Journal of neurology 245*, 6-13.

[8] Conway, K. A., Lee, S.-J., Rochet, J.-C., Ding, T. T., Williamson, R. E., and Lansbury, P. T. (2000) Acceleration of oligomerization, not fibrillization, is a shared property of both α-synuclein mutations linked to early-onset Parkinson's disease: implications for pathogenesis and therapy, *Proceedings of the National Academy of Sciences 97*, 571-576.

[9] Conlon, I. J., Dunn, G. A., Mudge, A. W., and Raff, M. C. (2001) Extracellular control of cell size, *Nature cell biology 3*, 918-921.

[10] Al-Habori, M. (2001) Macromolecular crowding and its role as intracellular signalling of cell volume regulation, *The international journal of biochemistry & cell biology 33*, 844-864.

[11] Zhu, Y. J., Lin, H., and LAL, R. (2000) Fresh and nonfibrillar amyloid β protein (1–40) induces rapid cellular degeneration in aged human fibroblasts: evidence for AβP-channel-mediated cellular toxicity, *The FASEB Journal 14*, 1244-1254.

[12] Nilsberth, C., Westlind-Danielsson, A., Eckman, C. B., Condron, M. M., Axelman, K., Forsell, C., Stenh, C., Luthman, J., Teplow, D. B., and Younkin, S. G. (2001) The'Arctic'APP mutation (E693G) causes Alzheimer's disease by enhanced Aβ protofibril formation, *Nature neuroscience 4*, 887-893.

[13] Sousa, M. M., Cardoso, I., Fernandes, R., Guimaraes, A., and Saraiva, M. J. (2001) Deposition of transthyretin in early stages of familial amyloidotic polyneuropathy: evidence for toxicity of nonfibrillar aggregates, *The American journal of pathology 159*, 1993-2000.

[14] Bucciantini, M., Giannoni, E., Chiti, F., Baroni, F., Formigli, L., Zurdo, J., Taddei, N., Ramponi, G., Dobson, C. M., and Stefani, M. (2002) Inherent toxicity of aggregates implies a common mechanism for protein misfolding diseases, *Nature 416*, 507-511.

[15] Kourie, J., and Shorthouse, A. (2000) Properties of cytotoxic peptide-formed ion channels, *American Journal of Physiology-Cell Physiology 278*, C1063-C1087.

[16] Kourie, J. I., and Henry, C. L. (2002) Ion channel formation and membrane-linked pathologies of misfolded hydrophobic proteins: The role of dangerous unchaperoned molecules, *Clinical and experimental pharmacology and physiology 29*, 741-753.

[17] Goedert, M., and Spillantini, M. G. (2006) A century of Alzheimer's disease, *science 314*, 777-781.

[18] Karlawish, J. (2011) Addressing the ethical, policy, and social challenges of preclinical Alzheimer disease, *Neurology 77*, 1487-1493.

[19] Blennow, K., de Leon, M., and Zetterberg, H. (2006) Alzheimer's Disease., *Lancet 368*, 387-403.

[20] Mattson, M. P. (2004) Pathways towards and away from Alzheimer's disease, *Nature 430*, 631-639.

[21] McKhann, G. M., Knopman, D. S., Chertkow, H., Hyman, B. T., Jack, C. R., Kawas, C. H., Klunk, W. E., Koroshetz, W. J., Manly, J. J., and Mayeux, R. (2011) The diagnosis of dementia due to

Alzheimer's disease: Recommendations from the National Institute on Aging-Alzheimer's Association workgroups on diagnostic guidelines for Alzheimer's disease, *Alzheimer's & Dementia 7*, 263-269.
[22] Hung, Y. H., Bush, A. I., and Cherny, R. A. (2010) Copper in the brain and Alzheimer's disease, *JBIC Journal of Biological Inorganic Chemistry 15*, 61-76.
[23] Barnham, K. J., and Bush, A. I. (2008) Metals in Alzheimer's and Parkinson's diseases, *Current opinion in chemical biology 12*, 222-228.
[24] Bush, A. I. (2003) The metallobiology of Alzheimer's disease, *Trends in neurosciences 26*, 207-214.
[25] Bush, A. I., Pettingell, W. H., Multhaup, G., d Paradis, M., Vonsattel, J.-P., Gusella, J. F., Beyreuther, K., Masters, C. L., and Tanzi, R. E. (1994) Rapid induction of Alzheimer A beta amyloid formation by zinc, *Science 265*, 1464-1467.
[26] Roberts, B. R., Ryan, T. M., Bush, A. I., Masters, C. L., and Duce, J. A. (2012) The role of metallobiology and amyloid-β peptides in Alzheimer's disease, *Journal of neurochemistry 120*, 149-166.
[27] Karran, E., Mercken, M., and De Strooper, B. (2011) The amyloid cascade hypothesis for Alzheimer's disease: an appraisal for the development of therapeutics, *Nature Reviews Drug Discovery 10*, 698-712.
[28] Beal, M. F. (1995) Aging, energy, and oxidative stress in neurodegenerative diseases, *Annals of neurology 38*, 357-366.
[29] Galindo, M. F., Ikuta, I., Zhu, X., Casadesus, G., and Jordán, J. (2010) Mitochondrial biology in Alzheimer's disease pathogenesis, *Journal of neurochemistry 114*, 933-945.
[30] Blass, J. P. (2000) The mitochondrial spiral: an adequate cause of dementia in the Alzheimer's syndrome, *Annals of the New York Academy of Sciences 924*, 170-183.
[31] Dumont, M., and Beal, M. F. (2011) Neuroprotective strategies involving ROS in Alzheimer disease, *Free radical biology and medicine 51*, 1014-1026.
[32] Zhu, X., Raina, A. K., Lee, H.-g., Casadesus, G., Smith, M. A., and Perry, G. (2004) Oxidative stress signalling in Alzheimer's disease, *Brain research 1000*, 32-39.
[33] LaFerla, F. M., Green, K. N., and Oddo, S. (2007) Intracellular amyloid-β in Alzheimer's disease, *Nature Reviews Neuroscience 8*, 499-509.
[34] Kepp, K. P. (2012) Bioinorganic chemistry of Alzheimer's disease, *Chemical reviews 112*, 5193-5239.
[35] Lovell, M. A. (2009) A potential role for alterations of zinc and zinc transport proteins in the progression of Alzheimer's disease, *Journal of Alzheimer's disease: JAD 16*, 471.
[36] Hardy, J., and Selkoe, D. J. (2002) The amyloid hypothesis of Alzheimer's disease: progress and problems on the road to therapeutics, *Science 297*, 353-356.
[37] Kayed, R., Head, E., Thompson, J. L., McIntire, T. M., Milton, S. C., Cotman, C. W., and Glabe, C. G. (2003) Common structure of soluble amyloid oligomers implies common mechanism of pathogenesis, *Science 300*, 486-489.
[38] Lesné, S., Koh, M. T., Kotilinek, L., Kayed, R., Glabe, C. G., Yang, A., Gallagher, M., and Ashe, K. H. (2006) A specific amyloid-β protein assembly in the brain impairs memory, *Nature 440*, 352-357.
[39] Hung, L. W., Ciccotosto, G. D., Giannakis, E., Tew, D. J., Perez, K., Masters, C. L., Cappai, R., Wade, J. D., and Barnham, K. J. (2008) Amyloid-β peptide (Aβ) neurotoxicity is modulated by the rate of peptide aggregation: Aβ dimers and trimers correlate with neurotoxicity, *The Journal of Neuroscience 28*, 11950-11958.
[40] Vigo-Pelfrey, C., Lee, D., Keim, P., Lieberburg, I., and Schenk, D. B. (1993) Rapid Communication: Characterization of β-Amyloid Peptide from Human Cerebrospinal Fluid, *Journal of neurochemistry 61*, 1965-1968.
[41] Hardy, J. (1997) Amyloid, the presenilins and Alzheimer's disease, *Trends in neurosciences 20*, 154-159.

[42] Carter, J., and Lippa, C. (2001) b-Amyloid, Neuronal Death and Alzheimer's Disease, *Current molecular medicine 1*, 733-737.
[43] Bate, C., Kempster, S., Last, V., and Williams, A. (2006) Interferon-γ increases neuronal death in response to amyloid-β1-42, *Journal of neuroinflammation 3*, 7.
[44] Walsh, D., Klyubin, I., Fadeeva, J., Rowan, M., and Selkoe, D. (2002) Amyloid-beta oligomers: their production, toxicity and therapeutic inhibition, *Biochemical Society Transactions 30*, 552-557.
[45] Demuro, A., Mina, E., Kayed, R., Milton, S. C., Parker, I., and Glabe, C. G. (2005) Calcium dysregulation and membrane disruption as a ubiquitous neurotoxic mechanism of soluble amyloid oligomers, *Journal of Biological Chemistry 280*, 17294-17300.
[46] Demuro, A., Parker, I., and Stutzmann, G. E. (2010) Calcium signaling and amyloid toxicity in Alzheimer disease, *Journal of Biological Chemistry 285*, 12463-12468.
[47] Caspersen, C., Wang, N., Yao, J., Sosunov, A., Chen, X., Lustbader, J. W., Xu, H. W., Stern, D., McKhann, G., and Yan, S. D. (2005) Mitochondrial Abeta: a potential focal point for neuronal metabolic dysfunction in Alzheimer's disease, *FASEB journal: official publication of the Federation of American Societies for Experimental Biology 19*, 2040-2041.
[48] Manczak, M., Anekonda, T. S., Henson, E., Park, B. S., Quinn, J., and Reddy, P. H. (2006) Mitochondria are a direct site of Aβ accumulation in Alzheimer's disease neurons: implications for free radical generation and oxidative damage in disease progression, *Human molecular genetics 15*, 1437-1449.
[49] Hoaglund, C. S., Valentine, S. J., Sporleder, C. R., Reilly, J. P., and Clemmer, D. E. (1998) Three-dimensional ion mobility/TOFMS analysis of electrosprayed biomolecules, *Analytical chemistry 70*, 2236-2242.
[50] Fenn, L. S., Kliman, M., Mahsut, A., Zhao, S. R., and McLean, J. A. (2009) Characterizing ion mobility-mass spectrometry conformation space for the analysis of complex biological samples, *Analytical and bioanalytical chemistry 394*, 235-244.
[51] Kebarle, P., and Verkerk, U. H. (2009) Electrospray: from ions in solution to ions in the gas phase, what we know now, *Mass Spectrometry Reviews 28*, 898-917.
[52] Breuker, K., and McLafferty, F. W. (2008) Stepwise evolution of protein native structure with electrospray into the gas phase, 10− 12 to 102 s, *Proceedings of the National Academy of Sciences 105*, 18145-18152.
[53] Moore, B. D., Rangachari, V., Tay, W. M., Milkovic, N. M., and Rosenberry, T. L. (2009) Biophysical Analyses of Synthetic Amyloid-β (1− 42) Aggregates before and after Covalent Cross-Linking. Implications for Deducing the Structure of Endogenous Amyloid-β Oligomers, *Biochemistry 48*, 11796-11806.
[54] Zovo, K., Helk, E., Karafin, A., Tõugu, V., and Palumaa, P. (2010) Label-free high-throughput screening assay for inhibitors of Alzheimer's amyloid-β peptide aggregation based on MALDI MS, *Analytical chemistry 82*, 8558-8565.
[55] Dole, M., Mack, L., Hines, R., Mobley, R., Ferguson, L., and Alice, M. d. (1968) Molecular beams of macroions, *The Journal of Chemical Physics 49*, 2240-2249.
[56] De La Mora, J. F. (2000) Electrospray ionization of large multiply charged species proceeds via Dole's charged residue mechanism, *Analytica chimica acta 406*, 93-104.
[57] Wilm, M., and Mann, M. (1996) Analytical properties of the nanoelectrospray ion source, *Analytical chemistry 68*, 1-8.
[58] Gaskell, S. J. (1997) Electrospray: principles and practice, *Journal of mass spectrometry 32*, 677-688.
[59] Iribarne, J., and Thomson, B. (1976) On the evaporation of small ions from charged droplets, *The Journal of Chemical Physics 64*, 2287-2294.
[60] Hogan Jr, C. J., Carroll, J. A., Rohrs, H. W., Biswas, P., and Gross, M. L. (2008) Combined charged residue-field emission model of macromolecular electrospray ionization, *Analytical chemistry 81*, 369-377.

[61] Sobott, F., Hernández, H., McCammon, M. G., Tito, M. A., and Robinson, C. V. (2002) A tandem mass spectrometer for improved transmission and analysis of large macromolecular assemblies, *Analytical chemistry 74*, 1402-1407.
[62] Chernushevich, I. V., and Thomson, B. A. (2004) Collisional cooling of large ions in electrospray mass spectrometry, *Analytical chemistry 76*, 1754-1760.
[63] Douglas, D. (2009) Linear quadrupoles in mass spectrometry, *Mass spectrometry reviews 28*, 937-960.
[64] Finnigan, R. E. (1994) Quadrupole mass spectrometers, *Analytical Chemistry 66*, 969A-975A.
[65] Bergmann, T., Martin, T., and Schaber, H. (1989) High-resolution time-of-flight mass spectrometer, *Review of Scientific Instruments 60*, 792-793.
[66] Mamyrin, B., Karataev, V., Shmikk, D., and Zagulin, V. (1973) The mass reflectron, a new non-magnetic time-of-flight mass spectrometer with high resolution, *Zh. Eksp. Teor. Fiz 64*, 82-89.
[67] Langevin, P. (1903) The ionisation of gases., *Annales De Chimi Et De Physique 28*, 289-384.
[68] Bradbury, N. E. (1931) The Mobility of Aged Ions in Air in Relation to the Nature of Gaseous Ions, *Physical Review 37*, 1311.
[69] Cravath, A. M. (1929) The rate of formation of negative ions by electron attachment, *Physical Review 33*, 605.
[70] van de Graaf, R. J. (1928) A new method of determining the mobility of ions or electrons in gases, *Philisophical Magazine Series 7 6*, 210-217.
[71] Uetrecht, C., Rose, R. J., van Duijn, E., Lorenzen, K., and Heck, A. J. (2010) Ion mobility mass spectrometry of proteins and protein assemblies, *Chemical Society Reviews 39*, 1633-1655.
[72] Smith, D. P., Knapman, T. W., Campuzano, I., Malham, R. W., Berryman, J. T., Radforda, S. E., and Ashcrofta, A. E. (2009) Deciphering drift time measurements from travelling wave ion mobility spectrometry-mass spectrometry studies, *European Journal of Mass Spectrometry 12*, 13.
[73] Ruotolo, B. T., Benesch, J. L., Sandercock, A. M., Hyung, S.-J., and Robinson, C. V. (2008) Ion mobility–mass spectrometry analysis of large protein complexes, *Nature Protocols 3*, 1139-1152.
[74] Revercomb, H., and Mason, E. A. (1975) Theory of plasma chromatography/gaseous electrophoresis. Review, *Analytical Chemistry 47*, 970-983.
[75] Thalassinos, K., and Scrivens, J. H. (2009) Applications of traveling wave ion mobility-mass spectrometry, *Practical aspects of trapped ion mass spectrometry: applications of ion trapping devices*, 205-235.
[76] Koomen, J. M., Ruotolo, B. T., Gillig, K. J., McLean, J. A., Russell, D. H., Kang, M., Dunbar, K. R., Fuhrer, K., Gonin, M., and Schultz, A. J. (2002) Oligonucleotide analysis with MALDI–ion-mobility–TOFMS, *Analytical and bioanalytical chemistry 373*, 612-617.
[77] Clemmer, D. E., and Jarrold, M. F. (1997) Ion mobility measurements and their applications to clusters and biomolecules, *Journal of Mass Spectrometry 32*, 577-592.
[78] Woods, A. S., Ugarov, M., Egan, T., Koomen, J., Gillig, K. J., Fuhrer, K., Gonin, M., and Schultz, J. A. (2004) Lipid/peptide/nucleotide separation with MALDI-ion mobility-TOF MS, *Analytical chemistry 76*, 2187-2195.
[79] Jackson, S. N., Ugarov, M., Egan, T., Post, J. D., Langlais, D., Albert Schultz, J., and Woods, A. S. (2007) MALDI-ion mobility-TOFMS imaging of lipids in rat brain tissue, *Journal of Mass Spectrometry 42*, 1093-1098.
[80] Kliman, M., May, J. C., and McLean, J. A. (2011) Lipid analysis and lipidomics by structurally selective ion mobility-mass spectrometry, *Biochimica et Biophysica Acta (BBA)-Molecular and Cell Biology of Lipids 1811*, 935-945.
[81] Niu, S., Rabuck, J. N., and Ruotolo, B. T. (2013) Ion mobility-mass spectrometry of intact protein–ligand complexes for pharmaceutical drug discovery and development, *Current opinion in chemical biology 17*, 809-817.
[82] Wyttenbach, T., von Helden, G., Batka, J. J., Carlat, D., and Bowers, M. T. (1997) Effect of the long-range potential on ion mobility measurements, *Journal of the American Society for Mass Spectrometry 8*, 275-282.

[83] McDaniel, E., Martin, D., and Barnes, W. (1962) Drift tube-mass spectrometer for studies of low-energy ion-molecule reactions, *Review of Scientific Instruments 33*, 2-7.
[84] Kuk, Y., Jarrold, M., Silverman, P., Bower, J., and Brown, W. (1989) Preparation and observation of Si 10 clusters on a Au (001)-(5× 20) surface, *Physical Review B 39*, 11168.
[85] Kemper, P. R., and Bowers, M. T. (1990) A hybrid double-focusing mass spectrometer—high-pressure drift reaction cell to study thermal energy reactions of mass-selected ions, *Journal of the American Society for Mass Spectrometry 1*, 197-207.
[86] Shvartsburg, A. A., Tang, K., and Smith, R. D. (2005) Optimization of the design and operation of FAIMS analyzers, *Journal of the American Society for Mass Spectrometry 16*, 2-12.
[87] Swearingen, K. E., and Moritz, R. L. (2012) High-field asymmetric waveform ion mobility spectrometry for mass spectrometry-based proteomics, *Expert review of proteomics 9*, 505-517.
[88] Borysik, A. J., Read, P., Little, D. R., Bateman, R. H., Radford, S. E., and Ashcroft, A. E. (2004) Separation of β2-microglobulin conformers by high-field asymmetric waveform ion mobility spectrometry (FAIMS) coupled to electrospray ionisation mass spectrometry, *Rapid communications in mass spectrometry 18*, 2229-2234.
[89] Giles, K., Pringle, S. D., Worthington, K. R., Little, D., Wildgoose, J. L., and Bateman, R. H. (2004) Applications of a travelling wave-based radio-frequency-only stacked ring ion guide, *Rapid Communications in Mass Spectrometry 18*, 2401-2414.
[90] Pringle, S. D., Giles, K., Wildgoose, J. L., Williams, J. P., Slade, S. E., Thalassinos, K., Bateman, R. H., Bowers, M. T., and Scrivens, J. H. (2007) An investigation of the mobility separation of some peptide and protein ions using a new hybrid quadrupole/travelling wave IMS/oa-ToF instrument, *International Journal of Mass Spectrometry 261*, 1-12.
[91] Shvartsburg, A. A., and Smith, R. D. (2008) Fundamentals of traveling wave ion mobility spectrometry, *Analytical chemistry 80*, 9689-9699.
[92] Bush, M. F., Hall, Z., Giles, K., Hoyes, J., Robinson, C. V., and Ruotolo, B. T. (2010) Collision cross sections of proteins and their complexes: a calibration framework and database for gas-phase structural biology, *Analytical chemistry 82*, 9557-9565.
[93] Campuzano, I., Bush, M. F., Robinson, C. V., Beaumont, C., Richardson, K., Kim, H., and Kim, H. I. (2011) Structural characterization of drug-like compounds by ion mobility mass spectrometry: comparison of theoretical and experimentally derived nitrogen collision cross sections, *Analytical chemistry 84*, 1026-1033.
[94] Salbo, R., Bush, M. F., Naver, H., Campuzano, I., Robinson, C. V., Pettersson, I., Jørgensen, T. J., and Haselmann, K. F. (2012) Traveling-wave ion mobility mass spectrometry of protein complexes: accurate calibrated collision cross-sections of human insulin oligomers, *Rapid Communications in Mass Spectrometry 26*, 1181-1193.
[95] Bush, M. F., Campuzano, I. D., and Robinson, C. V. (2012) Ion mobility mass spectrometry of peptide ions: effects of drift gas and calibration strategies, *Analytical chemistry 84*, 7124-7130.
[96] Henderson, S. C., Li, J., Counterman, A. E., and Clemmer, D. E. (1999) Intrinsic size parameters for Val, Ile, Leu, Gln, Thr, Phe, and Trp residues from ion mobility measurements of polyamino acid ions, *The Journal of Physical Chemistry B 103*, 8780-8785.
[97] Wyttenbach, T., Bushnell, J. E., and Bowers, M. T. (1998) Salt bridge structures in the absence of solvent? The case for the oligoglycines, *Journal of the American Chemical Society 120*, 5098-5103.
[98] Wyttenbach, T., von Helden, G., and Bowers, M. T. (1996) Gas-phase conformation of biological molecules: Bradykinin, *Journal of the American Chemical Society 118*, 8355-8364.
[99] Counterman, A. E., Valentine, S. J., Srebalus, C. A., Henderson, S. C., Hoaglund, C. S., and Clemmer, D. E. (1998) High-order structure and dissociation of gaseous peptide aggregates that are hidden in mass spectra, *Journal of the American Society for Mass Spectrometry 9*, 743-759.
[100] Valentine, S. J., Anderson, J. G., Ellington, A. D., and Clemmer, D. E. (1997) Disulfide-intact and-reduced lysozyme in the gas phase: conformations and pathways of folding and unfolding, *The Journal of Physical Chemistry B 101*, 3891-3900.

[101] Valentine, S. J., Counterman, A. E., and Clemmer, D. E. (1997) Conformer-dependent proton-transfer reactions of ubiquitin ions, *Journal of the American Society for Mass Spectrometry 8*, 954-961.
[102] Shelimov, K. B., Clemmer, D. E., Hudgins, R. R., and Jarrold, M. F. (1997) Protein structure in vacuo: Gas-phase conformations of BPTI and cytochrome c, *Journal of the American Chemical Society 119*, 2240-2248.
[103] Hoaglund, C. S., Liu, Y., Ellington, A. D., Pagel, M., and Clemmer, D. E. (1997) Gas-phase DNA: oligothymidine ion conformers, *Journal of the American Chemical Society 119*, 9051-9052.
[104] Thalassinos, K., Grabenauer, M., Slade, S. E., Hilton, G. R., Bowers, M. T., and Scrivens, J. H. (2008) Characterization of phosphorylated peptides using traveling wave-based and drift cell ion mobility mass spectrometry, *Analytical chemistry 81*, 248-254.
[105] Williams, J. P., and Scrivens, J. H. (2008) Coupling desorption electrospray ionisation and neutral desorption/extractive electrospray ionisation with a travelling-wave based ion mobility mass spectrometer for the analysis of drugs, *Rapid Communications in Mass Spectrometry 22*, 187-196.
[106] Leary, J. A., Schenauer, M. R., Stefanescu, R., Andaya, A., Ruotolo, B. T., Robinson, C. V., Thalassinos, K., Scrivens, J. H., Sokabe, M., and Hershey, J. W. (2009) Methodology for measuring conformation of solvent-disrupted protein subunits using T-WAVE ion mobility MS: an investigation into eukaryotic initiation factors, *Journal of the American Society for Mass Spectrometry 20*, 1699-1706.
[107] Hyung, S.-J., Robinson, C. V., and Ruotolo, B. T. (2009) Gas-phase unfolding and disassembly reveals stability differences in ligand-bound multiprotein complexes, *Chemistry & biology 16*, 382-390.
[108] Han, L., Hyung, S. J., and Ruotolo, B. T. (2012) Bound cations significantly stabilize the structure of multiprotein complexes in the gas phase, *Angewandte Chemie 124*, 5790-5793.
[109] Han, L., Hyung, S.-J., Mayers, J. J., and Ruotolo, B. T. (2011) Bound anions differentially stabilize multiprotein complexes in the absence of bulk solvent, *Journal of the American Chemical Society 133*, 11358-11367.
[110] Ruotolo, B. T., Hyung, S. J., Robinson, P. M., Giles, K., Bateman, R. H., and Robinson, C. V. (2007) Ion Mobility–Mass Spectrometry Reveals Long-Lived, Unfolded Intermediates in the Dissociation of Protein Complexes, *Angewandte Chemie International Edition 46*, 8001-8004.
[111] Eschweiler, J. D., Rabuck-Gibbons, J., Tian, Y., and Ruotolo, B. T. (2015) CIUSuite: A Quantitative Analysis Package for Collision Induced Unfolding Measurements of Gas-Phase Protein Ions, *In Preparation*.
[112] Han, L., Hyung, S.-J., and Ruotolo, B. T. (2013) Dramatically stabilizing multiprotein complex structure in the absence of bulk water using tuned Hofmeister salts, *Faraday discussions 160*, 371-388.
[113] Han, L., and Ruotolo, B. T. (2013) Traveling-wave ion mobility-mass spectrometry reveals additional mechanistic details in the stabilization of protein complex ions through tuned salt additives, *International Journal for Ion Mobility Spectrometry 16*, 41-50.
[114] Ruotolo, B. T., Giles, K., Campuzano, I., Sandercock, A. M., Bateman, R. H., and Robinson, C. V. (2005) Evidence for macromolecular protein rings in the absence of bulk water, *Science 310*, 1658-1661.
[115] Pace, C. N., Trevino, S., Prabhakaran, E., and Scholtz, J. M. (2004) Protein structure, stability and solubility in water and other solvents, *Philosophical Transactions of the Royal Society of London B: Biological Sciences 359*, 1225-1235.
[116] Wolynes, P. G. (1995) Biomolecular folding in vacuo!!!(?), *Proceedings of the National Academy of Sciences of the United States of America 92*, 2426.
[117] Scarff, C. A., Patel, V. J., Thalassinos, K., and Scrivens, J. H. (2009) Probing hemoglobin structure by means of traveling-wave ion mobility mass spectrometry, *Journal of the American Society for Mass Spectrometry 20*, 625-631.

[118] Bernstein, S. L., Dupuis, N. F., Lazo, N. D., Wyttenbach, T., Condron, M. M., Bitan, G., Teplow, D. B., Shea, J.-E., Ruotolo, B. T., and Robinson, C. V. (2009) Amyloid-β protein oligomerization and the importance of tetramers and dodecamers in the aetiology of Alzheimer's disease, *Nature chemistry 1*, 326-331.
[119] Smith, D. P., Radford, S. E., and Ashcroft, A. E. (2010) Elongated oligomers in β2-microglobulin amyloid assembly revealed by ion mobility spectrometry-mass spectrometry, *Proceedings of the National Academy of Sciences 107*, 6794-6798.
[120] Politis, A., Park, A. Y., Hyung, S.-J., Barsky, D., Ruotolo, B. T., and Robinson, C. V. (2010) Integrating ion mobility mass spectrometry with molecular modelling to determine the architecture of multiprotein complexes.
[121] Hyung, S.-J., DeToma, A. S., Brender, J. R., Lee, S., Vivekanandan, S., Kochi, A., Choi, J.-S., Ramamoorthy, A., Ruotolo, B. T., and Lim, M. H. (2013) Insights into antiamyloidogenic properties of the green tea extract (−)-epigallocatechin-3-gallate toward metal-associated amyloid-β species, *Proceedings of the National Academy of Sciences 110*, 3743-3748.
[122] Soper, M. T., DeToma, A. S., Hyung, S.-J., Lim, M. H., and Ruotolo, B. T. (2013) Amyloid-β–neuropeptide interactions assessed by ion mobility-mass spectrometry, *Physical Chemistry Chemical Physics 15*, 8952-8961.
[123] Dupuis, N. F., Wu, C., Shea, J.-E., and Bowers, M. T. (2011) The amyloid formation mechanism in human IAPP: dimers have β-strand monomer− monomer interfaces, *Journal of the American Chemical Society 133*, 7240-7243.
[124] Dupuis, N. F., Wu, C., Shea, J.-E., and Bowers, M. T. (2009) Human islet amyloid polypeptide monomers form ordered β-hairpins: a possible direct amyloidogenic precursor, *Journal of the American Chemical Society 131*, 18283-18292.
[125] Mesleh, M., Hunter, J., Shvartsburg, A., Schatz, G., and Jarrold, M. (1996) Structural information from ion mobility measurements: effects of the long-range potential, *The Journal of Physical Chemistry 100*, 16082-16086.
[126] Shvartsburg, A. A., and Jarrold, M. F. (1996) An exact hard-spheres scattering model for the mobilities of polyatomic ions, *Chemical Physics Letters 261*, 86-91.
[127] Bleiholder, C., Wyttenbach, T., and Bowers, M. T. (2011) A novel projection approximation algorithm for the fast and accurate computation of molecular collision cross sections (I). Method, *International Journal of Mass Spectrometry 308*, 1-10.
[128] Bleiholder, C., Contreras, S., Do, T. D., and Bowers, M. T. (2013) A novel projection approximation algorithm for the fast and accurate computation of molecular collision cross sections (II). Model parameterization and definition of empirical shape factors for proteins, *International Journal of Mass Spectrometry 345*, 89-96.
[129] Anderson, S. E., Bleiholder, C., Brocker, E. R., Stang, P. J., and Bowers, M. T. (2012) A novel projection approximation algorithm for the fast and accurate computation of molecular collision cross sections (III): Application to supramolecular coordination-driven assemblies with complex shapes, *International Journal of Mass Spectrometry 330*, 78-84.
[130] Bleiholder, C., Contreras, S., and Bowers, M. T. (2013) A novel projection approximation algorithm for the fast and accurate computation of molecular collision cross sections (IV). Application to polypeptides, *International Journal of Mass Spectrometry 354*, 275-280.
[131] Scarff, C. A., Thalassinos, K., Hilton, G. R., and Scrivens, J. H. (2008) Travelling wave ion mobility mass spectrometry studies of protein structure: biological significance and comparison with X-ray crystallography and nuclear magnetic resonance spectroscopy measurements, *Rapid Communications in Mass Spectrometry 22*, 3297-3304.
[132] Jarrold, M. F. (1999) Unfolding, refolding, and hydration of proteins in the gas phase, *Accounts of chemical research 32*, 360-367.
[133] Reimer, L. (2013) *Transmission electron microscopy: physics of image formation and microanalysis*, Vol. 36, Springer.

[134] Goldsbury, C. S., Wirtz, S., Müller, S. A., Sunderji, S., Wicki, P., Aebi, U., and Frey, P. (2000) Studies on the in vitro assembly of Aβ 1–40: implications for the search for Aβ fibril formation inhibitors, *Journal of structural biology 130*, 217-231.
[135] Goldsbury, C., Baxa, U., Simon, M. N., Steven, A. C., Engel, A., Wall, J. S., Aebi, U., and Müller, S. A. (2011) Amyloid structure and assembly: insights from scanning transmission electron microscopy, *Journal of structural biology 173*, 1-13.
[136] Gessel, M. M., Bernstein, S., Kemper, M., Teplow, D. B., and Bowers, M. T. (2012) Familial Alzheimer's disease mutations differentially alter amyloid β-protein oligomerization, *ACS chemical neuroscience 3*, 909-918.
[137] Bernstein, S. L., Wyttenbach, T., Baumketner, A., Shea, J.-E., Bitan, G., Teplow, D. B., and Bowers, M. T. (2005) Amyloid β-protein: monomer structure and early aggregation states of Aβ42 and its Pro19 alloform, *Journal of the American Chemical Society 127*, 2075-2084.
[138] Murray, M. M., Bernstein, S. L., Nyugen, V., Condron, M. M., Teplow, D. B., and Bowers, M. T. (2009) Amyloid β protein: Aβ40 inhibits Aβ42 oligomerization, *Journal of the American Chemical Society 131*, 6316-6317.
[139] Young, L. M., Cao, P., Raleigh, D. P., Ashcroft, A. E., and Radford, S. E. (2013) Ion mobility spectrometry–mass spectrometry defines the oligomeric intermediates in amylin amyloid formation and the mode of action of inhibitors, *Journal of the American Chemical Society 136*, 660-670.
[140] Grabenauer, M., Wyttenbach, T., Sanghera, N., Slade, S. E., Pinheiro, T. J., Scrivens, J. H., and Bowers, M. T. (2010) Conformational Stability of Syrian Hamster Prion Protein PrP (90− 231), *Journal of the American Chemical Society 132*, 8816-8818.
[141] Bernstein, S. L., Liu, D., Wyttenbach, T., Bowers, M. T., Lee, J. C., Gray, H. B., and Winkler, J. R. (2004) α-Synuclein: Stable compact and extended monomeric structures and pH dependence of dimer formation, *Journal of the American Society for Mass Spectrometry 15*, 1435-1443.
[142] Grabenauer, M., Wu, C., Soto, P., Shea, J.-E., and Bowers, M. T. (2009) Oligomers of the prion protein fragment 106− 126 are likely assembled from β-hairpins in solution, and methionine oxidation inhibits assembly without altering the peptide's monomeric conformation, *Journal of the American Chemical Society 132*, 532-539.
[143] Scarff, C. A., Sicorello, A., Tomé, R. J., Macedo-Ribeiro, S., Ashcroft, A. E., and Radford, S. E. (2013) A tale of a tail: Structural insights into the conformational properties of the polyglutamine protein ataxin-3, *International journal of mass spectrometry 345*, 63-70.
[144] Ekeowa, U. I., Freeke, J., Miranda, E., Gooptu, B., Bush, M. F., Pérez, J., Teckman, J., Robinson, C. V., and Lomas, D. A. (2010) Defining the mechanism of polymerization in the serpinopathies, *Proceedings of the National Academy of Sciences 107*, 17146-17151.
[145] Larini, L., Gessel, M. M., LaPointe, N. E., Do, T. D., Bowers, M. T., Feinstein, S. C., and Shea, J.-E. (2013) Initiation of assembly of tau (273-284) and its ΔK280 mutant: an experimental and computational study, *Physical Chemistry Chemical Physics 15*, 8916-8928.
[146] Baumketner, A., Bernstein, S. L., Wyttenbach, T., Bitan, G., Teplow, D. B., Bowers, M. T., and Shea, J. E. (2006) Amyloid β-protein monomer structure: A computational and experimental study, *Protein Science 15*, 420-428.
[147] Baumketner, A., Bernstein, S. L., Wyttenbach, T., Lazo, N. D., Teplow, D. B., Bowers, M. T., and Shea, J. E. (2006) Structure of the 21–30 fragment of amyloid β-protein, *Protein science 15*, 1239-1247.
[148] Murray, M. M., Krone, M. G., Bernstein, S. L., Baumketner, A., Condron, M. M., Lazo, N. D., Teplow, D. B., Wyttenbach, T., Shea, J.-E., and Bowers, M. T. (2009) Amyloid β-Protein: Experiment and Theory on the 21− 30 Fragment, *The Journal of Physical Chemistry B 113*, 6041-6046.
[149] Gessel, M. M., Wu, C., Li, H., Bitan, G., Shea, J.-E., and Bowers, M. T. (2011) Aβ (39–42) modulates Aβ oligomerization but not fibril formation, *Biochemistry 51*, 108-117.

[150] Kłoniecki, M., Jabłonowska, A., Poznański, J., Langridge, J., Hughes, C., Campuzano, I., Giles, K., and Dadlez, M. (2011) Ion mobility separation coupled with MS detects two structural states of Alzheimer's disease Aβ1–40 peptide oligomers, *Journal of molecular biology 407*, 110-124.
[151] Bleiholder, C., Do, T. D., Wu, C., Economou, N. J., Bernstein, S. S., Buratto, S. K., Shea, J.-E., and Bowers, M. T. (2013) Ion Mobility Spectrometry Reveals the Mechanism of Amyloid Formation of Aβ (25–35) and Its Modulation by Inhibitors at the Molecular Level: Epigallocatechin Gallate and Scyllo-inositol, *Journal of the American Chemical Society 135*, 16926-16937.
[152] Zheng, X., Gessel, M. M., Wisniewski, M. L., Viswanathan, K., Wright, D. L., Bahr, B. A., and Bowers, M. T. (2012) Z-Phe-Ala-diazomethylketone (PADK) disrupts and remodels early oligomer states of the Alzheimer disease Aβ42 protein, *Journal of Biological Chemistry 287*, 6084-6088.
[153] Pithadia, A. S., Kochi, A., Soper, M. T., Beck, M. W., Liu, Y., Lee, S., DeToma, A. S., Ruotolo, B. T., and Lim, M. H. (2012) Reactivity of diphenylpropynone derivatives toward metal-associated amyloid-β species, *Inorganic chemistry 51*, 12959-12967.
[154] Beck, M. W., Oh, S. B., Kerr, R. A., Lee, H. J., Kim, S. H., Kim, S., Jang, M., Ruotolo, B. T., Lee, J.-Y., and Lim, M. H. (2015) A rationally designed small molecule for identifying an in vivo link between metal–amyloid-β complexes and the pathogenesis of Alzheimer's disease, *Chemical Science 6*, 1879-1886.
[155] Wu, C., Murray, M. M., Bernstein, S. L., Condron, M. M., Bitan, G., Shea, J.-E., and Bowers, M. T. (2009) The structure of Aβ42 C-terminal fragments probed by a combined experimental and theoretical study, *Journal of molecular biology 387*, 492-501.
[156] Do, T. D., Economou, N. J., Chamas, A., Buratto, S. K., Shea, J.-E., and Bowers, M. T. (2014) Interactions between Amyloid-β and Tau Fragments Promote Aberrant Aggregates: Implications for Amyloid Toxicity, *The Journal of Physical Chemistry B 118*, 11220-11230.
[157] Smith, D. P., Giles, K., Bateman, R. H., Radford, S. E., and Ashcroft, A. E. (2007) Monitoring copopulated conformational states during protein folding events using electrospray ionization-ion mobility spectrometry-mass spectrometry, *Journal of the American Society for Mass Spectrometry 18*, 2180-2190.
[158] Smith, D. P., Woods, L. A., Radford, S. E., and Ashcroft, A. E. (2011) Structure and dynamics of oligomeric intermediates in β 2-microglobulin self-assembly, *Biophysical journal 101*, 1238-1247.
[159] Santambrogio, C., Ricagno, S., Sobott, F., Colombo, M., Bolognesi, M., and Grandori, R. (2011) Characterization of β2-microglobulin conformational intermediates associated to different fibrillation conditions, *Journal of Mass Spectrometry 46*, 734-741.
[160] Woods, L. A., Platt, G. W., Hellewell, A. L., Hewitt, E. W., Homans, S. W., Ashcroft, A. E., and Radford, S. E. (2011) Ligand binding to distinct states diverts aggregation of an amyloid-forming protein, *Nature chemical biology 7*, 730-739.
[161] Palmieri, L. C., Melo-Ferreira, B., Braga, C. A., Fontes, G. N., Mattos, L. J., and Lima, L. M. T. (2013) Stepwise oligomerization of murine amylin and assembly of amyloid fibrils, *Biophysical chemistry 180*, 135-144.
[162] Young, L. M., Saunders, J. C., Mahood, R. A., Revill, C. H., Foster, R. J., Tu, L.-H., Raleigh, D. P., Radford, S. E., and Ashcroft, A. E. (2015) Screening and classifying small-molecule inhibitors of amyloid formation using ion mobility spectrometry–mass spectrometry, *Nature chemistry 7*, 73-81.
[163] Young, L. M., Saunders, J. C., Mahood, R. A., Revill, C. H., Foster, R. J., Ashcroft, A., and Radford, S. (2015) ESI-IMS–MS: A method for rapid analysis of protein aggregation and its inhibition by small molecules, *Methods*.
[164] Grabenauer, M., Bernstein, S. L., Lee, J. C., Wyttenbach, T., Dupuis, N. F., Gray, H. B., Winkler, J. R., and Bowers, M. T. (2008) Spermine binding to Parkinson's protein α-synuclein and its disease-related A30P and A53T mutants, *The journal of physical chemistry B 112*, 11147-11154.

[165] Vlad, C., Lindner, K., Karreman, C., Schildknecht, S., Leist, M., Tomczyk, N., Rontree, J., Langridge, J., Danzer, K., and Ciossek, T. (2011) Autoproteolytic Fragments Are Intermediates in the Oligomerization/Aggregation of the Parkinson's Disease Protein Alpha-Synuclein as Revealed by Ion Mobility Mass Spectrometry, *ChemBioChem 12*, 2740-2744.
[166] Hilton, G. R., Thalassinos, K., Grabenauer, M., Sanghera, N., Slade, S. E., Wyttenbach, T., Robinson, P. J., Pinheiro, T. J., Bowers, M. T., and Scrivens, J. H. (2010) Structural analysis of prion proteins by means of drift cell and traveling wave ion mobility mass spectrometry, *Journal of the American Society for Mass Spectrometry 21*, 845-854.
[167] Nyon, M. P., Segu, L., Cabrita, L. D., Lévy, G. R., Kirkpatrick, J., Roussel, B. D., Patschull, A. O., Barrett, T. E., Ekeowa, U. I., and Kerr, R. (2012) Structural dynamics associated with intermediate formation in an archetypal conformational disease, *Structure 20*, 504-512.
[168] Benesch, J. L. (2009) Collisional activation of protein complexes: picking up the pieces, *Journal of the American Society for Mass Spectrometry 20*, 341-348.
[169] Hyung, S. J., and Ruotolo, B. T. (2012) Integrating mass spectrometry of intact protein complexes into structural proteomics, *Proteomics 12*, 1547-1564.

Chapter 2.

Amyloid β: Neuropeptide Interactions Assessed by Ion Mobility – Mass Spectrometry

Molly T. Soper, Alaina S. DeToma, Suk-Joon Hyung, Mi Hee Lim and Brandon T. Ruotolo (2013) Amyloid-β-neuropeptide interactions assessed by ion mobility-mass spectrometry, *Phys Chem Chem Phys 15,* 8952-8961

Recently, small peptides have been shown to modulate aggregation and toxicity of the amyloid β protein (Aβ). As such, these new scaffolds may help discover a new class of biotherapeutics useful in the treatment of Alzheimer's disease. Many of these inhibitory peptide sequences have been derived from natural sources or from Aβ itself (*e.g.* C-terminal Aβ fragments). In addition, much earlier work indicates that tachykinins, a broad class of neuropeptides, display neurotrophic properties, presumably through direct interactions with either Aβ or its receptors. Based on this work, we undertook a limited screen of neuropeptides using ion mobility-mass spectrometry to search for similar peptides with direct Aβ binding properties. Our results reveal that the neuropeptides leucine enkephalin (LE) and galanin interact with both the monomeric and small oligomeric forms of $A\beta_{1\text{-}40}$ to create a range of complexes having diverse stoichiometries, while some tachykinins (*i.e.*, substance P) do not. LE interacts with Aβ more strongly than galanin, and we utilized ion mobility-mass spectrometry, molecular dynamics simulations, gel electrophoresis/Western blot, and transmission electron microscopy to study the influence of this peptide on the structure of Aβ monomer, small Aβ oligomers, as well as the eventual formation of Aβ fibrils. We find that LE binds selectively within a region of Aβ between its N-terminal tail and hydrophobic core. Furthermore, our data indicate that LE modulates fibril generation, producing shorter fibrillary aggregates when added in stoichiometric excess relative to Aβ.

2.1. Introduction

Alzheimer's disease (AD) is currently the sixth leading cause of death worldwide, directly affecting over 24 million people globally[1]. Critically, of the top six causes of death, AD is the only cause for which the mortality rate has not decreased over the past 5 years[1, 2]. There are several competing hypotheses describing the onset and etiology of AD[3]. One of the most prominent of these theorems centers on the uncontrolled aggregation of Aβ peptides varying from 36-43 amino acids in length, produced from proteolytic cleavage of the amyloid precursor protein (APP) *in vivo*; these Aβ species proceed to form amyloid fibrils or plaques in the brain that are comprised primarily of $A\beta_{1-40}$ and $A\beta_{1-42}$[4, 5]. While the eventual formation of amyloid fibrils serves to demarcate the phenomenology of the disease, and fibrils are found prominently in the brains of AD patients, current data suggest that the causative Aβ-related agent, if any, takes the form of small oligomers that may range from dimers to dodecamers[6-10]. Because Aβ peptides aggregate both *in vivo* and *in vitro*, likely occupying a number of structural and oligomeric states simultaneously, the study of Aβ aggregation and its prevention has proven challenging for classical structural biology and biophysics tools[11].

A number of small peptides and small peptide fragments have been found to inhibit the formation of Aβ fibrils and, in some cases, possess protective or restorative properties with respect to the neuronal degeneration that accompanies AD[12-17]. Such peptides are sought after as potential biotherapeutics for AD primarily due to their natural ability to cross membranes and the blood-brain barrier[18, 19]. For example, fragment sequences derived from the C-terminal section of $A\beta_{1-42}$ (C-terminal fragments, CTFs) have been found to directly interact with full-length Aβ peptides and inhibit fibril formation and toxicity[14]. Similarly, proline-rich hydrophobic peptides have been found to alter $A\beta_{1-42}$ folding and fibril formation[20]. Seminal work in AD indicated that tachykinin neuropeptides possess the ability to ameliorate the neurotoxic effects of Aβ peptides[21]. Specifically substance P and physalaemin were found to be inhibitors of Aβ-induced neurotoxicity in hippocampal neurons at μM concentrations, whereas other related peptides did not display the same abilities. Whether the observed neurotrophic activity of these tachykinin peptides is related to their specific roles as neuronal agonists, or if they interact directly with soluble forms of Aβ monomers or oligomers is currently unknown.

Relatively recently, ion mobility-mass spectrometry (IM-MS) has been used to investigate a number of amyloid forming peptides and proteins, providing details on the structures and identities of the oligomers formed prior to amyloid fibril formation[22, 23]. IM separates peptides, proteins, and protein complexes according to differences in ion collision cross-section (CCS) and charge[24]. When combined with MS, this technology is a powerful approach to both complex mixture analysis[25] and for structural studies of heterogeneous biological complexes[26]. IM-MS has been used to identify the oligomers produced by β-microglobulin and transthyretin tetramer, [23, 27, 28] in the case of the former providing detailed structural and composition information on the soluble oligomers formed. Aβ has also been analyzed in detail using IM-MS, revealing much regarding the structure of soluble oligomers and the action of potential inhibitors on the fibril formation process *in vitro*. Specifically, IM-MS has been employed to assess the influence of the CTF $A\beta_{39-42}$ on the oligomerization of full length Aβ[14]. While the addition of CTF to full length Aβ did not alter fibril formation, IM-MS showed discrete differences in the oligomerization pathway of Aβ when bound to CTF in a manner linked to decreases in Aβ-induced neurotoxicity.

Inspired both by this previous IM-MS work on CTF-mediated Aβ oligomerization,[14] and also the earlier work described above relating tachykinin-type neuropeptides to neurotrophic effects in neurons doped with excess Aβ,[21] we screened a limited panel of neuropeptides for their direct interactions with Aβ monomers and small oligomers using IM-MS. While we find no evidence of direct interaction between substance P and monomeric/dimeric $A\beta_{1-40}$, we do detect Aβ interactions with leucine enkephalin (LE) and galanin. Of the two neuropeptides, LE displays a stronger noncovalent bond (Aβ:LE dissociation constant (K_d) equivalent to $A\beta_{1-40}$ dimer formation), and thus in this work we characterized this complex in detail using IM-MS, molecular dynamics (MD) simulations, gel electrophoresis, and transmission electron microscopy (TEM). Further analysis of Aβ:galanin interaction is detailed in Appendix 1. Concentration dependent doping of $A\beta_{1-40}$ with LE leads to the formation of peptide oligomers having a broad range of stoichiometries, and we find that subsequent LE additions to monomeric Aβ are less favored than multiple LE additions to the Aβ dimer. Furthermore, our MD data, filtered by CCS values, indicate that the most likely binding site for LE is within the N-terminus of the peptide, a region similar to other natural products that have been shown to inhibit Aβ fibril formation and neurotoxicity[29]. Finally, our gel data demonstrate that LE-doped $A\beta_{1-40}$ samples exhibits the increased amount of Aβ species with MW ≤ 25kDa, compared to that observed

under LE-untreated conditions. From TEM analysis, mainly truncated fibrillary Aβ are observed in contrast to the long amyloid fibrils typically formed by the peptide in isolation. We discuss these results in the context of biotherapeutic development for AD, as well as Aβ fibril formation in general.

2.2. Experimental

2.2.1. General

Reagents were purchased from commercial sources and used without further purification unless specified otherwise. $A\beta_{1-40}$ was purchased from Anaspec (Fremont, CA, USA). $A\beta_{1-40}$ was dissolved in the supplied 1% (v/v) ammonium hydroxide and diluted with pH 6.9 100mM ammonium acetate (Sigma-Aldrich, St. Louis, MO, USA). Peptide concentration for the stock solution was calculated from absorbance at 280nm (ε = 1490 M^{-1} cm^{-1}) using a Thermo Scientific Genesys 10UV spectrometer (Vernon Hills, IL, USA) or Agilent 8453 spectrophotometer (Santa Clara, CA, USA). LE acetate hydrate (YGGFL) was purchased from Sigma-Aldrich (St. Louis, MO, USA) and prepared in pH 6.9 100mM ammonium acetate. Somatostatin 14, substance P, galanin, and neurotensin were purchased from Anaspec and prepared in 100mM ammonium acetate. Sequence identity comparisons between different neuropeptides studied here were performed with the LALNVIEW tool, accessed through the ExPasy bioinformatics resources[30].

2.2.2. IM-MS

Mass spectra were collected on a quadrupole-ion mobility-time-of-flight (TOF) mass spectrometer (Synapt G2 HDMS, Waters, Milford, MA, USA) with a nano-electrospray ionization (nESI) source. Protein ions were generated using a nESI source and optimized to allow transmission of noncovalent protein complexes using electrospray capillaries prepared as described previously[31]. Protein complex ions were generated using an aliquot of the sample (*ca.* 7 µL) sprayed from the nESI emitter at a capillary voltage of 1.7kV. The source was operated in positive ion mode with the sample cone at 50 V. The bias voltage was 45 V, with backing pressure at 5.42 mbar and TOF pressure at 7.94 x 10^{-7} mbar. The travelling-wave IM separator was operated at a pressure of approximately 3.0 mbar of nitrogen and helium. Mass spectra were

calibrated externally using a solution of cesium iodide (100 mg mL^{-1}) and analyzed using MassLynx 4.1 and Driftscope 2.0 software (Waters, Milford, MA, USA). CCS (Ω) measurements were externally calibrated using a database of known values in helium, using values for peptides and proteins that bracket the likely CCS and ion mobility values of the unknown ions[27, 32]. We report the standard deviations (σ) from triplicate measurements of CCS, but real errors for these values must incorporate the errors involved in the calibration process (an additional ± 3%). Samples were prepared by mixing stock solutions (as prepared above) of neuropeptide and $A\beta_{1-40}$ at pH 6.9, to generate a final $A\beta_{1-40}$ concentration of 20 μM. Samples were incubated on ice for 1 h prior to IM-MS analysis.

2.2.3. Docking Studies

Flexible ligand docking studies were preformed using AutoDock Vina[33]. LE was created using PyMOL and studies were conducted against the $A\beta_{1-40}$ monomer (aqueous solution NMR structure PDB 2LFM)[34]. Twenty docking studies, one with each conformation within the PDB file, were performed. The structures for LE and $A\beta_{1-40}$ were prepared for use with AutoDock vina using AutoDock Tools[33]. All hydrogens were added to $A\beta_{1-40}$ and torsions were kept as the default selected in AutoDock Tools. The exhaustiveness for the docking studies was set at 8, resulting in 9 output models for each $A\beta_{1-40}$ conformation. Docked models of LE were visualized with $A\beta_{1-40}$ using PyMOL.

2.2.4. MD Simulations

Simulations were started using the minimized $A\beta_{1-40}$ solution NMR structure (PDB 2LFM)[34]. The simulations were performed using periodic boundary conditions in a dodecahedron with the minimum distance between the simulated molecules and the box wall being 1.0 nm. GROMACS ligand topology was prepared using the GlycoBioChem PRODRG2 server[35]. The MD simulations were carried out using the GROMACS software package[36] and GROMOS96 force field[37]. To constrain the bond length in the $A\beta_{1-40}$ and LE, the LINCS algorithm was used, allowing an integration time step of 2 fs. Long-range electrostatic interactions were treated with the particle mesh Ewald method. Temperature was maintained using the method of Berendsen *et al*[38]. The LE and the $A\beta_{1-40}$ were separately coupled to external temperature bath with a temperature-coupling constant of 0.1 ps.

The system was energy-minimized by steepest decent for 500 steps. After equilibration, simulated annealing was performed for the $A\beta_{1\text{-}40}$: LE complex in the gas-phase. The three most basic $A\beta_{1\text{-}40}$ side chains (R5, K16, and K28) were charged. The system was heated from 300 K to 500 K over 100 ps, then cooled down to 300 K over the next 100 ps. The cycle was repeated over 20 ns in order to allow for escape from local minima and enhance equilibration. For the $A\beta_{1\text{-}40}$: LE complex, 20 independent simulated annealing runs, each running for a total of 20 ns, were performed from the lowest energy complexes generated by AutoDock Vina. From the MD trajectory generated, 100 structures were sampled at 300 K and the CCS was calculated with Mobcal using the trajectory method algorithm[39, 40]. Models of the $A\beta_{1\text{-}40}$:LE complexes were visualized in PyMOL. In total 2000 structures were generated. Of the 1090 structures which were within ± 3% of the experimentally determined CCS, the 201 structures with lowest energy were analyzed to determine the $A\beta_{1\text{-}40}$ residues within 4 Å of LE. Standardized values (Z-scores) were calculated for each residue of $A\beta_{1\text{-}40}$ and plotted in standard deviation (σ) space in order to determine the relative likelihood of LE binding within a given region of Aβ.

2.2.5. K_d Measurements by MS

Dissociation constant (K_d) values for the neuropeptides with $A\beta_{1\text{-}40}$ were calculated using the relative intensity of each species from the mass spectra, as described previously[41]. We modified this method to accommodate multiple ligand binding events with the following assumptions: (1) the spray and detection efficiency of all species are similar, (2) the ligand concentration is sufficiently high so that $[L]_{eq}$ remains constant and (3) the ligand binds to the complex one at a time in a stepwise fashion.

For the equilibrium binding of A (unbound protein) and B (a ligand/binding partner):

$$A + B \leftrightarrow C_1 + C_2 + \cdots + C_x \quad (2.1)$$

$$R_x = \frac{[C_x]_{eq}}{[A]_{eq}} \quad (2.2)$$

Where R_x is an equilibrium quotient between the bound form of the protein (C_x, having x ligands attached) when interacting with ligand B, and tis unbound for (A).

$$[C_x]_{eq} = \frac{R_x([A]_0 - (\sum_{i=1}^{x-1}[C_i]_{eq}))}{1+R_x} \quad (2.3)$$

Eqn (2.3) above defines R_x for all bound forms of the protein (C_i) and:

$$K_{d_x} = \frac{[C_{(x-1)}]_{eq}[B]_{eq}}{[C_x]_{eq}} \quad (2.4)$$

Allows for the determination of K_d for any given step in the sequential equilibrium described in eqn (2.1), where C_0 = A. Standard deviation values (σ) for the K_d measurements reported here are shown from three replicate measurements.

2.2.6. Aβ Aggregation Experiments

Aβ experiments were performed according to the previously published methods[42-49]. Prior to experiments, $A\beta_{1-40}$ was dissolved in ammonium hydroxide (NH_4OH, 1% v/v, aqueous), aliquoted, and lyophilized overnight, and stored at -80 °C. A stock solution of fresh Aβ was prepared by dissolving the peptide in 1% NH_4OH (10 µL) and diluting with ddH_2O. The Aβ stock solution was diluted to a final concentration of 25 µM in a buffered solution containing ammonium acetate (100 mM, pH 6.9). The Aβ samples were incubated with 0, 1, 3, or 5 equiv. LE (1.2 mM stock solution in the same buffered solution) at 37 °C with constant agitation for 24h.

Samples from the experiment were analyzed by gel electrophoresis and visualized by Western blot using an anti-Aβ antibody (6E10)[42-49]. Each sample was separated on a 10-20% Tris-tricine gel (Invitrogen, Grand Island, NY, USA) and transferred onto a nitrocellulose membrane. The nitrocellulose was blocked with bovine serum albumin (BSA, 3% w/v, Sigma, St. Louis, USA) containing 0.1% Tween-20 (TBS-T, Sigma) for 2 h at room temperature. Afterward, the membrane was incubated with the anti-Aβ antibody 6E10 (1:2000, Covance, Princeton, NJ) in a solution of 2% BSA (w/v in TBS-T) overnight at 4 °C. The horseradish peroxidase-conjugated goat anti-mouse secondary antibody (1:5000, Cayman Chemical, Ann Arbor, MI, USA) in 2% BSA was added for 1 h at room temperature. The Thermo-Scientific SuperSignal West Pico Chemiluminescent Substrate was used to visualize the protein bands.

2.2.7 TEM

TEM images were taken using Phillips CM-100 transmission electron microscope (Microscopy and Image Analysis Laboratory, University of Michigan, MI, USA) using a magnification factor of 25 000. Samples for TEM were prepared according to the previously reported methods[42-47, 49].

Glow-discharged grids (Formar/Carbon 300-mesh, Electron Microscopy Sciences, Hatfield, PA, USA) were treated with Aβ samples from the *in vitro* inhibition experiments (5 µL) for 2 min at room temperature. Excess sample was removed using filter paper followed by washing with ddH_2O five times. Each grid was stained with uranyl aceteate (1% w/v ddH_2O, 5 µL, 1 min). Upon removal of excess uranyl acetate, the grids were dried for 15 min at room temperature.

2.3. Results

A limited neuropeptide screen for binding with $A\beta_{1\text{-}40}$ was conducted with five neuropeptides, varying in mass and structure. Masses of the neuropeptides in this study ranged from 555.62 Da (LE) to 3158.5 Da (galanin). $A\beta_{1\text{-}40}$ prepared for nESI-IM-MS analysis in 100 mM ammonium acetate results in a mass spectrum containing both 3^+ and 4^+ monomer and 5^+ dimer ions in high relative abundances (Figure 2.1). IM-MS analysis of this same dataset (data not shown) reveals evidence of additional oligomeric forms of the monomeric 4^+ peptide (*vide infra*). $A\beta_{1\text{-}40}$-neuropeptide binding was only detected between $A\beta_{1\text{-}40}$ and two neuropeptides, LE and galanin, under our experimental conditions (Figure 2.1). Complex formation between $A\beta_{1\text{-}40}$ and

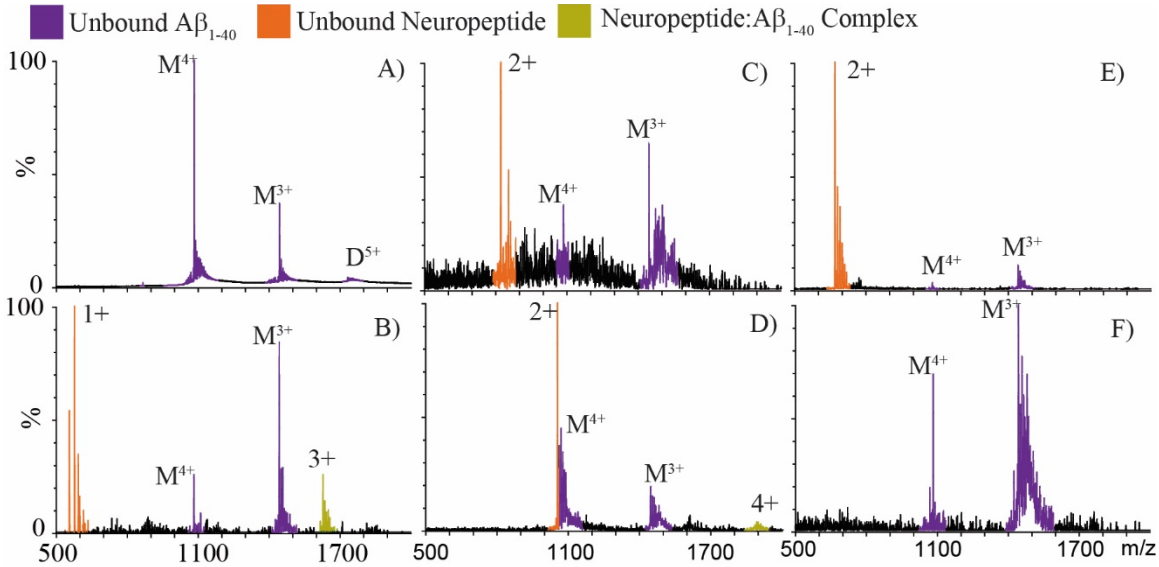

Figure 2.1 – Analyses of $A\beta_{1\text{-}40}$ incubated with one equivalent of each neuropeptide by nESI-IM-MS. A) Mass spectrum of $A\beta_{1\text{-}40}$ only, with signals corresponding to monomeric and dimeric peptides marked with a 'M' and 'D', respectively. Satellite peaks observed correspond to alkali metal adducts commonly observed in nESI-MS. $A\beta_{1\text{-}40}$ was then mixed with equivalent amounts of B) LE (free $[M+H]^+$ at m/z = 556.6), C) somatostatin (free $[M + 2H]^{2+}$ at m/z = 820.5), D) galanin (free $[M+3H]^{3+}$ at m/z = 1053.8), E) substance P (free $[M + 2H]^{2+}$at m/z = 675.5) and F) neurotensin (no free signal detected, peptide mass = 1674.0). LE and galanin are the two neuropeptides in this set where we detect complexes with $A\beta_{1\text{-}40}$ (complexes signals in green), while the other neuropeptides screened result in signals for unbound $A\beta_{1\text{-}40}$ (purple) and unbound neuropeptide (orange). Poorer signal intensities are recorded in panels C and F due to signal suppression surrounding the addition of the neuropeptide indicated.

substance P, somatostatin, or neurotensin is not evident in our dataset. The $A\beta_{1\text{-}40}$ binding strength is greater for LE than for galanin, as reported in the relative intensity differences detected by MS between the free $A\beta_{1\text{-}40}$ monomer peaks and the respective complex ion signals. Due to the apparently enhanced strength of the Aβ:LE interaction under the conditions of our screen relative to all other neuropeptides studied, we focused on characterizing the structure of this complex further.

Up to 80 µM LE was titrated into a 20 µM Aβ solution, and the resultant complexes were detected using IM-MS (Figure 2.2). The 1:1 complex of $A\beta_{1\text{-}40}$:LE is first observed in our IM-MS data when 10 µM LE is added. At a 1:2 ratio of $A\beta_{1\text{-}40}$: LE, the 1:2 and 1:3 complexes of $A\beta_{1\text{-}40}$:LE are detected, both of which occupy a 3^+ charge state (Figure 2.2B). Complexes of $A\beta_{1\text{-}40}$ dimer with LE are also observed with lower intensity in the $A\beta_{1\text{-}40}$:LE mixture (20/60 µM, respectively) (*vide infra*). The K_d value for each of the $A\beta_{1\text{-}40}$:LE complexes identified were calculated as an average across the concentration ramp (Table 2.1). Measured K_d values for Aβ:LE complexes are in the low µM range, with similar K_d values for both the monomer and dimer complexes. While the 1:1 complex exhibits a K_d of 61.7 µM (similar to the K_d we measure for the Aβ dimer, at 56 µM), the 1:2 and the 1:3 complexes possess K_d values of 99.2 and 55.7 µM respectively, indicating a slight thermodynamic barrier in the formation of Aβ:2LE. Aβ dimer, however, does not exhibit signs of a similar barrier, as LE-related K_d values are recorded to be 76.7 and 49.8 µM for the formation of the 2:1 and the 2:2 complexes, respectively.

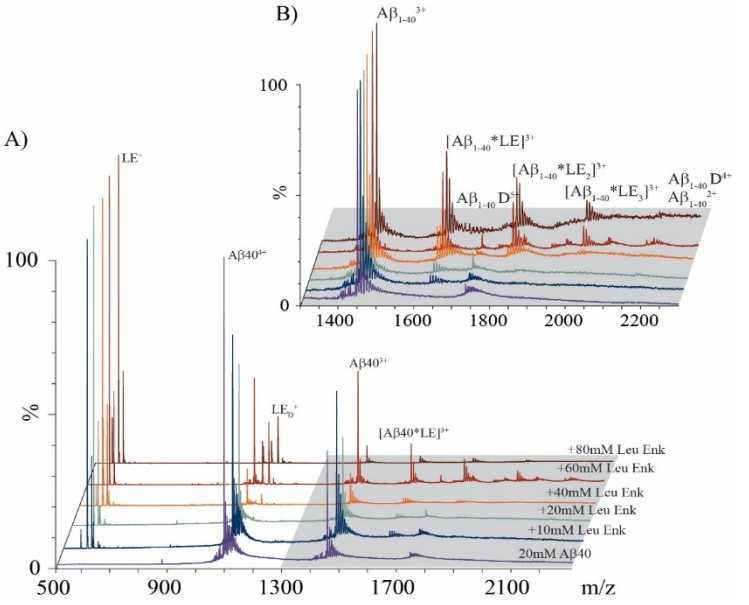

Figure 2.2 – A) MS spectra for $A\beta_{1\text{-}40}$ acquired at 20 µM (purple). $A\beta_{1\text{-}40}$ was then incubated with increasing concentrations of LE, ranging from 10-80 µM (stoichiometric ratios from 0.5 to 4). At sufficiently high LE concentrations, $A\beta_{1\text{-}40}$ is seen in complex with LE, producing Aβ:LE complexes ranging from 1:1 to 1:3. B) A magnified region of the spectrum shown in A (grey highlight), wher signals corresponding to Aβ:LE complexes are labeled.

Using IM-MS, it is possible to measure the CCSs of both free $A\beta_{1-40}$ and Aβ:LE complexes simultaneously (Figure 2.3). While the 3^+ charge state of $A\beta_{1-40}$ and the $A\beta_{1-40}$ monomer: LE complexes all occupy a single closely related family of structures, as evidenced by the drift time profiles recorded for these ions, the 4^+ $A\beta_{1-40}$ monomer has at least two main conformational

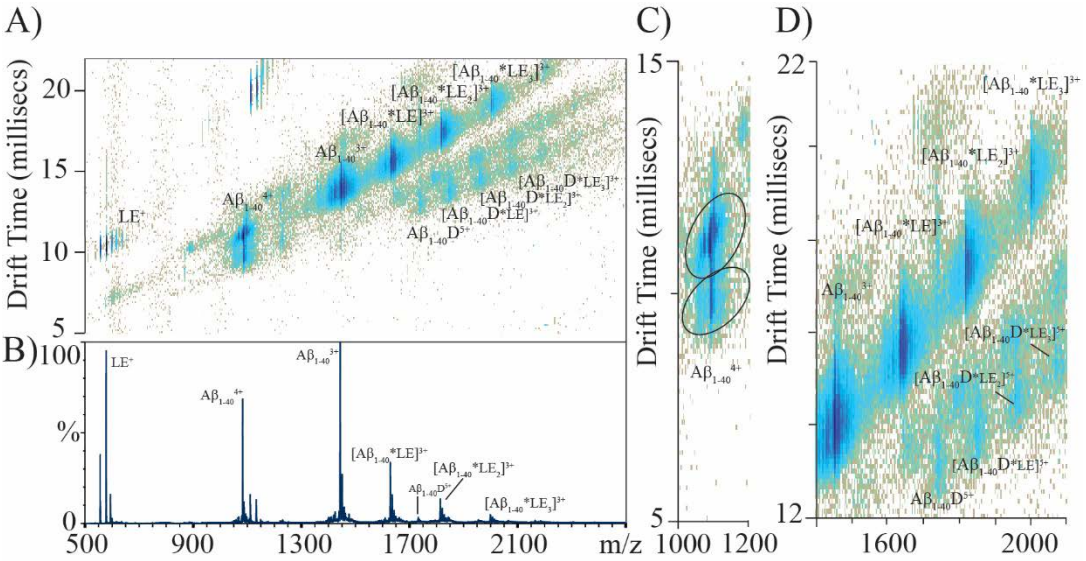

Figure 2.3 – A) IM-MS data for $A\beta_{1-40}$ (20 µM) incubated with LE (60 µM) for 1 h on ice, where Aβ:LE complexes are labeled, along with free peptide. IM separation allows for the identification of Aβ dimer complexes previously undetected by MS alone. $A\beta_{1-40}$ is seen in complex with LE at stoichiometric ratios up to 1:3 $A\beta_{1-40}$: LE and 2:3 $A\beta_{1-40}$: LE. B) MS dataset for the IM-MS plot shown in A. C) Two main conformations of $A\beta_{1-40}^{4+}$ are identified, with a third minor conformer, as observed previously[29]. D) A magnified region of the IM-MS data shown in A, showing detail on $A\beta_{1-40}^{3+}$:LE complexes. Monomer complexes are observed in greater relative abundance than those related to dimeric $A\beta_{1-40}$.

families, along with a third minor structure for which we did not record data here[29]. The more compact form of Aβ 4^+ has a CCS of 622 $Å^2$. These values are similar to previous reports[29]. The measured cross section of LE is 165 $Å^2$; however, the change in CCS of $A\beta_{1-40}$ monomer when in complex with LE is only 44-47 $Å^2$ indicating a closely packed interaction. The changes in size for the dimer complexes are similar in magnitude to those of the monomer (27-51 $Å^2$), also likely representing a tightly packed complex. The intensities that we observe for the Aβ dimer-based complexes are lower than those of the Aβ monomer-related complexes (Figure 2.3D), likely due to the lower concentration of free Aβ dimer in solution.

Table 2.1 – K_d values for LE:Aβ_{1-40} complexes measured by MS

Complex	K_d (μM)	σ
Aβ_{1-40} Dimer	56.0	44.7
[Aβ_{1-40} + LE]	61.7	27.2
[Aβ_{1-40} + LE_2]	99.2	30.6
[Aβ_{1-40} + LE_3]	55.7	21.7
[Aβ_{1-40} dimer + LE]	76.7	15.6
[Aβ_{1-40} dimer + LE_2]	49.8	6.5

To visualize the most likely configurations of the 1:1 Aβ_{1-40}:LE complex, rigid peptide-flexible ligand docking followed by simulated annealing MD was performed. Of the 2000 resultant structures after annealing simulations, 1090 had CCS values within 3% of the experimentally measured value for the complex (638 $Å^2$), as calculated by the trajectory method. These structures were additionally filtered by the energy axis from MD data, resulting in 201 sample structures that are mostly-likely to represent the structure of the gas-phase ions in our experiments. From this population, a lowest-energy sample configuration was compared to both the starting NMR (PDB ID: 2LFM) and LE docked structures in Figure 2.4B-D. We further analyzed the 201 low energy structures to determine the LE side-chain groups within 4 Å of any Aβ_{1-40} residue and counted these as potential interactions. As expected, models indicate, the hydrophobic residues Phe and Tyr in LE interacted more frequently with Aβ_{1-40} than the Leu and in much greater frequency than the two Gly residues. The Aβ_{1-40} region with most frequent LE interactions in our MD dataset lies in the region between residues Glu-3 and Lys-16, with the most frequent LE interactions occurring with the Arg-5, Tyr-10, Glu-11, Lys-16, and Glu-22 side chains. Generally, our MD results, filtered according to our experimental CCS data, indicate that LE interacts preferentially with the N-terminus and hydrophobic core of the Aβ_{1-40} monomer.

In order to assess whether the interaction of LE with Aβ_{1-40} could influence aggregation of the peptide, *in vitro* aggregation studies were conducted and samples of the resulting Aβ species were analyzed by gel electrophoresis/ Western blot and TEM. (Figure 2.5). The gel electrophoresis/Western blot results present the distribution of Aβ species, including aggregates that are able to penetrate the gel, based on their molecular weight (MW)[29, 43-46, 49]. Upon incubation of Aβ species with LE (1, 3 or 5 equiv.), the amount of Aβ species with MW ≤ 25 kDA, visualized in the gel, is relatively increased compared to that observed under LE-untreated conditions. (Figure 2.5A). For a qualitative comparison against these gel results, TEM was used

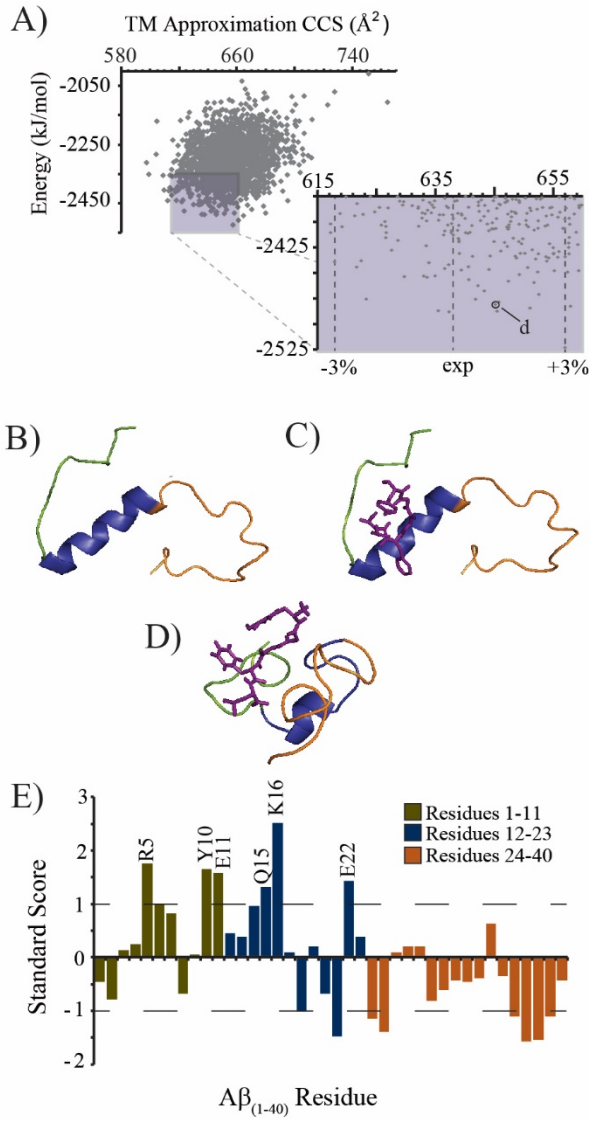

Figure 2.4 – A) Output from all molecular dynamics simulations. The lowest energy 201 structures with CCS values within ±3% of experimental are highlighted (purple box). B) The structure of Aβ monomer (PDB 2LFM). C) A docked structure of Aβ (PDB 2LFM) with LE using AutoDock Vina. D) A representative low energy model (indicated in A) from the main structural family identified from our MD simulations, in agreement with experimental CCS values. Colors represent the N-terminus (green), core/helix region (blue), and the C-terminus (orange). E) A plot of the standard score (Z-score) for Aβ residues within 4Å of the bound LE. Larger values denote contacts of greater significance on the standard deviation (σ) scale. Negative values denote contacts of reduced significance.

to identify whether LE could restructure gross Aβ aggregate morphology (Figure 2.5B). In the absence of LE, large Aβ aggregates with mainly fibrillary morphologies are indicated. On the other hand, from the samples containing Aβ and LE (3 or 5 equiv.), shorter fibrillar species are shown as the main Aβ species. Taken together, LE demonstrates an ability to moderately alter Aβ aggregate formation *in vitro*.

2.4. Discussion

Neuropeptide screening results shown in Figure 2.1 not only indicate Aβ:LE and Aβ:galanin complex formation, but also detect no direct complexes between Aβ and substance P, a neuropeptide known to possess neurotrophic properties with respect to Aβ-induced neurotoxicity[50]. This result suggests that either substance P interacts with larger toxic oligomers that are not detected in our IM-MS datasets, or that the action or substance P is related to its role as a neuronal agonist, where it may act to block Aβ interactions with critical cell surface receptors. The original work identifying the neurotrophic effects of tachykinin neuropeptides in the context of Aβ localized the critical amino acid sequence involved in the putative interaction to GSNKGAIIGLM, which shares broad sequence homology within the tachykinin family and corresponds to residues 25-35 of the Aβ peptide[21]. This sequence bears little resemblance to the amino acid sequence of either LE

(YGGFL) or galanin (GWTLNSAGYLLGPHAVGNHRSFSDKNGLTS). For example, the strongest identity between galanin and $A\beta_{25-35}$ exist in a six amino acid sequence between residues 23 and 28 in glanin and residues 2 through 7 in the Aβ fragment, resulting in only a 33% sequence identity within that region. Since early reports for Aβ:tachykinin interactions suggested that the C-terminus of Aβ played a role[21], the fact that our results for peptides that contain little sequence identity to tachykinins and target the N-terminus is not surprising. Interestingly, galanin has also been implicated in the etiology of AD, as the peptide has been found within fibrils innervating surviving cholinergic neurons[51]. While known physiological concentrations of both neuropeptides is insufficient to drive the formation of the relatively weak interactions discovered in this report *in vivo*, the local concentrations of these peptides, which generally co-localize with Aβ[52], may be sufficient to interact with Aβ and influence complex equilibria towards the complex formation.

IM-MS structure and oligomer population data for peptides and proteins must be interpreted carefully due to the relatively unique environment employed during the analysis. First, during the nESI process, many peptides may be trapped in rapidly evaporating droplets and are thus forced to generate artificial complexes due to solvent evaporation[53]. While this situation is typically avoided by simply lowering the overall sample concentration[26], the concentration accessed in this report is in excess of those that typically limit the production of ESI-artifact oligomers. The data in Figure 2.1, however, serve as control experiments in this regard, validating the specificity of the interactions identified for LE and galanin against a panel of either larger or similarly sized peptides. No Aβ complexes were detected for the other peptides in our panel (*i.e.* substance P, somatostatin, or neurotensin), even when added in large excess in solution, indicating that oligomers observed in our IM-MS data are both specific to LE and galanin and likely formed in solution. Since the structural measurements generated by IM-MS take place in the gas-phase, a certain amount of local structural rearrangement is expected for peptide complex ions. Such rearrangements can be observed in Figure 2.4D. The key to utilizing gas-phase IM-MS data effectively in assessing the structure of biomolecules is to seek evidence of correlated structural elements, rather than a wholesale identity between solvent-free and native-state structures[54]. However, we find that the binding region likely accessed by LE in solution is apparently retained in our lowest energy gas-phase structures and, indeed, throughout our simulation results (Figure 2.4E) despite the rearrangements observed for the Aβ peptide backbone. We also note that while

the Aβ data presented here focuses on positive ions, most reports of IM-MS data for this peptide contain data for negative ions in order to exploit its charge obtained in solution to simplify data interpretation and MD simulations[55]. While we are actively pursuing negative ion mode data for Aβ bound to neuropeptides, the data in this report focused on positive ions primarily to avoid the signal intensity and instrumental noise limitations associated with acquiring such data. We deemed ion signal intensity of primary importance in our studies due to the relatively weak Aβ:neuropeptide interactions we wished to probe.

Once we overcame the challenges associated with the collection and interpretation of IM-MS data on these complexes, we noted several advantages of the method for studying Aβ:neuropeptide complexes in comparison to other structural biology tools. The concentration range accessed by the IM-MS approach is comparatively low relative to other approaches that are capable of recording complex size and shape information[56-61]. In addition, due to the heterogeneous nature of the Aβ:LE complexes interrogated, most spectroscopic probes would report structure and K_d values averaged over many co-existing complexes and assemblies. We found IM analysis to be especially important in the detection of dimer-related complexes, which may have gone completely overlooked if detected by MS alone. The plots shown in Figure 2.3 group these signals together to form a trend line easily distinguished from other signals associated with Aβ and LE[62]. Trends observed for the CCS associated with the addition of LE to Aβ are especially informative (Table 2.2) and indicate that highly compact forms are favored for this complex in the context of both Aβ monomers and dimers. Interestingly, the compactness of the resulting complex recorded by IM-MS has no correlation with the resultant binding constant of that complex (K_d, Table 2.1), perhaps providing additional evidence of local structural rearrangements in these Aβ:LE assemblies upon introduction to the gas phase. Finally, the ability to evaluate individually the structure and stability of Aβ:LE complexes is a feat that few other techniques can accomplish, and as such the values reported here, while in broad agreement with other studies of Aβ stability[29] form a unique resource on Aβ:neuropeptide interactions.

Table 2.2 – CCS values for LE:$A\beta_{1-40}$ complexes measured by IM-MS

Complex	*m/z*	CCS ($Å^2$)	σ^a
LE^+	557.0	165	0.22
$A\beta_{1-40}{}^{4+}$	1083.5	622	13.2
$A\beta_{1-40}{}^{4+}$	1083.5	678	0.29
$A\beta_{1-40}{}^{3+}$	1444.3	594	0.38
$[A\beta_{1-40} + LE]^{3+}$	1629.6	638	0.84
$[A\beta_{1-40} + LE_2]^{3+}$	1815.0	683	0.43
$[A\beta_{1-40} + LE_3]^{3+}$	2000.3	731	0.18
$A\beta_{1-40}$ $Dimer^{5+}$	1733.0	946	12.7
$[A\beta_{1-40}$ dimer + $LE]^{5+}$	1844.2	982	0.21
$[A\beta_{1-40}$ dimer + $LE_2]^{5+}$	1955.4	1032	1.54
$[A\beta_{1-40}$ dimer + $LE_3]^{5+}$	2066.6	1060	22.6

[a] Standard deviation from measurements in triplicate. For real errors, including those from IM calibration, an additional ~3% must be added to these values.

The ability of endogenous or exogenous molecules to modulate Aβ aggregate formation has been of interest, primarily in an effort to redirect aggregation from producing toxic intermediates. Altering the thermodynamics and/or kinetic parameters of this process using molecules like LE could offer insight into this problem; however, traditional methods to access the degree of fibril formation, such as the fluorescence-based assay using the amyloid-specific dye thioflavin-T (ThT), do not always adequately represent these changes[29, 42, 63, 64]. In the case of LE, its inherent interactions with both ThT and Aβ aggregates would have interfered with data interpretation (data not shown). Thus gel electrophoresis/Western blot studies in conjunction with TEM could offer a more complete picture of the ability of LE to influence $A\beta_{1-40}$ aggregation. Upon incubation of Aβ with LE, there are slightly different distributions of peptide sizes detected by gel electrophoresis/Western blot studies, compared to that from the LE-untreated Aβ sample, indicating that LE could not completely block or alter the fibril formation trajectory. To complement these results, TEM images show differences in aggregate morphology that occur during aggregation when LE is present, particularly on larger aggregates. While the aggregate populations could not be completely characterized or quantified by TEM, primarily larger sized aggregates can be visualized. The TEM images display that samples containing excess LE (*e.i.* 3 or 5 equiv.) indicate altered aggregates of large sizes (*e.g.*, mainly shorter fibrils), which is consistent with the gel data that showed minimal changes to low MW populations. Thus, weak ligand binding may not preclude it from influencing downstream fibrillization provided that

interactions occur near the N-terminus of Aβ, similar to LE; however, adjustment of additional parameters in such compounds might be required to fully alter structural properties of Aβ aggregates at earlier stages.

The Aβ:LE binding region identified in Figure 2.4 possesses some features similar to the Aβ binding region previously identified in our work with (-)-epigallocatechin-3-gallage (EGCG), a natural product found in green tea[29]. Many previous reports have identified EGCG as a potent inhibitor of Aβ fibril formation and toxicity[65, 66]. Our very recent work has further indicated that the main role of EGCG in inhibiting Aβ fibril formation likely relies on critical interactions with bound metal ions, such as Cu(II) and Zn(II)[29]. Like LE, we found that the EGCG binds preferentially to the cleft between the N-terminus and central helix regions of metal-free $A\beta_{1\text{-}40}$[29]. EGCG and LE bind to this region of $A\beta_{1\text{-}40}$ with similar affinities (K_d relative to Aβ monomer for both LE and EGCG are both in the μM range) in the absence of metal ions; thus, both produce relatively similar downstream effects in Aβ fibril formation once bound (Figure 2.5). EGCG has been found to improve cell viability and recover neuronal activity when Aβ is present, thus making the natural product a key target in AD drug design efforts[29, 65]. While the data presented in this report is too preliminary to make similar claims related to the potential of LE as a general scaffold or optimization target for future AD therapies, it is clear from the data presented here

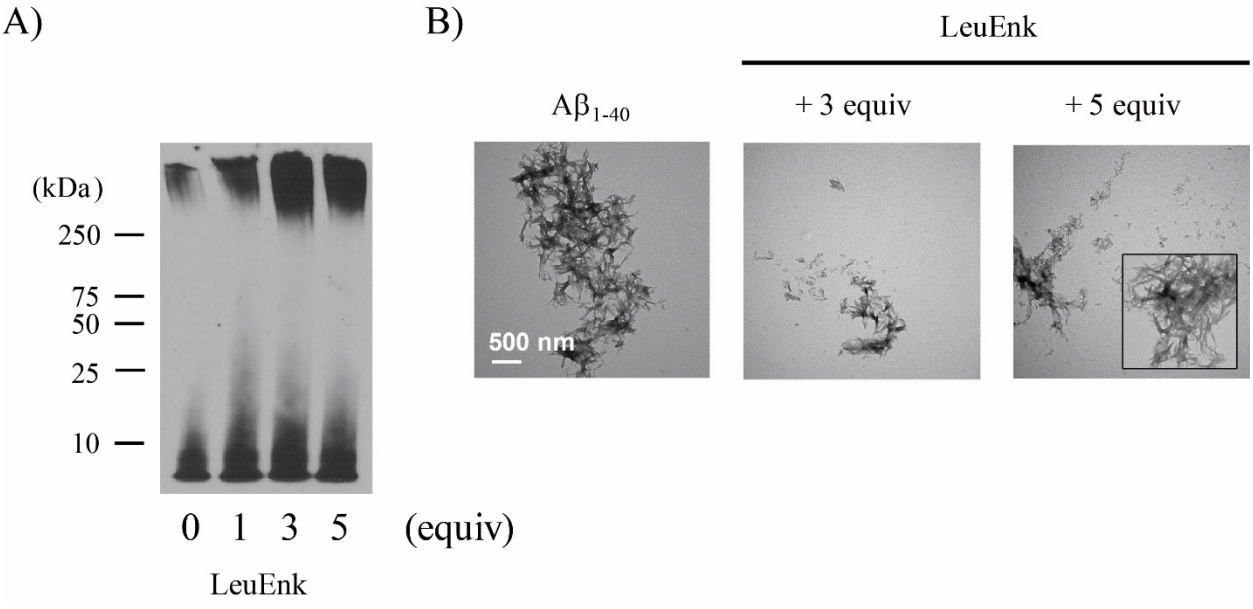

Figure 2.5 – Influence of LE on $A\beta_{1\text{-}40}$ aggregation *in vitro*. A) Visualization of Aβ species generated in the absence and presence of LE by gel electrophoresiss and Western blotting (6E10). Experimental conditions: $[A\beta_{1\text{-}40}]$ = 25 μM; [LE] = 0, 25, 75, or 125 μM; 100 mM ammonium acetate, pH 6.9; 37 °C; 24 h; agitation. B) TEM images of Aβ species in the absence and presence of LE (3 and 5 equiv.) from samples in A. The scale bar depicts 500 nm.

that the nature of the binder, as well as the binding site accessed, both play significant roles in tuning the ability of small molecules to modulate Aβ fibril formation and ameliorate disease phenotypes.

2.5. Conclusions

Here, we describe studies employing IM-MS, MD simulations, gel electrophoresis/Western blot, and TEM which determine both the presence and structure of Aβ:LE complexes, as well as their influence on Aβ oligomerization and fibril formation. In addition to LE, our IM-MS data on a limited panel of neuropeptides detected Aβ:galanin interactions, but no complexes were detected between Aβ and somatostatin, neurotensin, or substance P. The latter result is especially informative, as it indicates that previously identified neurotrophic effects for substance P relative to Aβ are likely the result of the neuropeptide interacting with larger Aβ oligomers or due to its agonist activity relative to neuronal receptor sites. Aβ:LE complexes ranging in stoichiometry from 1:1 to 2:3 are detected ion our dataset, and CCS values indicate that the complexes favor a compact configuration. A detailed IM-MS analysis of Aβ:LE complexes indicates that the small neuropeptide is likely bound in a cleft between the Aβ N-terminus and its hydrophobic core region in a manner similar to EGCG[29]. The gel/Western blot data suggest minimal change in the size distribution of the Aβ species incubated with LE, but TEM data for Aβ samples doped with LE display mainly shorter fibrils in lieu of potentially non-toxic amorphous aggregates that were observed in previous work using metal-containing Aβ samples doped with EGCG[29]. Overall, the dataset presented here generates intriguing correlations between binding affinity, binding site, and resultant fibril morphology that will likely aid in the pursuit of both small molecules and biotherapeutics for AD. Future work in our group will continue to pursue neuropeptides, including the interaction with galanin we observed in these data, as potential Aβ binders, fibril formation inhibitors, and neurotrophic agents.

2.6. Acknowledgements

Work presented here was supported by Russell Bornschein, in his aid in developing the K_d relationships shown in this work. In addition we thank Richard D. Smith (UM) and Jordan J. Clark (UM) for their aid in the MD simulations presented here. This work ws supported by funding from the NIH GM-095832 (to B.T.R), the Alfred P. Sloan Foundation and the Ruth K.

Broad Biomedical Research Foundation (to M.H.L.). M.T.S. was funded by an NIH Training Grant (T32 CA140044) and A.S.D acknowledges the National Science Foundation for a Graduate Research Fellowship.

2.7. References

[1] Brookmeyer, R., Johnson, E., Ziegler-Graham, K., and Arrighi, H. M. (2007) Forecasting the global burden of Alzheimer's disease, *Alzheimer's & dementia 3*, 186-191.

[2] Alzheimer's Association (2012) 2012 Alzheimer's disease facts and figures, *Alzheimer's & Dementia 8*, 131-168.

[3] Selkoe, D. J. (2001) Alzheimer's disease: genes, proteins, and therapy, *Physiological reviews 81*, 741-766.

[4] O'Brien, R. J., and Wong, P. C. (2011) Amyloid precursor protein processing and Alzheimer's disease, *Annual review of neuroscience 34*, 185.

[5] Harper, J. D., and Lansbury Jr, P. T. (1997) Models of amyloid seeding in Alzheimer's disease and scrapie: mechanistic truths and physiological consequences of the time-dependent solubility of amyloid proteins, *Annual review of biochemistry 66*, 385-407.

[6] Kirkitadze, M. D., Bitan, G., and Teplow, D. B. (2002) Paradigm shifts in Alzheimer's disease and other neurodegenerative disorders: the emerging role of oligomeric assemblies, *Journal of neuroscience research 69*, 567-577.

[7] Lesné, S., Koh, M. T., Kotilinek, L., Kayed, R., Glabe, C. G., Yang, A., Gallagher, M., and Ashe, K. H. (2006) A specific amyloid-β protein assembly in the brain impairs memory, *Nature 440*, 352-357.

[8] Necula, M., Kayed, R., Milton, S., and Glabe, C. G. (2007) Small molecule inhibitors of aggregation indicate that amyloid β oligomerization and fibrillization pathways are independent and distinct, *Journal of Biological Chemistry 282*, 10311-10324.

[9] Ono, K., Condron, M. M., and Teplow, D. B. (2009) Structure–neurotoxicity relationships of amyloid β-protein oligomers, *Proceedings of the National Academy of Sciences 106*, 14745-14750.

[10] Bernstein, S. L., Dupuis, N. F., Lazo, N. D., Wyttenbach, T., Condron, M. M., Bitan, G., Teplow, D. B., Shea, J.-E., Ruotolo, B. T., and Robinson, C. V. (2009) Amyloid-β protein oligomerization and the importance of tetramers and dodecamers in the aetiology of Alzheimer's disease, *Nature chemistry 1*, 326-331.

[11] Bitan, G., Fradinger, E. A., Spring, S. M., and Teplow, D. B. (2005) Neurotoxic protein oligomers—what you see is not always what you get, *Amyloid 12*, 88-95.

[12] Yamin, G., Ruchala, P., and Teplow, D. B. (2009) A peptide hairpin inhibitor of amyloid β-protein oligomerization and fibrillogenesis, *Biochemistry 48*, 11329-11331.

[13] Murray, M. M., Bernstein, S. L., Nyugen, V., Condron, M. M., Teplow, D. B., and Bowers, M. T. (2009) Amyloid β protein: Aβ40 inhibits Aβ42 oligomerization, *Journal of the American Chemical Society 131*, 6316-6317.

[14] Gessel, M. M., Wu, C., Li, H., Bitan, G., Shea, J.-E., and Bowers, M. T. (2011) Aβ (39–42) modulates Aβ oligomerization but not fibril formation, *Biochemistry 51*, 108-117.

[15] Bohrmann, B., Tjernberg, L., Kuner, P., Poli, S., Levet-Trafit, B., Näslund, J., Richards, G., Huber, W., Döbeli, H., and Nordstedt, C. (1999) Endogenous proteins controlling amyloid β-peptide polymerization possible implications for β-amyloid formation in the central nervous system and in peripheral tissues, *Journal of Biological Chemistry 274*, 15990-15995.

[16] Janusz, M., Woszczyna, M., Lisowski, M., Kubis, A., Macała, J., Gotszalk, T., and Lisowski, J. (2009) Ovine colostrum nanopeptide affects amyloid beta aggregation, *FEBS letters 583*, 190-196.

[17] Orner, B. P., Liu, L., Murphy, R. M., and Kiessling, L. L. (2006) Phage display affords peptides that modulate β-amyloid aggregation, *Journal of the American Chemical Society 128*, 11882-11889.
[18] Boado, R. J. (2008) A new generation of neurobiological drugs engineered to overcome the challenges of brain drug delivery, *Drug News Perspect 21*, 489-503.
[19] Egleton, R. D., and Davis, T. P. (1997) Bioavailability and transport of peptides and peptide drugs into the brain, *Peptides 18*, 1431-1439.
[20] Bharadwaj, P., Head, R., Martins, R., Raussens, V., Sarroukh, R., Jegasothy, H., Waddington, L., and Bennett, L. (2013) Modulation of amyloid-β 1-42 structure and toxicity by proline-rich whey peptides, *Food & function 4*, 92-103.
[21] Yankner, B. A., Duffy, L. K., and Kirschner, D. A. (1990) Neurotrophic and neurotoxic effects of amyloid beta protein: reversal by tachykinin neuropeptides, *Science 250*, 279-282.
[22] Baumketner, A., Bernstein, S. L., Wyttenbach, T., Bitan, G., Teplow, D. B., Bowers, M. T., and Shea, J. E. (2006) Amyloid β-protein monomer structure: A computational and experimental study, *Protein Science 15*, 420-428.
[23] Smith, D. P., Radford, S. E., and Ashcroft, A. E. (2010) Elongated oligomers in β2-microglobulin amyloid assembly revealed by ion mobility spectrometry-mass spectrometry, *Proceedings of the National Academy of Sciences 107*, 6794-6798.
[24] Clemmer, D. E., and Jarrold, M. F. (1997) Ion mobility measurements and their applications to clusters and biomolecules, *Journal of Mass Spectrometry 32*, 577-592.
[25] Bohrer, B. C., Merenbloom, S. I., Koeniger, S. L., Hilderbrand, A. E., and Clemmer, D. E. (2008) Biomolecule analysis by ion mobility spectrometry, *Annual review of analytical chemistry (Palo Alto, Calif.) 1*, 293.
[26] Benesch, J. L., Ruotolo, B. T., Simmons, D. A., and Robinson, C. V. (2007) Protein complexes in the gas phase: technology for structural genomics and proteomics, *Chemical reviews 107*, 3544-3567.
[27] Ruotolo, B. T., Hyung, S. J., Robinson, P. M., Giles, K., Bateman, R. H., and Robinson, C. V. (2007) Ion Mobility–Mass Spectrometry Reveals Long-Lived, Unfolded Intermediates in the Dissociation of Protein Complexes, *Angewandte Chemie International Edition 46*, 8001-8004.
[28] Borysik, A. J., Read, P., Little, D. R., Bateman, R. H., Radford, S. E., and Ashcroft, A. E. (2004) Separation of β2-microglobulin conformers by high-field asymmetric waveform ion mobility spectrometry (FAIMS) coupled to electrospray ionisation mass spectrometry, *Rapid communications in mass spectrometry 18*, 2229-2234.
[29] Hyung, S.-J., DeToma, A. S., Brender, J. R., Lee, S., Vivekanandan, S., Kochi, A., Choi, J.-S., Ramamoorthy, A., Ruotolo, B. T., and Lim, M. H. (2013) Insights into antiamyloidogenic properties of the green tea extract (−)-epigallocatechin-3-gallate toward metal-associated amyloid-β species, *Proceedings of the National Academy of Sciences 110*, 3743-3748.
[30] Duret, L., Gasteiger, E., and Perrièe, G. (1996) LALNVIEW: a graphical viewer for pairwise sequence alignments, *Computer applications in the biosciences: CABIOS 12*, 507-510.
[31] Hernández, H., and Robinson, C. V. (2007) Determining the stoichiometry and interactions of macromolecular assemblies from mass spectrometry, *Nature protocols 2*, 715-726.

[32] Bush, M. F., Hall, Z., Giles, K., Hoyes, J., Robinson, C. V., and Ruotolo, B. T. (2010) Collision cross sections of proteins and their complexes: a calibration framework and database for gas-phase structural biology, *Analytical chemistry 82*, 9557-9565.
[33] Trott, O., and Olson, A. J. (2010) AutoDock Vina: improving the speed and accuracy of docking with a new scoring function, efficient optimization, and multithreading, *Journal of computational chemistry 31*, 455-461.
[34] Vivekanandan, S., Brender, J. R., Lee, S. Y., and Ramamoorthy, A. (2011) A partially folded structure of amyloid-beta (1–40) in an aqueous environment, *Biochemical and biophysical research communications 411*, 312-316.
[35] SchuÈttelkopf, A. W., and Van Aalten, D. M. (2004) PRODRG: a tool for high-throughput crystallography of protein–ligand complexes, *Acta Crystallographica Section D: Biological Crystallography 60*, 1355-1363.
[36] Lindahl, E., Hess, B., and Van Der Spoel, D. (2001) GROMACS 3.0: a package for molecular simulation and trajectory analysis, *Journal of Molecular Modeling 7*, 306-317.
[37] van Gunsteren, W. F., Billeter, S., Eising, A., Hünenberger, P. H., Krüger, P., Mark, A. E., Scott, W., and Tironi, I. G. (1996) Biomolecular simulation: The {GROMOS96} manual and user guide.
[38] Berendsen, H. J., Postma, J. P. M., van Gunsteren, W. F., DiNola, A., and Haak, J. (1984) Molecular dynamics with coupling to an external bath, *The Journal of chemical physics 81*, 3684-3690.
[39] Mesleh, M., Hunter, J., Shvartsburg, A., Schatz, G., and Jarrold, M. (1996) Structural information from ion mobility measurements: effects of the long-range potential, *The Journal of Physical Chemistry 100*, 16082-16086.
[40] Shvartsburg, A. A., and Jarrold, M. F. (1996) An exact hard-spheres scattering model for the mobilities of polyatomic ions, *Chemical Physics Letters 261*, 86-91.
[41] Wang, W., Kitova, E. N., and Klassen, J. S. (2003) Influence of solution and gas phase processes on protein-carbohydrate binding affinities determined by nanoelectrospray Fourier transform ion cyclotron resonance mass spectrometry, *Analytical chemistry 75*, 4945-4955.
[42] Mancino, A. M., Hindo, S. S., Kochi, A., and Lim, M. H. (2009) Effects of clioquinol on metal-triggered amyloid-β aggregation revisited, *Inorganic chemistry 48*, 9596-9598.
[43] Hindo, S. S., Mancino, A. M., Braymer, J. J., Liu, Y., Vivekanandan, S., Ramamoorthy, A., and Lim, M. H. (2009) Small molecule modulators of copper-induced Aβ aggregation, *Journal of the American Chemical Society 131*, 16663-16665.
[44] Choi, J.-S., Braymer, J. J., Nanga, R. P., Ramamoorthy, A., and Lim, M. H. (2010) Design of small molecules that target metal-Aβ species and regulate metal-induced Aβ aggregation and neurotoxicity, *Proceedings of the National Academy of Sciences 107*, 21990-21995.
[45] Choi, J.-S., Braymer, J. J., Park, S. K., Mustafa, S., Chae, J., and Lim, M. H. (2011) Synthesis and characterization of IMPY derivatives that regulate metal-induced amyloid-β aggregation, *Metallomics 3*, 284-291.
[46] DeToma, A. S., Choi, J. S., Braymer, J. J., and Lim, M. H. (2011) Myricetin: a naturally occurring regulator of metal-induced amyloid-β aggregation and neurotoxicity, *ChemBioChem 12*, 1198-1201.
[47] Braymer, J. J., Choi, J.-S., DeToma, A. S., Wang, C., Nam, K., Kampf, J. W., Ramamoorthy, A., and Lim, M. H. (2011) Development of bifunctional stilbene

derivatives for targeting and modulating metal-amyloid-β species, *Inorganic chemistry 50*, 10724-10734.
[48] He, X., Park, H. M., Hyung, S.-J., DeToma, A. S., Kim, C., Ruotolo, B. T., and Lim, M. H. (2012) Exploring the reactivity of flavonoid compounds with metal-associated amyloid-β species, *Dalton Transactions 41*, 6558-6566.
[49] Pithadia, A. S., Kochi, A., Soper, M. T., Beck, M. W., Liu, Y., Lee, S., DeToma, A. S., Ruotolo, B. T., and Lim, M. H. (2012) Reactivity of diphenylpropynone derivatives toward metal-associated amyloid-β species, *Inorganic chemistry 51*, 12959-12967.
[50] Kowall, N. W., Beal, M. F., Busciglio, J., Duffy, L. K., and Yankner, B. A. (1991) An in vivo model for the neurodegenerative effects of beta amyloid and protection by substance P, *Proceedings of the National Academy of Sciences 88*, 7247-7251.
[51] Counts, S., Perez, S., and Mufson, E. (2008) Galanin in Alzheimer's disease: Neuroinhibitory or neuroprotective?, *Cellular and molecular life sciences: CMLS 65*, 1842.
[52] Swaab, D. (1982) Neuropeptides. their distribution and function in the brain, *Progress in brain research 55*, 97.
[53] Kitova, E. N., El-Hawiet, A., Schnier, P. D., and Klassen, J. S. (2012) Reliable determinations of protein–ligand interactions by direct ESI-MS measurements. Are we there yet?, *Journal of the American Society for Mass Spectrometry 23*, 431-441.
[54] Zhong, Y., Hyung, S.-J., and Ruotolo, B. T. (2012) Ion mobility–mass spectrometry for structural proteomics, *Expert review of proteomics 9*, 47-58.
[55] Teplow, D. B., Lazo, N. D., Bitan, G., Bernstein, S., Wyttenbach, T., Bowers, M. T., Baumketner, A., Shea, J.-E., Urbanc, B., and Cruz, L. (2006) Elucidating amyloid β-protein folding and assembly: a multidisciplinary approach, *Accounts of chemical research 39*, 635-645.
[56] Ruotolo, B. T., Benesch, J. L., Sandercock, A. M., Hyung, S.-J., and Robinson, C. V. (2008) Ion mobility–mass spectrometry analysis of large protein complexes, *Nature Protocols 3*, 1139-1152.
[57] McLean, J. A., Ruotolo, B. T., Gillig, K. J., and Russell, D. H. (2005) Ion mobility–mass spectrometry: a new paradigm for proteomics, *International Journal of Mass Spectrometry 240*, 301-315.
[58] Mertens, H. D., and Svergun, D. I. (2010) Structural characterization of proteins and complexes using small-angle X-ray solution scattering, *Journal of structural biology 172*, 128-141.
[59] Irvine, G. (1997) Size-exclusion high-performance liquid chromatography of peptides: a review, *Analytica chimica acta 352*, 387-397.
[60] Lebowitz, J., Lewis, M. S., and Schuck, P. (2002) Modern analytical ultracentrifugation in protein science: a tutorial review, *Protein Science 11*, 2067-2079.
[61] Bonvin, A. M., Boelens, R., and Kaptein, R. (2005) NMR analysis of protein interactions, *Current opinion in chemical biology 9*, 501-508.
[62] Ruotolo, B. T., Gillig, K. J., Stone, E. G., and Russell, D. H. (2002) Peak capacity of ion mobility mass spectrometry:: Separation of peptides in helium buffer gas, *Journal of Chromatography B 782*, 385-392.
[63] Suzuki, Y., Brender, J. R., Hartman, K., Ramamoorthy, A., and Marsh, E. N. G. (2012) Alternative pathways of human islet amyloid polypeptide aggregation distinguished by

19F nuclear magnetic resonance-detected kinetics of monomer consumption, *Biochemistry 51*, 8154-8162.
[64] Hudson, S. A., Ecroyd, H., Kee, T. W., and Carver, J. A. (2009) The thioflavin T fluorescence assay for amyloid fibril detection can be biased by the presence of exogenous compounds, *Febs Journal 276*, 5960-5972.
[65] Choi, Y.-T., Jung, C.-H., Lee, S.-R., Bae, J.-H., Baek, W.-K., Suh, M.-H., Park, J., Park, C.-W., and Suh, S.-I. (2001) The green tea polyphenol (−)-epigallocatechin gallate attenuates β-amyloid-induced neurotoxicity in cultured hippocampal neurons, *Life sciences 70*, 603-614.
[66] Bieschke, J., Russ, J., Friedrich, R. P., Ehrnhoefer, D. E., Wobst, H., Neugebauer, K., and Wanker, E. E. (2010) EGCG remodels mature α-synuclein and amyloid-β fibrils and reduces cellular toxicity, *Proceedings of the National Academy of Sciences 107*, 7710-7715.

Chapter 3.

Ion Mobility-Mass Spectrometry Reveals a Dipeptide That Acts as a Molecular Chaperone for Amyloid β

Previously, we discovered and structurally-characterized an Amyloid β_{1-40} ($A\beta_{1-40}$): leucine enkephalin (LE, YGGFL) complex. This work identified LE as a potentially-useful starting point for the discovery of peptide-related biotherapeutics for Alzheimer's Disease (AD). In order to better understand LE:Aβ complexes that are formed *in vitro*, we describe here the analysis of a series of site directed amino acid substitution variant versions of LE and Aβ, covering the LE sequence in its entirety, as well as a large number of selected residues of $A\beta_{1-40}$ (residues: D1, E3, F4, R5, H6, Y10, E11, H13, H14, Q15, K16, E22, K28, and V40). Ion mobility- mass spectrometry (IM-MS) and molecular dynamics (MD) simulations reveal that the hydrophobic C-terminus of LE (residues FL) is crucial for the formation of Aβ:LE. As such we explore here the interaction of the dipeptide phenylalanine-leucine (FL) with wild both type (WT) and variant forms of Aβ using IM-MS, MD, Transmission Electron Microscopy (TEM) and circular dichroism (CD) spectroscopy in order to structurally characterize Aβ:FL. We find that FL binds within the region between the N-terminus and the hydrophobic core, most specifically at residue Y10 and Q15. We further show that FL is able to prevent Aβ fibril formation, thus providing another step toward the discovery of a potent AD therapeutic.

3.1 Introduction

The utility of IM-MS as a tool for drug development, especially in the context of protein misfolding diseases such as Alzheimer's Disease (AD) and Type II Diabetes, has recently emerged[1-10]. While many hypotheses surrounding the causation of AD are proposed, a prominent theory is that the uncontrolled aggregation of Aβ peptides, which form small toxic oligomers

(dimer to dodecamer) leads ultimately to neuronal cell death[11-15]. As Aβ aggregation allows for many oligomeric states simultaneously, studying Aβ oligomers for the purposes of drug discovery is difficult with classical biophysics and structural biology techniques[16]. IM-MS allows for the use of low concentrations, small sample volumes, and separates protein oligomers based on mass and collision cross section (CCS)[17-19] making it an ideal technology for the analysis of Aβ-small molecule complexes .

We previously reported on a set of experiments that identified Aβ-Neuropeptide complexes , and having the ultimate goal of identifying a peptide, or peptide fragment, which might inhibit Aβ fibril formation and provide a scaffold for future potential biotherapeutics[20]. In these data, we found evidence of interactions between $A\beta_{1-40}$ and both leucine enkephalin (LE) and galanin. We characterized the former in detail, providing CCSs, binding affinities (K_d), and molecular dynamics (MD) simulations. In addition, we studied the ability of LE to inhibit Aβ fibril formation using both TEM and gel electrophoresis. Complexes containing Aβ and LE were detected in stoichiometric ratios ranging from 1:1 to 1:3, and from 2:1 to 2:3 Aβ:LE. At increased concentrations of LE, our data indicated that attachment to Aβ dimers is favored over binding to the monomeric form. K_d values were measured in the μM range for these complexes, and molecular dynamics (MD) led the determination of the likely binding location of LE, along the N-terminus of the Aβ sequence, similar to other natural products[5]. TEM and gel data reported a truncation of Aβ fibrils and an increased amount of lower molecular weight Aβ oligomers when incubated in excess with LE, compared with control.

Here we report on IM-MS measurements of complexes formed between Aβ and the site directed amino acid substitutions of the entire sequence of LE, which indicate that the hydrophobic C-terminal residues (phenylalanine and leucine) are critical for the formation of Aβ:LE interactions. Furthermore, we study the dipeptide phenylalanine-leucine (FL) and its complexes formed with Aβ sequence variants. For 1:1 Aβ:FL complexes, we identify residues Y10 and Q15 as possessing key interactions with FL, necessary for strong complex formation. This observation matches well with the predicted location of FL binding from MD simulations of Aβ:LE[20]. MD simulations of Aβ:FL were conducted and models filtered using IM-MS data. From these, we predict FL interacts with Aβ primarily through Y10, and that these interactions occur mostly through a series of specific interactions with the C-terminal residue of FL.

Importantly, FL interacts more strongly with Aβ dimers, and Aβ:FL complexes containing the more pathogenic $A\beta_{1-42}$, appear to bind in a similar mode to that of $A\beta_{1-40}$:FL. Finally, we use TEM analysis to study Aβ fibril formation in the presence of FL, finding strong evidence of the inhibition of fibrilization. We conclude by discussing the potential impact of FL as a scaffold for the future development of AD therapies.

3.2 Experimental

3.2.1 General

Reagents were purchased from commercial sources and used without further purification unless otherwise specified. $A\beta_{1-40}$ was purchased from Anaspec (Fremont, CA, USA). Alanine mutations were custom synthesized and received at a purity of at least 95% (GenScript,). Aβ variants (1 mg) were dissolved in 200 µL 1% (v/v) ammonium hydroxide and diluted with pH 6.9 100 mM ammonium acetate (Sigma-Aldrich, St. Louis, MO, USA) to a total volume of 1500 µL. Peptides were then injected into a Slide-A-Lyzer Dialysis Cassette (2K MWCO, 3 mL volume, Thermo Scientific). 100mM ammonium acetate was added to fill volume of cassette capacity, and dialysis was performed over a 24 h period. Samples were then removed from the cassette, flash frozen with liquid nitrogen and lyophilized overnight. Peptides were reconstituted using 200 µL 1% (v/v) ammonium hydroxide and diluted with pH 6.9 100 mM ammonium acetate to a total volume of 1500 µL. Peptide concentration for the stock solution was calculated from absorbance at 280nm (ε = 1490 M^{-1} cm^{-1}). Peptides were aliquoted and stored at -80 °C. LE acetate hydrate (YGGFL) was purchased from Sigma-Aldrich (St. Louis, MO, USA) and prepared in pH 6.9 100mM ammonium acetate. FL was synthesized by AnaSpec, and prepared in dimethylsulfoxide (Sigma-Aldrich, St. Louis, MO).

3.2.2. IM-MS

Mass spectra were collected on a quadrupole-ion mobility-time-of-flight (TOF) mass spectrometer (Synapt G1 HDMS, Waters, Milford, MA, USA) with a nano-electrospray ionization (nESI) source. Protein ions were generated using a nESI source and optimized to allow transmission of noncovalent protein complexes using electrospray capillaries prepared as described previously[21]. Protein complex ions were generated using an aliquot of the sample (*ca.* 7 µL) sprayed from the nESI emitter at a capillary voltage of 1.2kV. The source was operated in

positive ion mode with the sample cone at 35 V and extraction cone at 1.0V. The bias voltage was 21 V, with backing pressure at 2.32 mbar and TOF pressure at 1.81 x 10^{-6} mbar. The travelling-wave IM separator was operated at a pressure of approximately 3.0 mbar of nitrogen. Mass spectra were calibrated externally using a solution of cesium iodide (100 mg mL^{-1}) and analyzed using MassLynx 4.1 and Driftscope 2.0 software (Waters, Milford, MA, USA). CCS (Ω) measurements were externally calibrated using a database of known values in helium, using values for peptides and proteins that bracket the likely CCS and ion mobility values of the unknown ions[22, 23]. Samples were prepared by mixing stock solutions (as prepared above) of neuropeptide and $A\beta_{1-40}$ variants at pH 6.9, to generate a final $A\beta_{1-40}$ concentration of 20 µM, with 2.88% v/v DMSO present in all samples. Samples were incubated on ice for 1 h prior to IM-MS analysis.

3.2.3. Docking Studies

Flexible ligand docking studies were preformed using AutoDock Vina[24]. FL was created using PyMOL and studies were conducted against the $A\beta_{1-40}$ monomer (aqueous solution NMR structure PDB 2LFM)[25] and $A\beta_{1-42}$ (aqueous solution NMR structure PDB 1Z0Q)[26]. Twenty docking studies with $A\beta_{1-40}$ and thirty docking studies with $A\beta_{1-42}$, one with each conformation within the PDB files, were performed. The structures for FL and Aβ were prepared for use with AutoDock vina using AutoDock Tools[24]. All hydrogens were added to Aβ and torsions were kept as the default selected in AutoDock Tools. The exhaustiveness for the docking studies was set at 8, resulting in 9 output models for each Aβ conformation. Docked models of FL were visualized with Aβ using PyMOL.

3.2.4. MD Simulations

Simulations were started using the minimized Aβ solution NMR structures (PDB 2LFM or PDB 1Z0Q)[25, 26]. Charges were applied to R5, K16, and K28 to mimic the 3+ charge state observed in the gas phase. The simulations were performed using periodic boundary conditions in a dodecahedron with the minimum distance between the simulated molecules and the box wall being 1.0 nm. GROMACS ligand topology was prepared using the GlycoBioChem PRODRG2 server[27]. The MD simulations were carried out using the GROMACS software package[28] and GROMOS96 force field[29]. To constrain the bond length in the Aβ and FL, the LINCS algorithm was used, allowing an integration time step of 2 fs. Long-range electrostatic interactions were

treated with the particle mesh Ewald method. Temperature was maintained using the method of Berendsen *et al*[30]. The FL and the Aβ were separately coupled to external temperature bath with a temperature-coupling constant of 0.1 ps.

The system was energy-minimized by steepest decent for 500 steps. After equilibration, simulated annealing was performed for the Aβ: FL complex in the gas-phase. The three most basic Aβ side chains (R5, K16, and K28) were charged. The system was heated from 300 K to 500 K over 100 ps, then cooled down to 300 K over the next 100 ps. The cycle was repeated over 20 ns in order to allow for escape from local minima and enhance equilibration. For the $A\beta_{1-40}$: FL complex, 20 independent simulated annealing runs, each running for a total of 20 ns, were performed from the lowest energy complexes generated by AutoDock Vina. For the $A\beta_{1-42}$: FL complex, 30 independent simulated annealing runs, each running for a total of 20 ns, were performed from the lowest energy complexes generated by AutoDock Vina. From the MD trajectory generated, 100 structures were sampled at 300 K and the CCS was calculated with Mobcal using the trajectory method algorithm[31, 32]. Models of the Aβ:FL complexes were visualized in PyMOL. In total 2000 structures were generated for $A\beta_{1-40}$ and 3000 structures for $A\beta_{1-42}$. Of the structures which were within ± 3% of the experimentally determined CCS, the 200 structures with lowest energy were analyzed to determine the Aβ residues within 4 Å of FL. Standardized values (Z-scores) were calculated for each residue of $A\beta_{1-40}$ and $A\beta_{1-42}$ and plotted in standard deviation (σ) space in order to determine the relative likelihood of FL binding within a given region of Aβ.

3.2.5. Hierarchical Clustering Analysis

Structures of $A\beta_{1-40}$:FL, following MD simulations, which were within ± 3% of the experimental CCS, and which matched site directed amino acid substitution experiments (FL was within 4 Å of Aβ residue Y10 and Q15). This reduced the set of possible structures from 963 to 60. We then characterized the structural families present in the dataset using hierarchical clustering. Aβ candidate structures were temporarily stripped of their ligands while being aligned using the Kabsch algorithm[33], and pairwise RMSD values were calculated for each structure in the dataset. These pairwise RMSD values were then used as a distance matrix for hierarchical clustering using the average linkage clustering module from Scipy[34]. Intra and inter-cluster RMSD values were analyzed and it was found that the dataset could reasonably be broken into 5 clusters,

allowing for facile interpretation of the dataset. For each structural cluster, and average structure was calculated to represent the structural family, and all ligands were then superimposed on the representative structure, revealing strong structure-specific ligand clustering, in addition to an averaged ligand location. Structures were visualized in PyMOL.

3.2.6 K_d Measurements by MS

Dissociation constant (K_d) values for the neuropeptides with $A\beta_{1\text{-}40}$ were calculated using the relative intensity of each species from the mass spectra, as described previously[35]. Previously[20], we modified this method to accommodate multiple ligand binding events with the following assumptions: (1) the spray and detection efficiency of all species are similar, (2) the ligand concentration is sufficiently high so that $[L]_{eq}$ remains constant and (3) the ligand binds to the complex one at a time in a stepwise fashion. Here we present further modification to better represent multiple ligand binding stoichiometry.

For the equilibrium binding of A (unbound protein) and B (a ligand/binding partner):

$$A + B \leftrightarrow C_1 + C_2 + \cdots + C_x \quad (3.1)$$

$$R_x = \frac{[C_x]_{eq}}{[A]_{eq}} \quad (3.2)$$

Where R_x is an equilibrium quotient between the bound form of the protein (C_x, having x ligands attached) when interacting with ligand B, and is unbound for (A).

$$[C_x]_{eq} = \frac{R_x([A]_0 - (\sum_{i=1}^{x-1} y[C_i]_{eq}))}{1 + yR_x} \quad (3.3)$$

Eqn (3.3) above defines R_x for all bound forms of the protein (C_i), where y is the number of species A in the complex and:

$$K_{d_x} = \frac{[C_{(x-1)}]_{eq}[B]_{eq}}{[C_x]_{eq}} \quad (3.4)$$

Allows for the determination of K_d for any given step in the sequential equilibrium described in eqn (3.1), where C_0 = A. Standard deviation values (σ) for the K_d measurements reported here are shown from three replicate measurements.

3.2.7 TEM

Negatively stained specimens for transmission electron microscopy were prepared by applying 5 μL of peptide solution to hydrophilic 400 mesh carbon-coated formvar support films mounted on copper grids (Ted Pella, Inc.). The samples were allowed to adhere for 3 min, rinsed twice with distilled water, and stained for 60-90 s with 1% uranyl acetate (Ted Pella, Inc.). All samples were imaged at an accelerating voltage of 60 kV in a CM-100 electron microscope (Philips, Inc.). Samples were prepared in 100 mM ammonium acetate, with 2.88% DMSO at a concentration of 25 μM Aβ and allowed to incubate at room temperature for 24 h.

3.3 Results and Discussion

As a follow up to our previous work investigating the detailed structures of LE:Aβ complexes,[20] we undertook a series of IM-MS experiments using a comprehensive set of site-directed amino acid substituted forms of LE (YGGFL). Each of these five LE variants was first evaluated using MS intensity values under controlled conditions as a quantitative measure of $A\beta_{1\text{-}40}$ complex formation. (Figure 3.1A). Substitution of the first three residues in the LE sequence (tyrosine and both glycine residues) yield complex ion signals similar to control experiments under our experimental conditions. However, when the two hydrophobic C-terminal residues (phenylalanine and leucine) were substituted, neither of these variants are observed to generate signals associated with complex formation, indicating their importance in Aβ:LE binding overall.

Using the information provided by Figure 3.1A, we filtered our previous model structures for the Aβ:LE complex[20], resulting in a refined population of models where Aβ constituents are within 4 Å of either the phe or leu residues of LE. This newly-refined model population was used to calculate standardized probability values for each residue of $A\beta_{1\text{-}40}$ in terms of their phe or leu contacts. This analysis highlights several regions of importance, which are shown in Figures 3.1B and C, where a standard score greater than 1 indicates an increased significance of the contact observed between the indicated Aβ residue and either the phe or leu on LE, respectively. $A\beta_{1\text{-}40}$ residues which most frequently interact with phe are Y10, H14, Q15, K16, E22 and D23, and those interacting most frequently with leu are R5, Y10, E11, H14, Q16, K16, and K28. Those interacting significantly with both residues are Y10, H14, Q15, K16. This analysis agrees overall with our previous models of Aβ:LE complexes, from which we concluded that LE binding likely occurs in the N-terminal/ hydrophobic core region of Aβ, similar behavior to other natural products[5, 20]. As such R5, Y10, E11, H14, Q15, K16, E22, and K28 alanine substitution

variants of Aβ were targeted for downstream experiments. Of the remaining alanine variants, D1A and V40A, as terminal ends were assumed to be negative controls. H6A and H13A were selected as a control for H14A while E3 serves as a control for E11A and E22A. Each of these to ensure if K_d had changed it was due to a specific location of the residue, not just the side chain

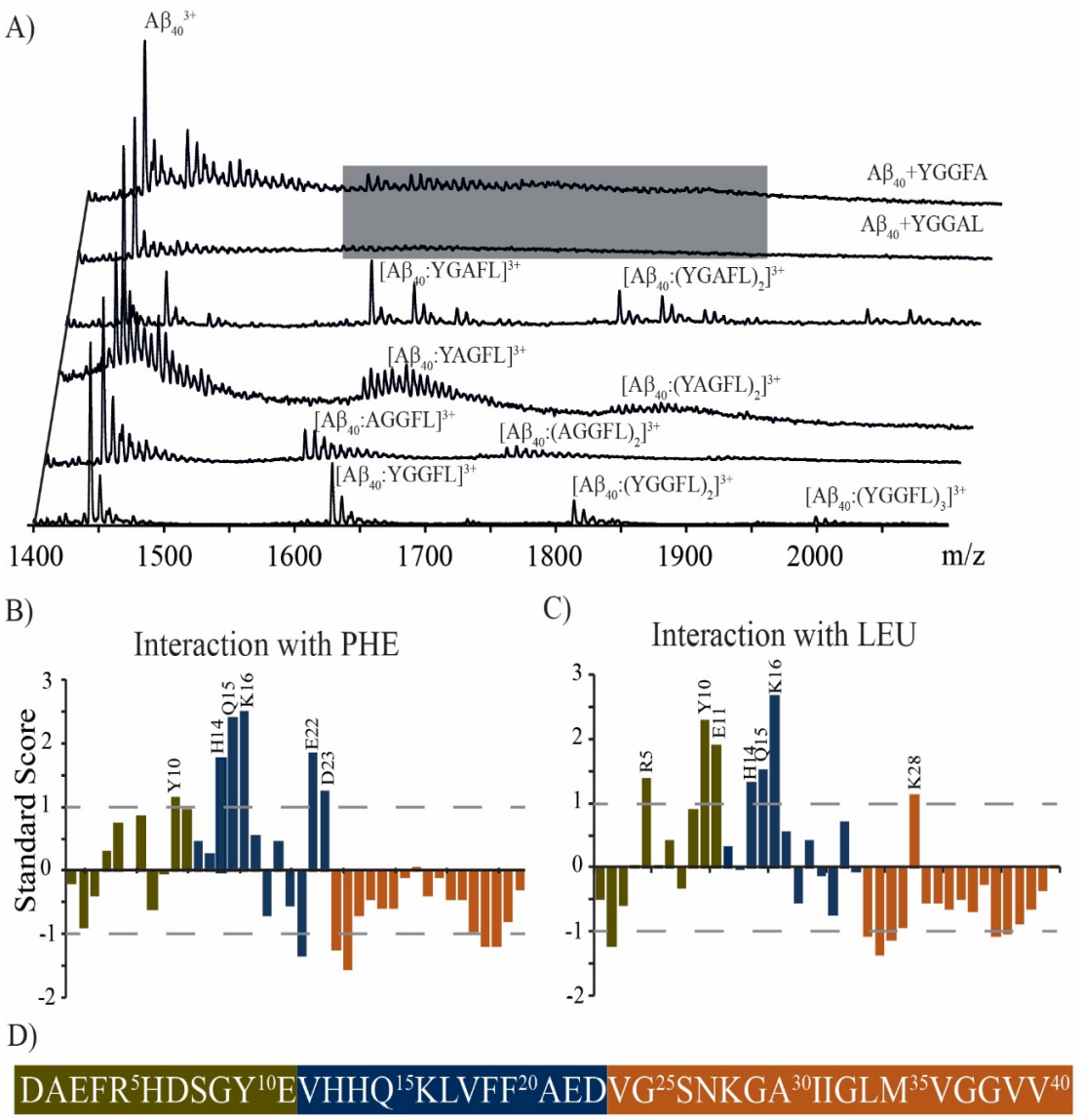

Figure 3.1 – Interactions between $A\beta_{1\text{-}40}$ and LE variants. A) IM-MS analysis of alanine substituted variants of LE reveals complexes formed between $A\beta_{1\text{-}40}$ and AGGFL, YAGFL, and YGAFL in a manner similar to WT LE. On the other hand, samples containing YGGAL and YGGFL produce no measureable complex signals, indicating phe and leu to be critical for the interaction with Aβ. B and C) Plots of the standard score (Z-score) for Aβ residues that are within 4Å of the phe and leu in LE. D) Sequence of $A\beta_{1\text{-}40}$, where the N-terminus (green) is defined as residues 1-11, the hydrophobic core (blue) is residues 12-23, and the C-terminus is residues 24-40. This color-coding for $A\beta_{1\text{-}40}$ applies to all figures.

composition. The control F4A, has been suspected in interactions with other potential AD therapeutics[6], and so was tested here.

As our data strongly indicates that it is primarily the hydrophobic C-terminus of LE that is responsible for its binding to Aβ, we moved to focus our experimental efforts on the dipeptide phenylalanine-leucine (FL). IM-MS data acquired from solutions continuing 20 µM $A\beta_{1\text{-}40}$ and FL ranging from 10 – 80 µM, reveals the formation of $A\beta_{1\text{-}40}$:FL complexes in ratios of 1:1- 1:4, 2:1- 2:5, 3:1- 3:4, and 4:1 (Figure 3.2A). Companion MD simulations of $A\beta_{1\text{-}40}$: FL complexes yields significant interactions between the dipeptide and R5, Y10, K16, D23, S26, N27, and K28 from the Aβ sequence. This result agrees in part with our analysis of $A\beta_{1\text{-}40}$:LE models discussed above, which predicted R5, Y10, K16, D23, and K28 as likely FL binding sites. While $A\beta_{1\text{-}40}$ is found in greater quantities *in vivo*, $A\beta_{1\text{-}42}$ is theorized to be the more pathogenic variant and aggregates more rapidly, making it more difficult to study *in vitro*. IM-MS data shown in Figure

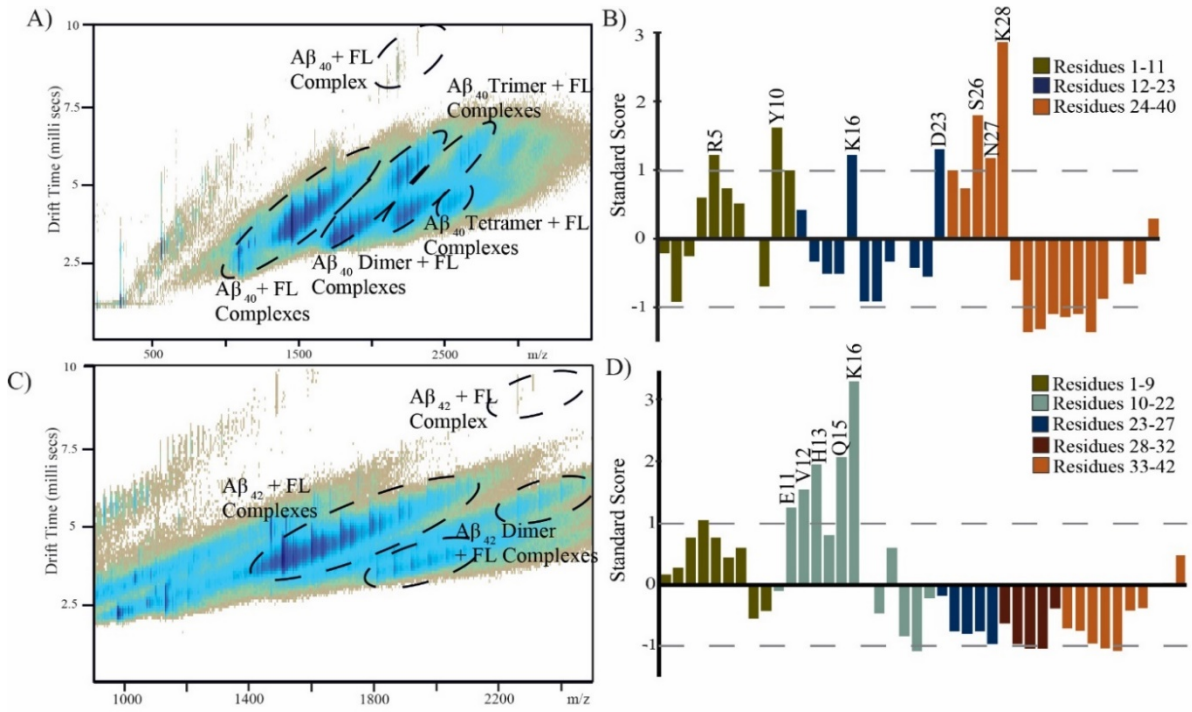

Figure 3.2 – Interaction between Aβ with the dipeptide FL. A) IM-MS data shows the presence of $A\beta_{1\text{-}40}$ in complex with FL as a monomer, dimer, trimer, and tetramer at 20 µM Aβ: 60 µM FL. Multiple copies of FL attach to each oligomer under these concentrations, while at lower FL concentrations (10 and 20 µM) only 1:1 complexes are observed. B and D) Plots of the standard score (Z-score) for Aβ residues within 4Å of the bound FL. Larger values denote contacts of greater significance on the standard deviation (σ) scale. Negative values denote contacts of reduced significance. C) IM-MS data shows the presence of $A\beta_{1\text{-}42}$ in complex with FL as both monomer and dimer, with up to 4 copies of FL binding to each oligomer at 20 µM Aβ: 60 µM FL. As with $A\beta_{1\text{-}40}$, with lower concentrations of FL, fewer FL copies are bound.

3.2C indicates that $A\beta_{1-42}$ binds FL, exhibiting K_d and complex stoichiometry values similar to that of $A\beta_{1-40}$. Low energy models generated for $A\beta_{1-42}$: FL complexes exhibit a strong preference toward binding within the hydrophobic core of $A\beta_{1-42}$, specifically with residues E11, V12, H13, Q15, and K16, an observation that is generally retained from our $A\beta_{1-40}$ MD and experimental data as well.

To more-clearly elucidate the binding location of FL within the $A\beta_{1-40}$ sequence, K_d values were extracted from the MS data acquired for all alanine substituted Aβ variants listed above, in addition to control variants: D1A, E3A, F4A, H6A, H13A, and V40A. All control residues represent regions of the Aβ sequence that MD IM-MS-filtered models did not highlight as critical for LE binding. Of the fourteen alanine variants, only three produced K_d values significantly greater than those recorded for the WT $A\beta_{1-40}$:FL 1:1 complex (K_d = 58.1 ± 25.9 μM). These variants include Y10A, Q15A, and E22A (K_d = 135 ± 71.3 μM, 126 ± 86.6 μM, 112 ± 53 μM respectively). Neighboring variants E11A, H14A and K16A do not deviate significantly from WT. In fact the mutations R5A, K16A, and K28A all fall within error of the WT value, demonstrating the lysine and arginine residues of Aβ have no impact on FL binding. Of the control cases, D1A, E3A and H13A behaved similarly to the WT as expected. The 1:1 complex of F4A:FL was only observed twice in seven samples, one at low concentration of FL and one at high, measured K_d, was averaged to 117 μM, but without a standard deviation. $A\beta_{1-40}$ F4A which was detected outside of the complex was heavily adducted with non-volatile salts, calling to question their effect on the binding events. In contrast to those which were within error of the WT, two variants, H6A and V40A, produced significantly reduced K_d values relative to WT, 27.5 ± 14.8 μM and 17.2 ± 8.5 μM respectively. Taken together, these data indicate that residues Y10, Q15, and E22 likely provide key molecular contacts that stabilize the $A\beta_{1-40}$:FL complex, while H6 and V40 provide a destabilizing or screening effect that, when removed, improves the strength of the resulting complex significantly. In order to validate the structures of the variant forms of $A\beta_{1-40}$ are not significantly altered from that of the WT sequence, CD spectroscopy data was acquired for all alanine variants and WT Aβ peptides (data shown in appendix II). While Y10A and Q15A peptides have CD signatures similar to that of $A\beta_{1-40}$, the CD spectrum acquired for E22A exhibits a pronounced β-sheet structure similar to that of $A\beta_{1-42}$. The known familial mutation E22G (Arctic mutation) of $A\beta_{1-40}$ has shown an increased propensity for aggregation and behavior mimicking $A\beta_{1-42}$[36]. The alanine variant E22A differs

from this mutation by only a methyl group and was suspected to mimic E22G structurally, making the CD results unsurprising. As such, CD data supports an analysis of our IM-MS K_d data interpreted on the basis of only the altered molecular contacts within the FL:Aβ binding surface for Y10A and Q15A, but strongly suggests that E22A K_d data is a product of both altered

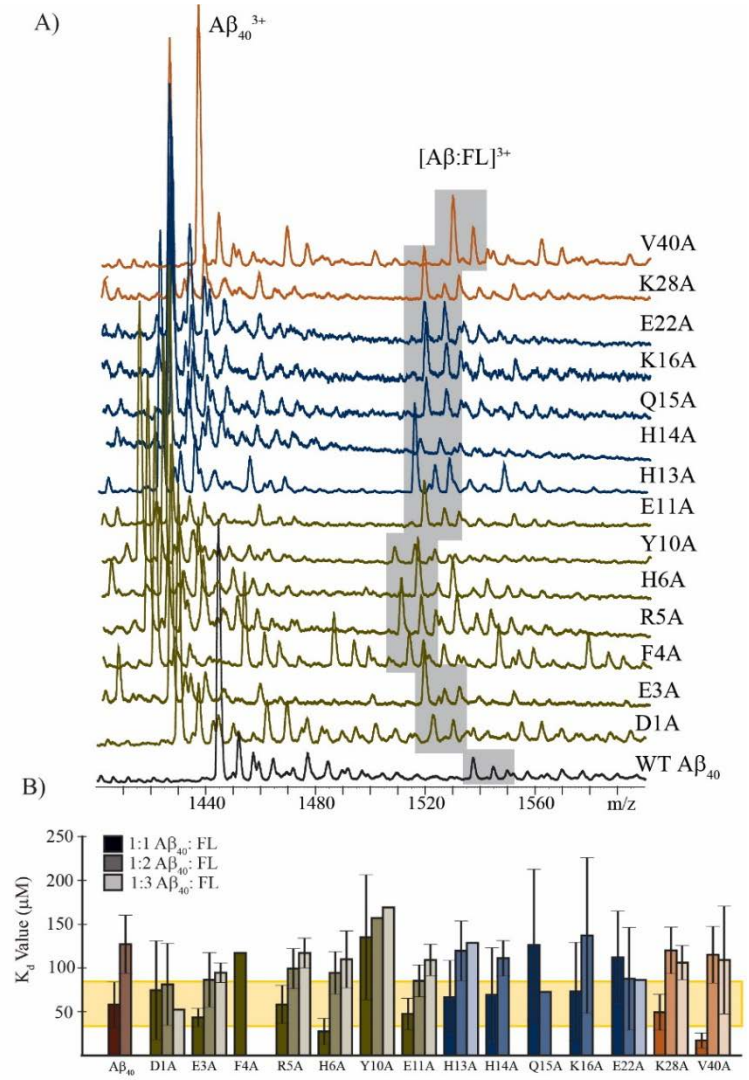

Figure 3.3 – Site directed amino acid substitution effects on FL biding. A) Shown is a representative spectra of 20 μM $A\beta_{1\text{-}40}$ variant incubated with 80 μM FL for 1 h on ice. The grey boxed region indicates the 1:1 complex detected at a 3+ charge state. Signal for the 1:1 complexes of Y10A: FL and Q15A: FL show decreases in intensity when compared to the WT interaction. B) K_d values calculated for each amino acid substitution. Error bars indicate 1 standard deviation (σ). WT interaction is shown in red. The yellow bar is ±1(σ) of the 1:1 complex. The 1:1 interactions are shown as the darkest shade, 1:2 in medium shade, and 1:3 as the lightest. Of the 1:1 interactions only Y10A, Q15A, and E22A are above 1 σ different than the WT. All 1:2 interactions fell within standard deviation of the WT 1:2 interaction and a WT 1:3 interaction could not be measured in triplicate

peptide conformation and available FL interactors within the Aβ sequence. Multiple FL binding events to Aβ (1:2 and 1:3 Aβ:FL) yielded weaker K_d values than that of the 1:1 interaction for all variants where 1:2 or 1:3 complexes were detected. Additionally all measurements of the 1:2 complex were within error of each other, indicating no strong preferences in higher-order FL binding among those tested here. K_d values for alanine variants with LE, as well as values acquired for higher order Aβ:LE complexes, are available with discussion in appendix II.

To evaluate the ability of FL to alter Aβ fibril formation, TEM images were acquired for $A\beta_{1\text{-}40}$ samples containing FL. For example, the features observed in the TEM data shown in Figure 3.4 have a marked dependence upon FL concentration, with long mature fibril structures observed for Aβ samples where no FL is added, to truncated fibril structures in samples where equimolar FL is added, and a complete abrogation of Aβ fibril formation when excess FL is present. Truncated fibrils observed by TEM upon equimolar FL addition to Aβ samples are less dense when compared to control samples, further indicating that mature fibril formation is weakly inhibited under these conditions. The weakly-stained forms observed under conditions of FL excess appear universally amorphous, indicating that while Aβ aggregation still occurs, it likely does so through an altered route that may not produce toxic species, which have been observed in previous studies[37].

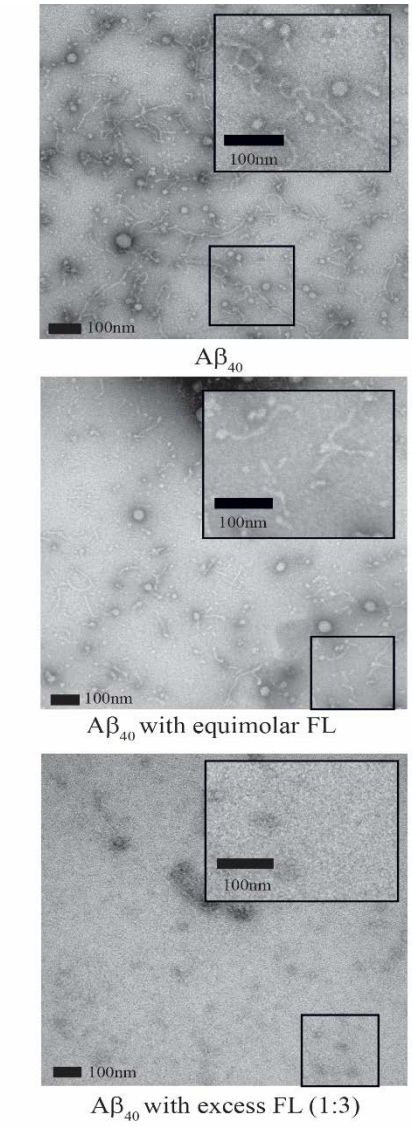

Figure 3.4 – TEM images of $A\beta_{1\text{-}40}$ incubated with equimolar or excess FL (as labeled), displaying reduced fibril formation upon FL addition.

Using all the data described above, we filtered the output of MD simulations to produce a range of models that describe the molecular details of the $A\beta_{1\text{-}40}$:FL complexes observed in our experiments. Our workflow begins by filtering all models that have CCS values outside of our experimental error (652.6 ± 22.1 Å^2 for the $A\beta_{1\text{-}40}$:FL complex). Next, we remove all models that lack clear interactions (contact within 4 Å) between FL and Y10 and Q15, which our experimental data

suggest are key elements for the efficient formation of a stable $A\beta_{1-40}$:FL complex. Hierarchical clustering of this filtered model pool yields five structural families. Figure 3.5A shows the output of our clustering algorithm, along with low-resolution averaged peptide structures that depict an averaged location for FL binding on the Aβ surface. In most, FL is cradled between the N-terminus and the hydrophobic core while the c-terminus is further away. In two of the families however, the FL appears to be closer to C-terminal residues. In families where FL is closer to the C-terminal, the structural average appears to be more compact. A detailed, manual analysis of these five structural families reveals common themes in the molecular contacts created between FL and the Q15 residue within the Aβ sequence. Three examples of these details are shown in Figure 3.6, where we highlight bonding of FL and Aβ residue Q15. A bond distance of 2.8 Å between one oxygen of leucine and NE2 of Q15 is observed in the lowest energy structure matching our experimental restraints (Figure 3.6A). The ligand boding is stabilized by R5, H6, and D7 with hydrogen bonding distances of 3.1 Å and 3.2 Å between R5 and D7 with the oxygen of F, and a 3.8 Å bond between the nitrogen of F and H6. In this particular model, Y10 is too far away from the oxygen on L to hydrogen bond. In another low energy structure, FL is wrapped tightly within the Aβ structure (Figure 3.6B). Here hydrogen bonding occurs between NE2 of Q15 and the oxygen on F (2.7 Å). While there are no contacts

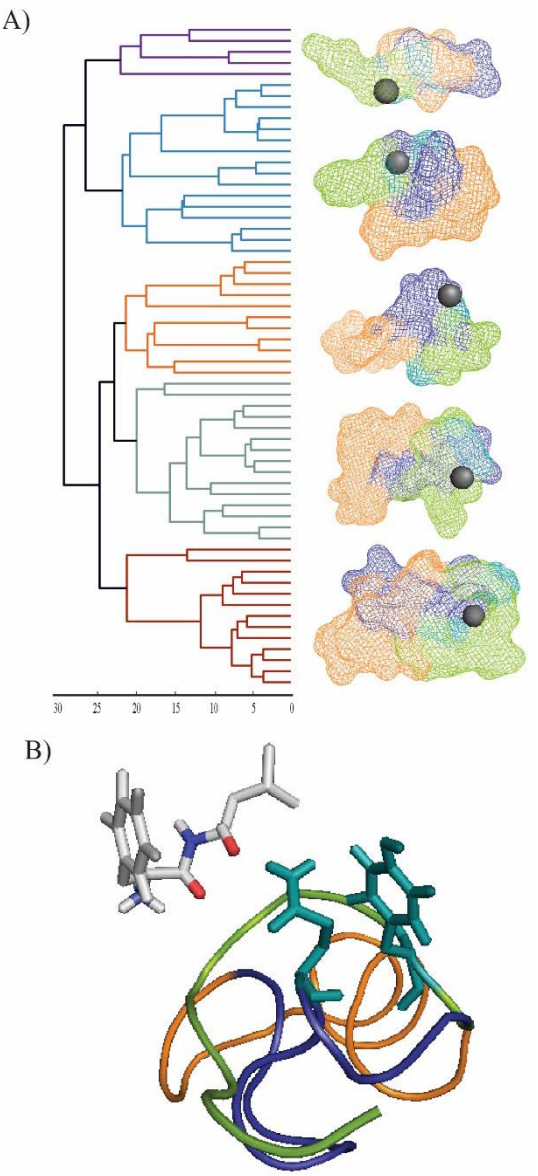

Figure 3.5 – Hierarchical clustering analysis and model visualization of $A\beta_{1-40}$:FL complexes. A) Clustering hierarchy, and the averaged family structure for each cluster. B) High resolution representative of Aβ:FL complex. Where Q15 and Y10 (teal) primarily interact with the leucine of FL. N-terminus (green), hydrophobic core (blue), C-terminus (orange), and FL (grey, oxygen in red, nitrogen in blue).

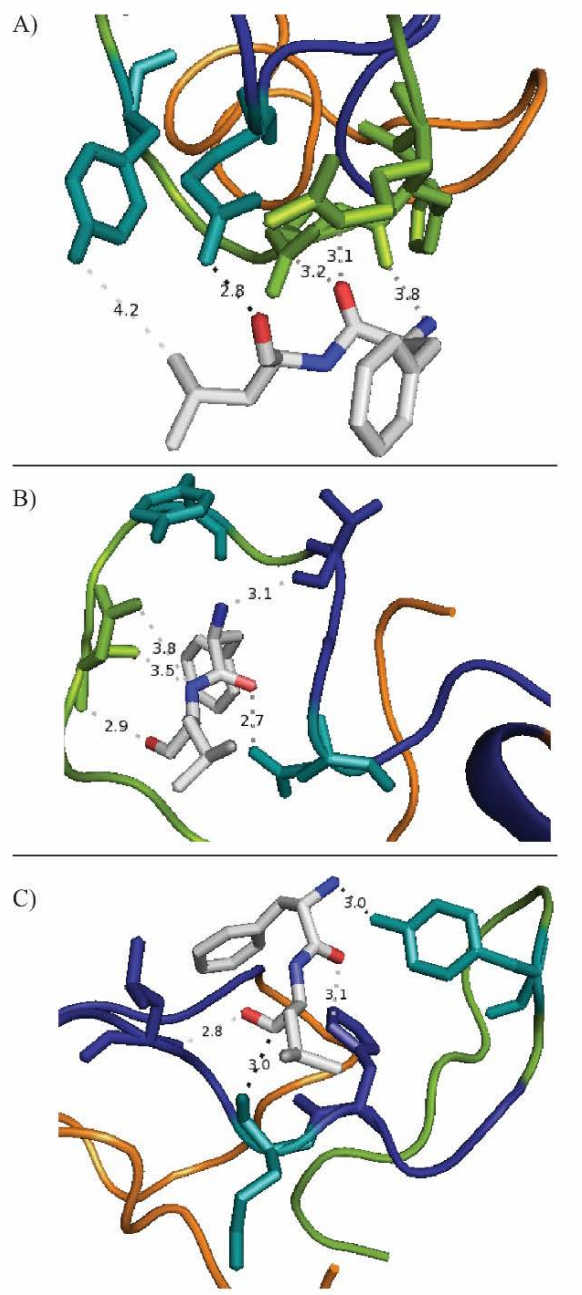

Figure 3.6 – Detailed interaction of Aβ:FL from the lowest energy structure of three clusters. Hydrogen bonding occurs most frequently with the backbone of FL. Bond distances with Q15 range from 2.7-3.0 Å. A and B) models in which Y10 has a hydrogen within 4 Å, but no heavy bonding atoms. C) Model in which Y10 and Q15 both hydrogen bond with FL. Y10 and Q 15 are shown in teal, FL in white with nitrogen in blue and oxygen in red.

less than 4 Å between FL and Y10 in this model, the ring structure surrounds the FL pocket. The interaction is stabilized with a 3.1 Å bond between the carboxylic acid oxygen on V12 and the backbone nitrogen on F, in addition to 3 hydrogen bonds between D7 and L. Despite the Y10 not being close enough for hydrogen bonding in the two models discussed thus far, another low energy structure from a different cluster does demonstrate bonding (Figure 3.6C). Here, Y10 has a hydrogen bond distance of 3.0 Å with the backbone nitrogen of F, and Q15 bonds with a distance of 3.0 Å between the oxygen on Q15 and the alpha carbon of L. The interaction is further stabilized with hydrogen bonding between an oxygen of L and N of L17 (2.8 Å) and ND1 of H14 and the oxygen of F (3.1 Å). Models which do not show binding to Y10 pass through our initial filter because hydrogen atoms are within 4 Å, however, hydrogen bond distances refer to heavy atom to heavy atom distances only. We note that all FL hydrogen bonding captured within our models occur along the backbone. As the hydrogen bonds are weak interactions, we believe data here only captures a subset of all potential interactions. Side-chain specific interactions are thus suggested to be possible, but undocumented in the three lowest energy models detailed here.

3.4 Conclusion

Through a comprehensive set of IM-MS and MD simulation results for a comprehensive series of amino acid LE variants, we have identified the two C-terminal residues within the pentapeptide as critical for its previously-reported interaction with Aβ. A subsequent IM-MS analysis of Aβ complexes formed with the isolated FL dipeptide from LE revealed both equivalent binding strengths to the full length construct, and improved attachment to higher-order Aβ oligomers. Through detailed IM-MS, TEM, and CD spectroscopy covering 14 alanine variants of $A\beta_{1\text{-}40}$, carefully selected through an analysis of MD simulation output, we have narrowed the potential sites of FL contact on the $A\beta_{1\text{-}40}$ surface to the Y10 and Q15 residues. Molecular models extensively filtered through a range of structural biology data indicate that FL primarily interacts with Q15 through hydrogen bonding to the FL backbone, and that the dipeptide is cradled between the N-terminus and the hydrophobic core in a manner similar to previous Aβ binders of therapeutic note. Critically, TEM data shows that FL inhibits $A\beta_{1\text{-}40}$ fibril formation, which further points to its potential as a foundation for future AD therapeutics. To move forward, we look towards chemical modification of the FL dipeptide in the creation of a therapeutic library for screening purposes. Modifications should reduce cellular toxicity and increase binding affinity. Additionally, NH_2-FL and FL-Ac variants are of interest, as it has been shown $A\beta_{42}$ C-terminal fragment NH_2-VVIA decreases the toxicity of oligomers[38]. Further, a screen for interaction with other dipeptides may discover complexes with greater binding affinity and provide a stronger starting scaffold to build therapeutics from.

3.5 Acknowledgements

Thank you to M. Ivanova for the collection of TEM images and preliminary input on interpretation. Additionally J. Clark for his assistance and advice in determining modes of binding. R. Kerr for his discussion of Aβ variants and preparation ideas. K. Korshaven and M. Wolf for assistance in troubleshooting CD. Also, J.D. Eschweiler for his development of the hierarchical clustering analysis code.

3.6 References

[1] Young, L. M., Saunders, J. C., Mahood, R. A., Revill, C. H., Foster, R. J., Tu, L.-H., Raleigh, D. P., Radford, S. E., and Ashcroft, A. E. (2015) Screening and classifying small-molecule inhibitors of amyloid formation using ion mobility spectrometry–mass spectrometry, *Nature chemistry 7*, 73-81.

[2] Young, L. M., Saunders, J. C., Mahood, R. A., Revill, C. H., Foster, R. J., Ashcroft, A., and Radford, S. (2015) ESI-IMS–MS: A method for rapid analysis of protein aggregation and its inhibition by small molecules, *Methods*.

[3] Woods, L. A., Platt, G. W., Hellewell, A. L., Hewitt, E. W., Homans, S. W., Ashcroft, A. E., and Radford, S. E. (2011) Ligand binding to distinct states diverts aggregation of an amyloid-forming protein, *Nature chemical biology 7*, 730-739.

[4] Young, L. M., Cao, P., Raleigh, D. P., Ashcroft, A. E., and Radford, S. E. (2013) Ion mobility spectrometry–mass spectrometry defines the oligomeric intermediates in amylin amyloid formation and the mode of action of inhibitors, *Journal of the American Chemical Society 136*, 660-670.

[5] Hyung, S.-J., DeToma, A. S., Brender, J. R., Lee, S., Vivekanandan, S., Kochi, A., Choi, J.-S., Ramamoorthy, A., Ruotolo, B. T., and Lim, M. H. (2013) Insights into antiamyloidogenic properties of the green tea extract (−)-epigallocatechin-3-gallate toward metal-associated amyloid-β species, *Proceedings of the National Academy of Sciences 110*, 3743-3748.

[6] Beck, M. W., Oh, S. B., Kerr, R. A., Lee, H. J., Kim, S. H., Kim, S., Jang, M., Ruotolo, B. T., Lee, J.-Y., and Lim, M. H. (2015) A rationally designed small molecule for identifying an in vivo link between metal–amyloid-β complexes and the pathogenesis of Alzheimer's disease, *Chemical Science 6*, 1879-1886.

[7] Pithadia, A. S., Kochi, A., Soper, M. T., Beck, M. W., Liu, Y., Lee, S., DeToma, A. S., Ruotolo, B. T., and Lim, M. H. (2012) Reactivity of diphenylpropynone derivatives toward metal-associated amyloid-β species, *Inorganic chemistry 51*, 12959-12967.

[8] Bleiholder, C., Do, T. D., Wu, C., Economou, N. J., Bernstein, S. S., Buratto, S. K., Shea, J.-E., and Bowers, M. T. (2013) Ion Mobility Spectrometry Reveals the Mechanism of Amyloid Formation of Aβ (25–35) and Its Modulation by Inhibitors at the Molecular Level: Epigallocatechin Gallate and Scyllo-inositol, *Journal of the American Chemical Society 135*, 16926-16937.

[9] Gessel, M. M., Wu, C., Li, H., Bitan, G., Shea, J.-E., and Bowers, M. T. (2011) Aβ (39–42) modulates Aβ oligomerization but not fibril formation, *Biochemistry 51*, 108-117.

[10] Zheng, X., Gessel, M. M., Wisniewski, M. L., Viswanathan, K., Wright, D. L., Bahr, B. A., and Bowers, M. T. (2012) Z-Phe-Ala-diazomethylketone (PADK) disrupts and remodels early oligomer states of the Alzheimer disease Aβ42 protein, *Journal of Biological Chemistry 287*, 6084-6088.

[11] Kirkitadze, M. D., Bitan, G., and Teplow, D. B. (2002) Paradigm shifts in Alzheimer's disease and other neurodegenerative disorders: the emerging role of oligomeric assemblies, *Journal of neuroscience research 69*, 567-577.

[12] Lesné, S., Koh, M. T., Kotilinek, L., Kayed, R., Glabe, C. G., Yang, A., Gallagher, M., and Ashe, K. H. (2006) A specific amyloid-β protein assembly in the brain impairs memory, *Nature 440*, 352-357.

[13] Necula, M., Kayed, R., Milton, S., and Glabe, C. G. (2007) Small molecule inhibitors of aggregation indicate that amyloid β oligomerization and fibrillization pathways are independent and distinct, *Journal of Biological Chemistry 282*, 10311-10324.
[14] Ono, K., Condron, M. M., and Teplow, D. B. (2009) Structure–neurotoxicity relationships of amyloid β-protein oligomers, *Proceedings of the National Academy of Sciences 106*, 14745-14750.
[15] Bernstein, S. L., Dupuis, N. F., Lazo, N. D., Wyttenbach, T., Condron, M. M., Bitan, G., Teplow, D. B., Shea, J.-E., Ruotolo, B. T., and Robinson, C. V. (2009) Amyloid-β protein oligomerization and the importance of tetramers and dodecamers in the aetiology of Alzheimer's disease, *Nature chemistry 1*, 326-331.
[16] Bitan, G., Fradinger, E. A., Spring, S. M., and Teplow, D. B. (2005) Neurotoxic protein oligomers—what you see is not always what you get, *Amyloid 12*, 88-95.
[17] Clemmer, D. E., and Jarrold, M. F. (1997) Ion mobility measurements and their applications to clusters and biomolecules, *Journal of Mass Spectrometry 32*, 577-592.
[18] Bohrer, B. C., Merenbloom, S. I., Koeniger, S. L., Hilderbrand, A. E., and Clemmer, D. E. (2008) Biomolecule analysis by ion mobility spectrometry, *Annual review of analytical chemistry (Palo Alto, Calif.) 1*, 293.
[19] Benesch, J. L., Ruotolo, B. T., Simmons, D. A., and Robinson, C. V. (2007) Protein complexes in the gas phase: technology for structural genomics and proteomics, *Chemical reviews 107*, 3544-3567.
[20] Soper, M. T., DeToma, A. S., Hyung, S.-J., Lim, M. H., and Ruotolo, B. T. (2013) Amyloid-β–neuropeptide interactions assessed by ion mobility-mass spectrometry, *Physical Chemistry Chemical Physics 15*, 8952-8961.
[21] Hernández, H., and Robinson, C. V. (2007) Determining the stoichiometry and interactions of macromolecular assemblies from mass spectrometry, *Nature protocols 2*, 715-726.
[22] Ruotolo, B. T., Hyung, S. J., Robinson, P. M., Giles, K., Bateman, R. H., and Robinson, C. V. (2007) Ion Mobility–Mass Spectrometry Reveals Long-Lived, Unfolded Intermediates in the Dissociation of Protein Complexes, *Angewandte Chemie International Edition 46*, 8001-8004.
[23] Bush, M. F., Hall, Z., Giles, K., Hoyes, J., Robinson, C. V., and Ruotolo, B. T. (2010) Collision cross sections of proteins and their complexes: a calibration framework and database for gas-phase structural biology, *Analytical chemistry 82*, 9557-9565.
[24] Trott, O., and Olson, A. J. (2010) AutoDock Vina: improving the speed and accuracy of docking with a new scoring function, efficient optimization, and multithreading, *Journal of computational chemistry 31*, 455-461.
[25] Vivekanandan, S., Brender, J. R., Lee, S. Y., and Ramamoorthy, A. (2011) A partially folded structure of amyloid-beta (1–40) in an aqueous environment, *Biochemical and biophysical research communications 411*, 312-316.
[26] Tomaselli, S., Esposito, V., Vangone, P., van Nuland, N. A., Bonvin, A. M., Guerrini, R., Tancredi, T., Temussi, P. A., and Picone, D. (2006) The α-to-β Conformational Transition of Alzheimer's Aβ-(1–42) Peptide in Aqueous Media is Reversible: A Step by Step Conformational Analysis Suggests the Location of β Conformation Seeding, *ChemBioChem 7*, 257-267.
[27] SchuÈttelkopf, A. W., and Van Aalten, D. M. (2004) PRODRG: a tool for high-throughput crystallography of protein–ligand complexes, *Acta Crystallographica Section D: Biological Crystallography 60*, 1355-1363.

[28] Lindahl, E., Hess, B., and Van Der Spoel, D. (2001) GROMACS 3.0: a package for molecular simulation and trajectory analysis, *Journal of Molecular Modeling 7*, 306-317.
[29] van Gunsteren, W. F., Billeter, S., Eising, A., Hünenberger, P. H., Krüger, P., Mark, A. E., Scott, W., and Tironi, I. G. (1996) Biomolecular simulation: The {GROMOS96} manual and user guide.
[30] Berendsen, H. J., Postma, J. P. M., van Gunsteren, W. F., DiNola, A., and Haak, J. (1984) Molecular dynamics with coupling to an external bath, *The Journal of chemical physics 81*, 3684-3690.
[31] Mesleh, M., Hunter, J., Shvartsburg, A., Schatz, G., and Jarrold, M. (1996) Structural information from ion mobility measurements: effects of the long-range potential, *The Journal of Physical Chemistry 100*, 16082-16086.
[32] Shvartsburg, A. A., and Jarrold, M. F. (1996) An exact hard-spheres scattering model for the mobilities of polyatomic ions, *Chemical Physics Letters 261*, 86-91.
[33] Kabsch, W. (1976) A solution for the best rotation to relate two sets of vectors, *Acta Crystallographica Section A: Crystal Physics, Diffraction, Theoretical and General Crystallography 32*, 922-923.
[34] Jones, E., Oliphant, T., and Peterson, P. (2014) {SciPy}: Open source scientific tools for {Python}.
[35] Wang, W., Kitova, E. N., and Klassen, J. S. (2003) Influence of solution and gas phase processes on protein-carbohydrate binding affinities determined by nanoelectrospray Fourier transform ion cyclotron resonance mass spectrometry, *Analytical chemistry 75*, 4945-4955.
[36] Paivio, A., Jarvet, J., Graslund, A., Lannfelt, L., and Westlind-Danielsson, A. (2004) Unique physicochemical profile of β-amyloid peptide variant Aβ1-40E22G protofibrils: Conceivable neuropathogen in arctic mutant carriers, *Journal of molecular biology 1*, 145-159.
[37] Walsh, D., Klyubin, I., Fadeeva, J., Rowan, M., and Selkoe, D. (2002) Amyloid-beta oligomers: their production, toxicity and therapeutic inhibition, *Biochemical Society Transactions 30*, 552-557.
[38] Li, H., Du, Z., Lopes, D. H., Fradinger, E. A., Wang, C., and Bitan, G. (2011) C-terminal tetrapeptides inhibit Aβ42-induced neurotoxicity primarily through specific interaction at the N-terminus of Aβ42, *Journal of medicinal chemistry 54*, 8451-8460.

Chapter 4.

Ion Mobility Mass Spectrometry Analysis of Ubiquitin and Ubiquilin2 Aggregates

4.1. Introduction

It is well understood that ubiquitin is crucial to protein degradation[1, 2]. Three key enzymes responsible for this process are E-activating, E-conjugating, and E-ligases[3, 4]. Where the E-activating enzyme links its active site cysteine to the c-terminus of ubiquitin. The ubiquitin conjugating enzyme forms catalytically activated intermediates. These may form polyubiquitin chains with E-ligases[5, 6]. The ligases can then form isopeptide bonds between the c-terminus of ubiquitin and lysine (K48 of ubiquitin) on an already ubiquitin tagged target protein, or lysine on the target protein[6]. This polyubiquitin chain signals the 26S proteasome for degredation[7]. A growing body of work suggests transition metals to be associated with the regulation of this process[8]. Dysfunction of the pathway can also be correlated with neurodegerateive diseases, which are further correlated with metal dyshomeostasis [9, 10]. In this chapter, IM-MS is used to characterize the structural effects of copper binding on ubiquitin aggregation *in vitro* in attempts to better understand its possible interaction in protein degradation and neurodegenerative diseases. We find, under conditions of three fold excess copper per ubiquitin subunit, that aggregation of ubiquitin increases, and have observed compaction of the ubiquitin monomer upon copper binding.

It is evident that neurodegenerative diseases having etiologies that rely upon protein aggregation are, by definition, complex and multifaceted disorders. In addition to the discussion above, the ubiquitin-like protein family (UBQLN1-4), is associated with both Alzheimer's and Parkinson's diseases[11]. Additionally, dominant X-linked juvenile and adult-onset familial amyotrophic lateral sclerosis (ALS) is thought to be caused by mutations in UBQLN2[12, 13]. The UBQLN2 protein is comprised of an ubiquitin-like domain, heat-shock-chaperonin-binding motifs, PXX repeats, and

an ubiquitin-associated domain. Mutations of UBQLN2 linked with ALS include P497H, P497S, P506T, P509S and P525S and are found in the PXX repeat region. All UBQLN family proteins have an ubiquitin-like domain and an ubiquitin-associated domain on the termini but the middle region is variable. This structural motif allows these proteins to be involved with directing the proteosomal degradation process[14]. Cells expressing proline mutations of UBQLN2 demonstrated impaired function of the ubiquitin-protesome degradation pathway, indicating ALS and ALS/dementia are associated with altered protein clearance and homeostasis[12]. P506T UBQLN2 inclusions were found in the spinal cord and hippocampus of ALS patients displaying dementia[12]. Little is known of these inclusions bodies, and the direct rolls of potential UBQLN2 aggregates in human disease [12, 13, 15, 16]. In addition to the studies discussed above, we endeavor here to determine structural differences between UBQLN2 wild type and the P506T mutant, and detect differences in protein aggregation using IM-MS and collision induced unfolding (CIU)[17, 18]. We find that both WT and P506T Ubiquilin2 have similar propensity for dimerization and nearly indistinguishable unfolding pathways.

4.2. Experimental Methods

4.2.1. Ubiquitin Preparation

Ubiquitin (from bovine erythrocytes, Sigma-Aldrich) and Recombinant Human Linear Tetra-Ubiquitin/Ub4, CF (R&D systems) were dissolved in 200mM ammonium acetate (BioUltra for molecular biology, Sigma) to 50-100 µM, aliquoted as necessary and stocks stored at -80 °C. Tri-ubiquitin (linear, Enzo Life Sciences) was left as received in 50 mM TRIS pH 8.0 containing 50 mM sodium chloride. Prior to IM-MS experiments all ubiquitin samples were buffer exchanged using 6kDA MWCO buffer exchange columns (bio-rad) for desalting of ubiquitin and tetra-ubiquitin, and for buffer exchange of tri-ubiquitin into 200 mM ammonium acetate. Proteins (10-15 µM) were incubated on ice for 3 h in 75/25 v/v 200 mM ammonium acetate/200 mM triethyl ammonium acetate buffer (TEAA, Sigma) unless otherwise specified. Copper (II) acetate was added at concentrations specified.

Linear Tri-Ubiquitin (L3UB, 10 µM) was incubated with 30 µM CuAc. While this represents a 3x excess of copper to the L3UB complex, with 100% binding efficiency each of the ubiquitin subunits could be copper bound, leaving no excess. To match the 3 fold excess for each subunit

represented for monoubiquitin incubation with 90 µM CuAc would be required. This concentration would greatly increase the noise of our spectrum and likely mask populations of ions with very low intensities, needing further clean up steps prior to analysis and so was not tested. Similarly linear tetra-ubiqutin (L4UB, 15 µM) was incubated with 15 µM and 45 µM CuAc, where 180 µM CuAc would be required for a 3 fold excess with respect to the number of ubiquitin domains.

4.2.2. Ubiquilin Preparation

Ubiquilin (WT and P506T) were expressed and purified by collaborators, Magdalenea Ivanova, and received in 100 mM ammonium acetate, pH 6.9. Samples were desalted using 6kDA MWCO buffer exchange columns (bio-rad), and kept on ice.

4.2.3. IM-MS – Ubiquitin Aggregation

Mass spectra were collected on a quadrupole-ion mobility-time-of-flight (TOF) mass spectrometer (Synapt G2 HDMS, Waters, Milford, MA, USA) with a nano-electrospray ionization (nESI) source. Protein ions were generated using a nESI source and optimized to allow transmission of noncovalent protein complexes using electrospray capillaries prepared as described previously[19]. Protein complex ions were generated using an aliquot of the sample (*ca.* 3 µL) sprayed from the nESI emitter at a capillary voltage of 1.2– 1.65 kV. The source was operated in positive ion mode with the sample cone at 20- 50 V. The bias voltage was 50 V, with backing pressure at 2.9- 6.1 mbar and TOF pressure at 1.47×10^{-6} mbar. The travelling-wave IM separator was operated at a pressure of approximately 3.0 mbar of nitrogen. Mass spectra were calibrated externally using a solution of cesium iodide (100 mg mL^{-1}) and analyzed using MassLynx 4.1 and Driftscope 2.0 software (Waters, Milford, MA, USA). Aggregate populations were selected in Driftscope, and percentages of the population calculated by dividing the signal intensity for the species of interest by the total ion population signal intensity. Averages were calculated on one sample using three different nESI needles, and error reported is one standard deviation.

4.2.4. IM-MS – Ubiquilin Aggregation

Mass spectra were collected as in 4.2.3. Ions were generated with the nESI emitter at a capillary voltage of 1.4 kV. The source was operated in positive ion mode with the sample cone at 40 V.

The bias voltage was 45 V, with backing pressure at 2.9 mbar and TOF pressure at 1.46 x 10^{-6} mbar. The travelling-wave IM separator was operated at a pressure of approximately 3.0 mbar of nitrogen. Mass spectra were analyzed using MassLynx 4.1 and Driftscope 2.0 software. Aggregate populations were selected in Driftscope, and percentages of the population calculated by dividing the signal intensity for the species of interest by the total ion population signal intensity.

The 14+ charge states for both the WT and P506T were selected in a MS/MS experiment for CIU fingerprint analysis. Prior to the ion mobility cell, ions were activated in the trap region by increasing the voltage applied in this area. By ramping the voltage, and measuring the resulting drift time of the unfolded structure at each voltage, a CIU fingerprint can be created. CIU fingerprints were collected over a trap collision energy range of 30-150 V, in steps of 5 V. Data was analyzed and fingerprints created using home built software, CIUSuite.

4.3. Results and Discussion

4.3.1. Ubiquitin in the Presence of Copper

Initial studies of 15 µM ubiquitin (Ubq) in 200 mM ammonium acetate were incubated with 45µM copper (II) acetate (CuAc) at 4 °C for 24 h to facilitate copper binding and promote aggregation while preventing protein degradation. While consistent evidence of Ubq aggregation beyond dimer formation was not observed under these conditions, we did identify a compaction in both the monomer and dimer upon copper binding. Each copper binding event led to further Ubq compaction. It is therefore possible that subsequent copper binding events allow for previously extended conformations to adopt a more compact, and likely more stable, structures in solution, that are then broadly conserved in our gas-phase

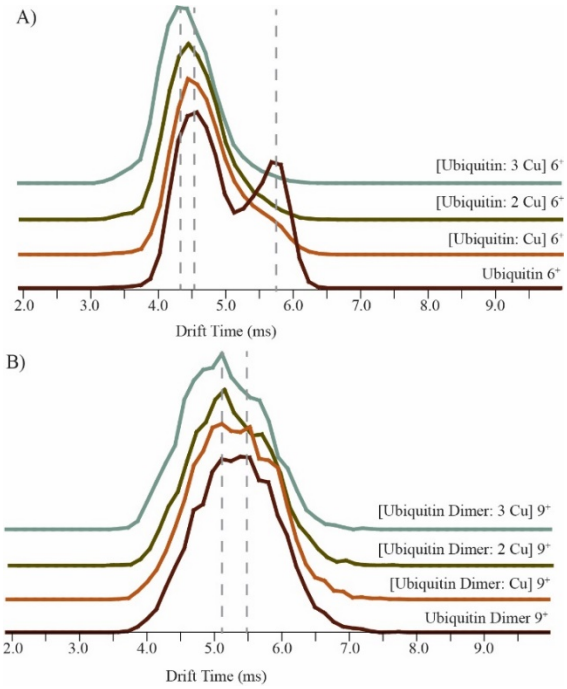

Figure 4.1 – Shift in structural populations upon copper binding. A) Ubiquitin monomer in the 6^+ charge state occupies two structural populations in the apo state. Each copper binding event shifts the populations to a more compact structure, with the 3 bound copper population being smaller even than the most compact form of the apo population. B) Upon copper binding to the Ubiquitin 9^+ dimer, the population shifts to lower drift times.

measurements. For example, the apo 6^+ monomeric ubiquitin occupies two structural families under our conditions, compact and extended (Figure 4.1). Upon binding a single copper, the observed population shifts dramatically toward compact conformers; a small amount of the extended structure appears as a shoulder. With the addition of further copper to Ubq only compact conformational families are observed. It is of note these Cu-bound compact states are slightly smaller than the compact conformer family found in the apo state. Although overall signal intensity is lower for the dimer when compared with monomeric Ubq signals, we see a similar trend for the 9^+ dimer, with the shifting of the IM drift time centroid from 5.42 to 5.12 ms (a shift of 7.6%). This shift is less substantial than measured for the Ubq monomer (a shift of 28.9%), with the dimer only occupying a single monomodal conformational family in its apo state. In samples prepared using 75/25 v/v ammonium acetate/ triethyl ammonium acetate (TEAA), this phenomenon was not observed. Monomeric ubiquitin only occupied one structural population, the more compact state. The dimer as well showed no significant shift in drift time upon copper addition.

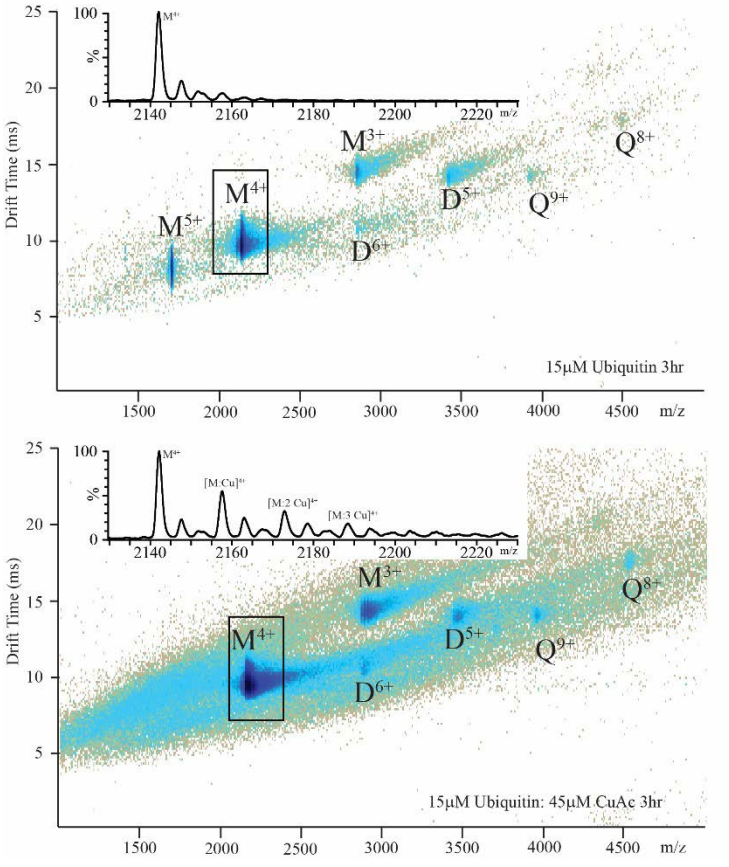

Figure 4.2 – IM-MS data of copper incubated ubiquitin. Upon incubation with 45 µM copper acetate (CuAc), 15 µM monomeric ubiquitin (M) aggregates to form increased amounts of dimer (D) and tetramer (Q). Increased noise in the sample is from excess CuAc in solution. Up to three copper adducts are observed on the M^{4+} species as shown in the MS inset.

While no shift in Ubq IM drift time was observed with samples having TEAA present, after a 3 h incubation on ice with a three-fold excess of CuAc, IM-MS data revealed that the sample contained 94.4% (± 2.75%) monomer, 4.0% (± 3.2%) dimer, and 1.6% (± 0.5%) tetramer. In contrast, control samples having no added CuAc contained 97.4% (± 1.5%) monomer, 2.5% (± 1.3%), and 0.3%

(± 0.05%) tetramer. This represents a 1.6 fold increase in Ubq dimer concentration, and a 5.3 fold increase in the Ubq tetramer concentration. Of note, no trimer was observed in either the control or the copper incubated samples leading to the conclusion that the tetramer was formed through a specific dimer-dimer addition event, and not through non-specific aggregation. IM-MS data for these samples are shown in Figure 4.2. In Cu-containing samples, the small amount of monomer 5^+ observed under non-metal containing conditions is no longer observable, and the dimer and tetramer signals have increased in intensity. An increased amount of background noise is also observed in Cu-containing spectra, due to salt-cluster associated chemical noise. Our MS data supports the addition of up to three Cu ions to Ubq (Figure 4.2 insets), although only one copper binding site has been identified at His68[20]. Zinc and platinum have been shown previously to bind three copies to Ubq at His68, Met1, and Lys6 (platinum)/Glu18 (zinc)[21], although the same studies did not investigate Cu binding.

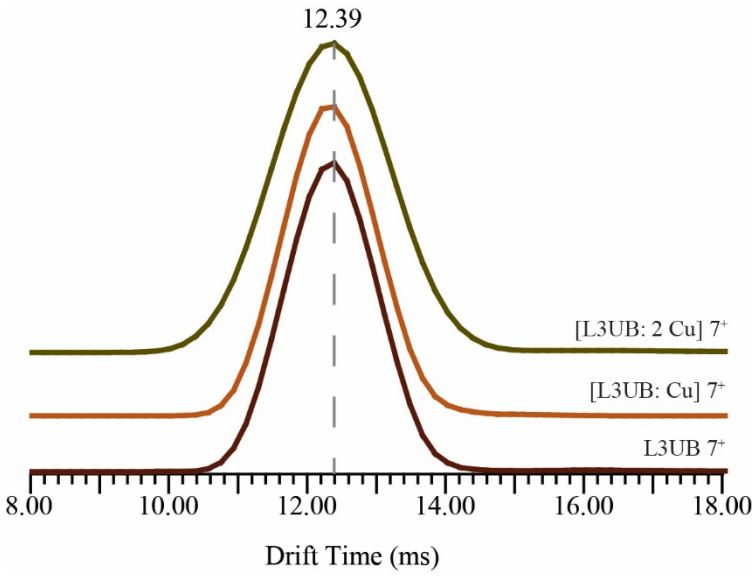

Figure 4.3 – Drift Time Analysis of L3UB. The L3UB monomer at a 7^+ charge state occupies a since conformational family. Upon addition of a 3x excess of CuAc in 75/25 ammonium acetate/ TEAA. No shift in conformational state is observed after 3 h incubation.

While incubation of copper with the monomer of Ubq seems to increase the Ubq dimer and tetramer population substantially, we moved to confirm this overall result by studying linear tri- and tetra-ubiquitin analogs. As for single domain constructs of Ubq, L3UB measured in 75/25 ammonium acetate/TEAA revealed no evidence of compaction upon Cu addition (Figure 4.3). After 3 h on ice, Cu-free L3UB monomer occupies 83.9% of the total IM-MS signal intensity and its dimer (six total Ubq domains) occupies 16.1% (σ = 4.44 %). Upon incubation with CuAc incubation at a 1:1 ratio (stoichiometric with respect to the number of ubiquitin domains), L3UB monomer makes up 77.2% of the signal intensity while dimer accounts for 22.8% (σ = 5.3%). This represents an

increase in dimeric state by 1.4 fold, a nearly 4.5 fold greater increase than observed for Cu-mediated dimerization in monodomain Ubq. (Figure 4.4 Left).

In contrast to Ubq and L3UB, linear tetra-ubiquitin (L4UB), incubated at 15 µM under conditions similar to those described above, we do not observe evidence of Cu-mediated dimer or trimer formation by IM-MS (CuAc, 15 µM and 45 µM, Figure 4.4 Right). CuAc concentrations of 15 µM and 45 µM represent enough copper to fully occupy 1/4th and 3/4th of the ubiquitin domains within L4UB respectively. Large amounts of L4UB ion charge stripping

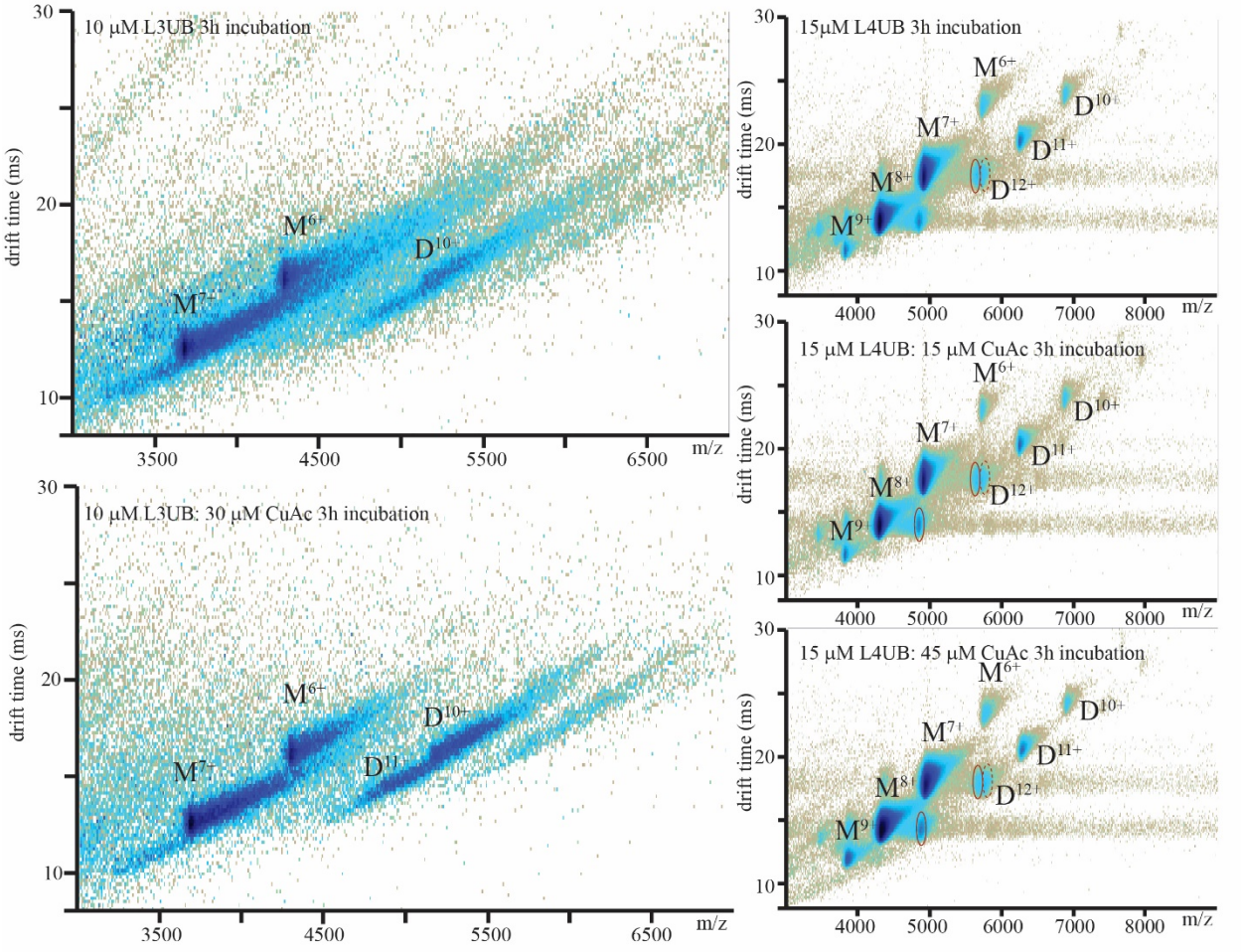

Figure 4.4 – IM-MS data showing incubation of polyubiquitin with CuAc. Left) Top – control of linear tri-ubiquitin after a 3 h incubation on ice. The majority of signal is tri-ubiquitin (M), with a small amount of its dimer (D). Increased background noise is likely attributed to TRIS acetate and Sodium Chloride not entirely removed following buffer exchange. Bottom- Incubation with 3x CuAc. Dimer signal increases in intensity by 6.7%. Peak broadening is due to copper adduction. Right) Top – control of linear tetra-ubiquitin after 3 h incubation on ice. The majority of signal is tetra-ubiquitin (M) with small amounts of its dimer (D). Charge stripping from the M^{8+} and M^{7+} is observed. Separation of the charge stripped M^{6+} and D^{12+} is possible due to varying amounts of adducts shifting the mass of the oligomers. The charge stripped species is circled in a solid line. Dimer is circled with a dashed-line. Middle and Bottom – Incubation with 15 µM or 45 µM CuAc. Distribution of oligomers does not shift.

are observed from the 8+ and 7+ charge states observed by MS (circled with a solid line in the right panel of figure 4.4). We also observe a shifted L4UB intact mass in a manner consistent with Cu addition to the structure. All three L4UB samples tested (control, 15 µM CuAc, 45 µM CuAc) contained protein ion signal identified as 99% monomer, and 1% dimer. The lack of any detectable evidence for Cu-mediated protein association in L4UB samples can likely be attributed to the lack of sufficient CuAc in solution to drive the oligomerization. The samples described here, which include 45 µM CuAc, represent the upper-end of the salt tolerance of nESI prior to the onset of significant chemical noise and ion suppression effects. As such, the data shown here cannot be used to differentiate between L4UB aggregation resistance and the need for Cu excess to initiate Cu-mediated Ubq-protein association and aggregation. While further study will be needed to ascertain to the propensity of L4UB to undergo Cu-mediated aggregation, our data clearly show enhanced aggregation and the formation of compact structures upon the introduction of Cu for the smaller Ubq and L3UB constructs.

4.3.2 Ubiquilin2 WT and P506T Mutation

The ubiquitin-like protein UB2 and its P506T mutant form are studied here using IM-MS in order to determine if different dimerzation propensities *in vitro* can describe their disease associations *in vivo*. In addition, we applied CIU in an effort to detect any differences in stability between these two proteoforms. Figure 4.5 shows our IM-MS results, with signals for both monomer and dimer distributions for both WT and P506T UB2 constructs detected. WT UB2 is dominated by monomeric protein signal, which accounts for 87.1% ± 0.2% of the total IM-MS signal observed, and 12.9% dimer. Similarly, IM-MS data for P506T reveals the protein to be

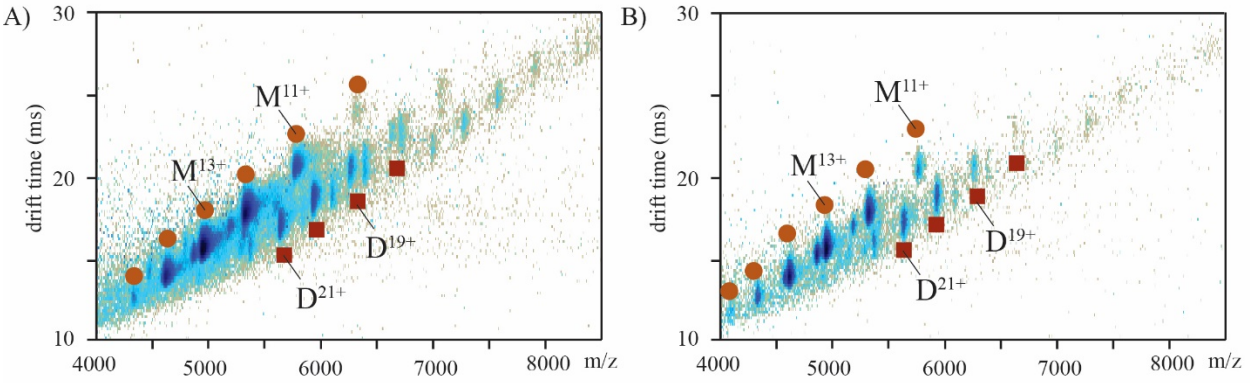

Figure 4.5 – IM-MS data of Ubiquilin2 proteins. Orange circles label species which are monomeric, while the red squares highlight those which are dimers. A) Wild Type Ubiquilin2. B) P506T Ubiquilin2. While more heavily adducted than the P506T, the WT UB2 is 87.1% monomer and 12.9% dimer. Mutant P506T is 88.6% monomer, and 11.4% dimer.

primarily monomeric under our conditions (88.6% ± 1.4%) with an amount of dimer (11.4%) similar to WT. The monomeric portion of P506T is more than one standard deviation higher than that of the WT, indicating a slightly lower propensity for dimerization for the mutant protein in this sample preparation. The IM drift times of each species also appear identical, further indicating that the WT and P506T are indistinguishable under native conditions.

While structurally indistinguishable to course-grained measurements of protein fold, such as IM-MS, if the P506T were to cause structural instability in the detailed tertiary/secondary structure of the protein, this may be detectable by CIU. A single charge state (14+) for both the WT and P506T was quadruople-selected for CIU fingerprint analysis (Figure 4.6). Both the WT and P506T UB2 follow nearly identical unfolding patterns. For both, three main CIU features are detected, the first of which is centered at ~15 ms IM drift time, and is stable through 60 V. At 65 V a new CIU feature appears, with an IM centroid of ~20 ms and remains stable through 95 V. For activation voltages between 105 and 150 V a third CIU transition is observed at ~22 ms. A difference plot shows areas of significant deviation between CIU data acquired for both UB2 proteoforms. By computing the root-mean squared deviation at each pixle within the difference plot shown in Figure 4.6, we can quantify the difference between the two data set as 3.36. This type of small of a value is typical of fingerprints which can be considered identical, as described previously[22].

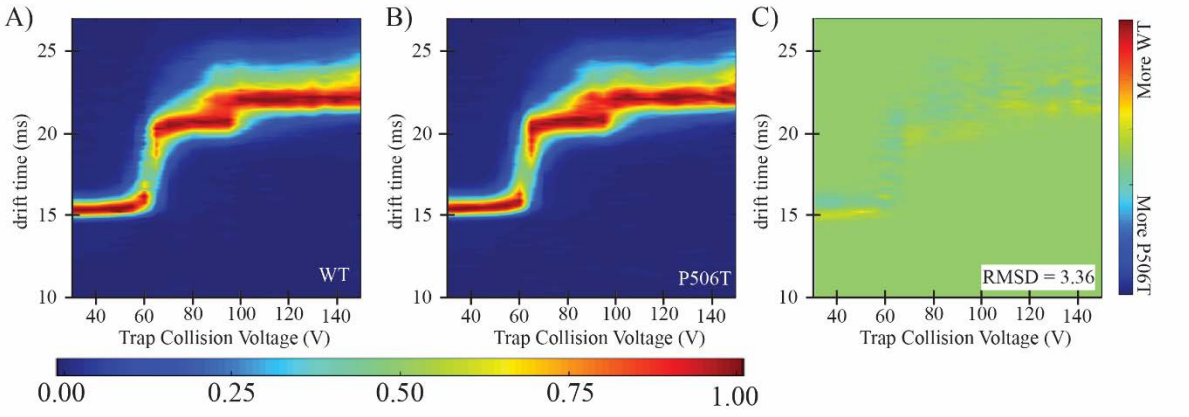

Figure 4.6 – Collision induced unfolding of the 14+ charge state of WT and P506T UB2. A) Unfolding fingerprint for WT UB2. Three distinct conformations are observed, one at drift time ~15 ms, one at ~20 ms, and one at ~ 21ms. B) Unfolding fingerprint for P506T UB2. Three distinct conformations are again observed, at the same drift times as those of the WT. Scale bar ranges from Blue to Red, where the more red the color the more intense the signal. C) Difference plot comparing WT and P506T. More blue indicates a more P506T like area, more yellow represents more WT. With an RMSD of 3.36, the fingerprints would be considered indistinguishable from one another.

Taken together, IM-MS and CIU indicates that the two UB2 forms studied here are nearly indistinguishable under native conditions (pH ~7) in terms of their structures and stabilities. Both protein samples contain approximately 88% monomer and 12% dimer, possess the same gas-phase stabilities and unfold following the same CIU pathway. Slight variations in the CIU stabilities observed can be readily attributed to increased salt adduct stabilization for the WT protein, as confirmed by MS[23]. While differences between the WT and mutant are not observed in these initial studies, it does not necessarily contradict previous work. For example, based on these proteins differential ability to alter protein degredation, future experiments should certainly target in vitro addition of proteosomal subunits to observe differential protein binding [12]. In addition, the pH and ionic strength dependence of UB2 aggregation was not explored here, and since our data strongly indicate similar native states, unfolded forms of UB2 present in solution may be a likely source of aggregation propensity detected for these proteins *in vivo*.

4.4. Conclusions

Here we have explored the aggregation propensity of two proteins important to the proteasomal degradation pathway, which when impaired can lead to dementia. The first, ubiquitin, signals for the degradation of other proteins upon tagging with polyubiquitin, and it has been suggested that transition metals may play an important role in this process. Our studies find that when incubated with an excess of copper acetate, copper binding causes a shift to a more compact monomeric and dimeric forms of Ubq. When incubated with excess copper in 75/25 v/v ammonium acetate/TEAA, dramatically increased amounts of dimer and tetramer are detected. The tetramer observed is likely formed through a dimer-dimer addition, as no trimer is detected, strongly indicating that this pathway is borne of specific protein-protein binding interfaces. L3UB exhibits the same propensity for aggregation when incubated with excess copper, however L4UB does not appear to be effected by copper after an incubation for 3 h with sub-stoichiometric amounts of Cu. It is possible conditions tested here did not reach the concentrations of copper required for aggregation of L4UB, and future experiments should aim to push the boundaries on Cu addition in nESI-MS in order to fully explore the aggregation of larger Ubq constructs. Further, the series of linear polyubiquitins is commercially available up to a decameric chain, it would be valuable to see which ubiquitin chain lengths are most susceptible

to aggregation in the presence of Cu in order to fully delineate the potential role of these forms in neurodegenerative disease etiologies.

Ubiquilin2, a protein linked with ALS through mutations, shares structural similarities to ubiquitin. The N-terminus contains an ubiquitin-like domain, and an ubiquitin-associated domain is found on the C-terminus. IM-MS and CIU experiments did not detect any differences between the WT and P506T mutations under native conditions in terms of their structures, aggregation propensities, or gas-phase stabilities. This however does not mean that the two variants are identical to one another broadly speaking. Further experiments which could be probed with IM-MS would include ubiquilin2-ubiquitin binding experiments, as it is known that the P506T mutation impairs the proteasomal degradation pathway. Additionally, it would be interesting to probe the interactions of UB2 with copper, to determine if binding occurs to the ubiquitin-like domain and facilitates an increased amount of dimerization as observed for the ubiquitin alone. In addition, a broader scope of solution conditions, including changes to protein solution pH, ionic strength, and temperature, could be used to investigate the aggregation propensity of UB2 constructs more using IM-MS.

4.5. Acknowledgements

Thank you to Alexander Brown for his dedicated work in developing solution conditions for the ubiquitin-copper interaction experiments, and collection of initial data which indicated a compaction of the monomer in 200 mM ammonium acetate. Additionally, Magdalena Ivanova for the expression and purification of the UB2 WT and P506T.

4.6. References

[1] Hershko, A., Ciechanover, A., and Rose, I. (1981) Identification of the active amino acid residue of the polypeptide of ATP-dependent protein breakdown, *Journal of Biological Chemistry 256*, 1525-1528.

[2] Tai, H.-C., and Schuman, E. M. (2008) Ubiquitin, the proteasome and protein degradation in neuronal function and dysfunction, *Nature Reviews Neuroscience 9*, 826-838.

[3] Hershko, A., Heller, H., Elias, S., and Ciechanover, A. (1983) Components of ubiquitin-protein ligase system. Resolution, affinity purification, and role in protein breakdown, *Journal of Biological Chemistry 258*, 8206-8214.

[4] Ciechanover, A., Elias, S., Heller, H., and Hershko, A. (1982) " Covalent affinity" purification of ubiquitin-activating enzyme, *Journal of Biological Chemistry 257*, 2537-2542.

[5] Sakata, E., Yamaguchi, Y., Miyauchi, Y., Iwai, K., Chiba, T., Saeki, Y., Matsuda, N., Tanaka, K., and Kato, K. (2007) Direct interactions between NEDD8 and ubiquitin E2 conjugating enzymes upregulate cullin-based E3 ligase activity, *Nature structural & molecular biology 14*, 167-168.

[6] Sakata, E., Satoh, T., Yamamoto, S., Yamaguchi, Y., Yagi-Utsumi, M., Kurimoto, E., Tanaka, K., Wakatsuki, S., and Kato, K. (2010) Crystal structure of UbcH5b∼ ubiquitin intermediate: insight into the formation of the self-assembled E2∼ Ub conjugates, *Structure 18*, 138-147.

[7] Pickart, C. M. (2000) Ubiquitin in chains, *Trends in biochemical sciences 25*, 544-548.

[8] Opazo, C. M., Greenough, M. A., and Bush, A. I. (2014) Copper: from neurotransmission to neuroproteostasis, *Frontiers in aging neuroscience 6*.

[9] Rubinsztein, D. C. (2006) The roles of intracellular protein-degradation pathways in neurodegeneration, *Nature 443*, 780-786.

[10] Bush, A. I. (2003) The metallobiology of Alzheimer's disease, *Trends in neurosciences 26*, 207-214.

[11] Mah, A. L., Perry, G., Smith, M. A., and Monteiro, M. J. (2000) Identification of ubiquilin, a novel presenilin interactor that increases presenilin protein accumulation, *The Journal of cell biology 151*, 847-862.

[12] Deng, H.-X., Chen, W., Hong, S.-T., Boycott, K. M., Gorrie, G. H., Siddique, N., Yang, Y., Fecto, F., Shi, Y., and Zhai, H. (2011) Mutations in UBQLN2 cause dominant X-linked juvenile and adult-onset ALS and ALS/dementia, *Nature 477*, 211-215.

[13] Mori, F., Tanji, K., Odagiri, S., Toyoshima, Y., Yoshida, M., Ikeda, T., Sasaki, H., Kakita, A., Takahashi, H., and Wakabayashi, K. (2012) Ubiquilin immunoreactivity in cytoplasmic and nuclear inclusions in synucleinopathies, polyglutamine diseases and intranuclear inclusion body disease, *Acta neuropathologica 124*, 149-151.

[14] Ko, H. S., Uehara, T., Tsuruma, K., and Nomura, Y. (2004) Ubiquilin interacts with ubiquitylated proteins and proteasome through its ubiquitin-associated and ubiquitin-like domains, *FEBS letters 566*, 110-114.

[15] Fahed, A. C., McDonough, B., Gouvion, C. M., Newell, K. L., Dure, L. S., Bebin, M., Bick, A. G., Seidman, J. G., Harter, D. H., and Seidman, C. E. (2014) UBQLN2 mutation causing heterogeneous X-linked dominant neurodegeneration, *Annals of neurology 75*, 793-798.

[16] Rutherford, N. J., Lewis, J., Clippinger, A. K., Thomas, M. A., Adamson, J., Cruz, P. E., Cannon, A., Xu, G., Golde, T. E., and Shaw, G. (2013) Unbiased screen reveals ubiquilin-1 and-2 highly associated with huntingtin inclusions, *Brain research 1524*, 62-73.

[17] Ruotolo, B. T., Hyung, S. J., Robinson, P. M., Giles, K., Bateman, R. H., and Robinson, C. V. (2007) Ion Mobility–Mass Spectrometry Reveals Long-Lived, Unfolded Intermediates in the Dissociation of Protein Complexes, *Angewandte Chemie International Edition 46*, 8001-8004.

[18] Hyung, S.-J., Robinson, C. V., and Ruotolo, B. T. (2009) Gas-phase unfolding and disassembly reveals stability differences in ligand-bound multiprotein complexes, *Chemistry & biology 16*, 382-390.

[19] Hernández, H., and Robinson, C. V. (2007) Determining the stoichiometry and interactions of macromolecular assemblies from mass spectrometry, *Nature protocols 2*, 715-726.

[20] Arena, G., Bellia, F., Frasca, G., Grasso, G., Lanza, V., Rizzarelli, E., Tabbì, G., Zito, V., and Milardi, D. (2013) Inorganic stressors of ubiquitin, *Inorganic chemistry 52*, 9567-9573.

[21] Arnesano, F., Belviso, B. D., Caliandro, R., Falini, G., Fermani, S., Natile, G., and Siliqi, D. (2011) Crystallographic Analysis of Metal-Ion Binding to Human Ubiquitin, *Chemistry-A European Journal 17*, 1569-1578.

[22] Eschweiler, J. D., Rabuck-Gibbons, J., Tian, Y., and Ruotolo, B. T. (2015) CIUSuite: A Quantitative Analysis Package for Collision Induced Unfolding Measurements of Gas-Phase Protein Ions, *In Preparation*.

[23] Han, L., Hyung, S. J., and Ruotolo, B. T. (2012) Bound cations significantly stabilize the structure of multiprotein complexes in the gas phase, *Angewandte Chemie 124*, 5790-5793.

Chapter 5.

Conclusions and Future Directions

5.1 Conclusions

The analysis of proteins associated with misfolding diseases is a complex problem. Traditional structural biology techniques may struggle with the heterogeneity of samples, low concentrations of intermediate species, and the rapid aggregation of these systems. However the combination of ion mobility with mass spectrometry allows us to overcome these difficulties. nESI-MS allows us to detect low μM concentrations of analyte, and identify oligomeric species with accurate mass. Ion mobility assists in additional separation making analysis of complex samples possible. As each of the IM and MS experiments take place in the sub second time scale, the capture of oligomeric species in the lag phase of aggregation is possible. To date systems such as amyloid β[1], β2-microglobulin[2], islet amyloid polypeptide/ amylin[3], α-synuclein[4], prion protein[5], transthyretin[6], Alpha 1-antitrypsin[7], insulin[8], ataxin-3[9], and tau[10] have been studied by IM-MS. This has allowed for the elucidation of structural information, aggregation pathways, and recently screening of drug molecules proposed to inhibition of aggregation[11]. IM-MS has been applied to the study of protein aggregation pathways in multiple ways. This includes assessment of the conversion of natively-structured monomeric proteins into partially unfolded, disease-associated forms. It also represents a crucial method for monitoring the transition between disordered aggregates and β-structured aggregates. Accurate size measurement allows for the building of models which best represent interactions, and IM-MS combined with traditional methods such as NMR, X-ray crystallography, TEM, and gel electrophoresis can refine these models to the most accurate representation.

The utilization of IM-MS for the study of amyloid β (chapters 2 & 3) as well as ubiquitin and ubiquilin2 (chapter 4) builds upon an already thriving field, contributing analysis of interaction partners in the form of neuropeptides, amino acid fragments, and transition metals. We have

screened Aβ for interaction with neuropeptides, finding binding events with leucine enkephalin and galanin. Additionally, site-directed amino acid substitution revealed the c-terminal hydrophobic residues of leucine enkephalin to be critical for the interaction of Aβ:LE. Following this discovery we analyzed the interaction of the dipeptide phenylalanine-leucine with Aβ, measuring K_d values when incubated with alanine mutations of Aβ to determine a binding location. Through these experiments, we find the interaction of Aβ residues Q15 and Y10 to be the most preferred binding partners of FL. All Aβ IM-MS experiments were accompanied with simulated annealing and the modeling filtered with experimental data to find the most accurate representations of the interaction. Modeling predicts this interaction to be mainly through hydrogen bonding.

Turning our attention next to larger aggregation prone proteins, also associated with neurophysiological disorders, we studied the aggregation effects of copper on ubiquitin. Mono, linear tri- and linear tetra ubiquitin were incubated with copper, revealing an increase in the dimeric forms of mono and tri ubiqutin. Incubation with tetra ubiquitin did not reveal further aggregation, although this could be due to the copper concentration in solution. Additionally the ubiquitin-like Ubiquilin2 WT and P506T mutation were compared for aggregation propensity and stability using CIU. No initial differences have been detected in the monomeric stability and each have approximately the same percentage of dimer formation.

5.2. Future Directions

5.2.1. Screen Interaction of Aβ and a Library of Dipeptides/ Rationally Designed Molecules

We have characterized the interaction of the dipeptide FL with Aβ through measurement of binding strength and site-directed amino acid substitutions. Aβ residues Q15 and Y10 are thought to hydrogen bond with FL. Additional experiments on the Aβ:FL system with IM-MS alone would not prove to provide additional information. However toxicity studies would provide answers to unknown questions.

In previously published works with Aβ:ligand interactions compactions of the Aβ monomer was observed upon ligand binding[12, 13]. At this time, the compaction cannot be tied with drug characteristic or efficacy. In the LE and FL binding events, compaction of the monomer is not observed. We hypothesize that this could be due to the flexibility of the LE and FL ligands,

whereas previous ligands are much more rigid in structure. Adding double bonds to the backbone of FL can increase rigidity. Additionally, the cyclo(FL) dipeptide will be much more rigid than the FL dipeptide tested in chapter 3, while still maintaining hydrophobicity and access to side chains. If compaction of the monomer is observed upon cyclo(FL) binding or more rigid FL structures, we can begin to develop a mechanism regarding ligand characteristics and efficacy in preventing oligomer formation with regards to compaction.

Other modifications to the FL dipeptide which may lend additional information on the mode of binding include NH_2-FL and FL-Ac to assess the effect of charge and toxicity of the fragment. Altering the side chain of phenylalanine, potentially swapping it with a tyrosine residue, can be used to test the hydrophobicity effects on binding and additionally test for the regional specificity of binding. Lastly, measuring binding affinity of the d-amino acid variant of FL can test the effects of stereochemistry on binding, while simultaneously allowing FL to avoid degradation in the cell.

Already IM-MS is proposed as a high throughput tool for the screening of drug libraries[13-15]. Thus, future IM-MS experiments should include screening a library of rationally designed small molecules based on FL. These molecules would ideally have properties aimed at increasing interaction strengths/specificity, allowing for blood/brain barrier permeability, reducing toxicity, and maintaining stabilization of small oligomers/ preventing fibril formation.

Additionally, FL is one of four hundred dipeptide permutations. The likelihood that LF also binds Aβ is quite high. Of interest would be a screen of dipeptide permutations, starting with those containing leucine and followed by those containing phenylalanine. Aβ contains two phenylalanine residues at locations 19 and 20, which have been demonstrated to be a part of the hydrophobic core region responsible for aggregation. Potentially FF could interact here. Following a dipeptide screen, rational design using the dipeptide with the highest binding affinity could produce additional libraries for testing.

5.2.2. Molecular Modeling Simulations to Address Solution Equilibrium

The molecular dynamics simulations presented in chapters 2 and 3, use a two-step approach. The first being a docking simulation using Audodock Vina, which holds the protein target rigid, while the flexible ligand is docked primarily based on stereochemistry. In these simulations, the

starting Aβ structure comes from the aqueous NMR structure retrieved from the protein data bank. This is done to reduce computational time and resources. An alternative approach, would be to assess the ligand binding in a simulation to mimic solution phase binding. This would allow for a much larger pool of starting monomeric structures, and mimic solution phase equilibria. These experiments would then be followed with simulated annealing, filtering and clustering analysis as described in chapter 3.

5.2.3. Further Characterization of Ubiquitin and Ubiquitin Like Protein

The concentrations of copper used in L4UB experiments (45 μM) did not influence the aggregation of L4UB. Future experiments should push the boundaries on copper concentrations to see if this is an effect of saturation. To achieve these concentrations, L4UB (15 μM) should be incubated with at least 60 μM copper acetate, and up to 180 μM, followed by a buffer exchange step to remove excess copper from the solution prior to IM-MS experiments. Further, the series of linear polyubiquitins is available up to a decameric chain, it would be of interest to see which ubiquitin chain lengths are most susceptible to aggregation in the presence of copper. Additionally, the polyubiquitin used in these studies was linear. Ubiquitin linked by lys48 traditionally signals for degredation, while those linked at lys63 preform non-proteolytic functions[16]. Additional studies could probe the aggregation propensity for those polyubiquitin species linked a lys48 in comparison to linear and lys63.

As demonstrated in chapter 4, ubiquilin2 WT and P506T vary little structurally as analyzed by IM-MS on the monomeric level under native conditions. A broader scope of solution conditions, including changes to protein solution pH, ionic strength, and temperature could be used to investigate differences. It is known that the P506T mutation impairs the proteasomal degradation pathway and thus studying the interaction of Ubiquilin2 and ubiquitin through IM-MS is of interest. Through our studies with ubiquitin and copper, there is evidence of copper mediated aggregation. Incubation of copper with Ubiquilin2 WT and P506T to test their aggregation is also of interest.

5.2.4. Application of IM-MS to the Cancer Associated Protein p53

While uncontrolled protein aggregation has been implicated in the etiology of many diseases, it has only recently been linked with cancer. Recent data indicate that mutant forms of the tumor-

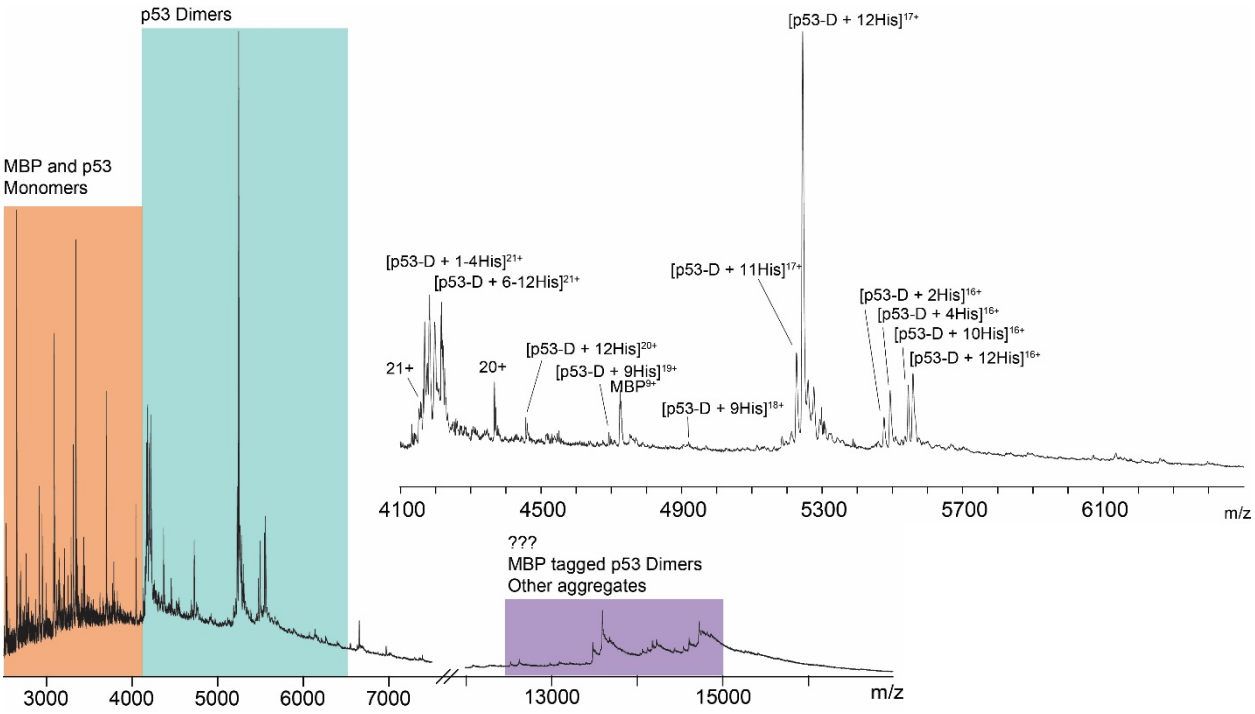

Figure 5.1- p53 protein analysis using the LCT Premier Mass Spectrometer. Initial studies using the LCT, show p53 monomers, and dimers. Sample received were tagged with MBP and a histidine tag. Inset is of the green region. Fragmentation of the MBP from the p53 also removes various number of histidine, complicating analysis. Also observed were unidentified aggregates at a very high m/z

suppressor protein, p53, undergo an aggregation and recruit WT p53 protein as part of its oncogenic activity[17]. Work moving forward can take the protocols developed in this thesis and apply them to cancer-related protein aggregation. Specifically, to perform a step-wise assessment of p53 aggregation using both wild type versions of the protein and oncogenic mutants (*e.g.* R273H) in an isolated fashion by IM-MS. These experiments would use MS and tandem MS measurements to confirm the stoichiometry of complexes detected beyond the expected tetramer and IM measurements to assess the sizes of the complexes. Accurate size information should be a priority during this phase, using the simple systems to optimize intact complexes before moving on to more complex assemblies. Previous measurements of the intact complex demonstrate the feasibility of our approach to this system[18-20]. Following this, the step-wise introduction of various interaction agents should be performed calculating the K_d and protein dynamics through subunit exchange. Starting interactions to be tested could include p63, p73, GTPBP4 and DNA segments as a control. Preliminary results using the Waters LCT Premier mass spectrometer are shown in figure 5.1. Monomeric and p53 are easily identified, with

various amounts of tag present. Protein sample preparation and cleaning needs to be optimized prior to further analysis.

5.3. References

[1] Bernstein, S. L., Dupuis, N. F., Lazo, N. D., Wyttenbach, T., Condron, M. M., Bitan, G., Teplow, D. B., Shea, J.-E., Ruotolo, B. T., and Robinson, C. V. (2009) Amyloid-β protein oligomerization and the importance of tetramers and dodecamers in the aetiology of Alzheimer's disease, *Nature chemistry 1*, 326-331.

[2] Smith, D. P., Radford, S. E., and Ashcroft, A. E. (2010) Elongated oligomers in β2-microglobulin amyloid assembly revealed by ion mobility spectrometry-mass spectrometry, *Proceedings of the National Academy of Sciences 107*, 6794-6798.

[3] Dupuis, N. F., Wu, C., Shea, J.-E., and Bowers, M. T. (2009) Human islet amyloid polypeptide monomers form ordered β-hairpins: a possible direct amyloidogenic precursor, *Journal of the American Chemical Society 131*, 18283-18292.

[4] Bernstein, S. L., Liu, D., Wyttenbach, T., Bowers, M. T., Lee, J. C., Gray, H. B., and Winkler, J. R. (2004) α-Synuclein: Stable compact and extended monomeric structures and pH dependence of dimer formation, *Journal of the American Society for Mass Spectrometry 15*, 1435-1443.

[5] Grabenauer, M., Wu, C., Soto, P., Shea, J.-E., and Bowers, M. T. (2009) Oligomers of the prion protein fragment 106− 126 are likely assembled from β-hairpins in solution, and methionine oxidation inhibits assembly without altering the peptide's monomeric conformation, *Journal of the American Chemical Society 132*, 532-539.

[6] Hyung, S.-J., Robinson, C. V., and Ruotolo, B. T. (2009) Gas-phase unfolding and disassembly reveals stability differences in ligand-bound multiprotein complexes, *Chemistry & biology 16*, 382-390.

[7] Ekeowa, U. I., Freeke, J., Miranda, E., Gooptu, B., Bush, M. F., Pérez, J., Teckman, J., Robinson, C. V., and Lomas, D. A. (2010) Defining the mechanism of polymerization in the serpinopathies, *Proceedings of the National Academy of Sciences 107*, 17146-17151.

[8] Salbo, R., Bush, M. F., Naver, H., Campuzano, I., Robinson, C. V., Pettersson, I., Jørgensen, T. J., and Haselmann, K. F. (2012) Traveling-wave ion mobility mass spectrometry of protein complexes: accurate calibrated collision cross-sections of human insulin oligomers, *Rapid Communications in Mass Spectrometry 26*, 1181-1193.

[9] Scarff, C. A., Sicorello, A., Tomé, R. J., Macedo-Ribeiro, S., Ashcroft, A. E., and Radford, S. E. (2013) A tale of a tail: Structural insights into the conformational properties of the polyglutamine protein ataxin-3, *International journal of mass spectrometry 345*, 63-70.

[10] Larini, L., Gessel, M. M., LaPointe, N. E., Do, T. D., Bowers, M. T., Feinstein, S. C., and Shea, J.-E. (2013) Initiation of assembly of tau (273-284) and its ΔK280 mutant: an experimental and computational study, *Physical Chemistry Chemical Physics 15*, 8916-8928.

[11] Young, L. M., Saunders, J. C., Mahood, R. A., Revill, C. H., Foster, R. J., Tu, L.-H., Raleigh, D. P., Radford, S. E., and Ashcroft, A. E. (2015) Screening and classifying small-molecule inhibitors of amyloid formation using ion mobility spectrometry–mass spectrometry, *Nature chemistry 7*, 73-81.

[12] Hyung, S.-J., DeToma, A. S., Brender, J. R., Lee, S., Vivekanandan, S., Kochi, A., Choi, J.-S., Ramamoorthy, A., Ruotolo, B. T., and Lim, M. H. (2013) Insights into antiamyloidogenic properties of the green tea extract (−)-epigallocatechin-3-gallate toward metal-associated amyloid-β species, *Proceedings of the National Academy of Sciences 110*, 3743-3748.

[13] Beck, M. W., Oh, S. B., Kerr, R. A., Lee, H. J., Kim, S. H., Kim, S., Jang, M., Ruotolo, B. T., Lee, J.-Y., and Lim, M. H. (2015) A rationally designed small molecule for identifying an in vivo link between metal–amyloid-β complexes and the pathogenesis of Alzheimer's disease, *Chemical Science 6*, 1879-1886.
[14] Niu, S., Rabuck, J. N., and Ruotolo, B. T. (2013) Ion mobility-mass spectrometry of intact protein–ligand complexes for pharmaceutical drug discovery and development, *Current opinion in chemical biology 17*, 809-817.
[15] Young, L. M., Saunders, J. C., Mahood, R. A., Revill, C. H., Foster, R. J., Ashcroft, A., and Radford, S. (2015) ESI-IMS–MS: A method for rapid analysis of protein aggregation and its inhibition by small molecules, *Methods*.
[16] Li, W., and Ye, Y. (2008) Polyubiquitin chains: functions, structures, and mechanisms, *Cellular and Molecular Life Sciences 65*, 2397-2406.
[17] Xu, J., Reumers, J., Couceiro, J. R., De Smet, F., Gallardo, R., Rudyak, S., Cornelis, A., Rozenski, J., Zwolinska, A., and Marine, J.-C. (2011) Gain of function of mutant p53 by coaggregation with multiple tumor suppressors, *Nature chemical biology 7*, 285-295.
[18] Joerger, A. C., Rajagopalan, S., Natan, E., Veprintsev, D. B., Robinson, C. V., and Fersht, A. R. (2009) Structural evolution of p53, p63, and p73: implication for heterotetramer formation, *Proceedings of the National Academy of Sciences 106*, 17705-17710.
[19] Natan, E., Baloglu, C., Pagel, K., Freund, S. M., Morgner, N., Robinson, C. V., Fersht, A. R., and Joerger, A. C. (2011) Interaction of the p53 DNA-binding domain with its n-terminal extension modulates the stability of the p53 tetramer, *Journal of molecular biology 409*, 358-368.
[20] Pagel, K., Natan, E., Hall, Z., Fersht, A. R., and Robinson, C. V. (2013) Intrinsically disordered p53 and its complexes populate compact conformations in the gas phase, *Angewandte Chemie International Edition 52*, 361-365.

Appendices

Appendix I. Chapter 2 Supporting Information

I.I IM-MS analysis of Aβ-galanin and Aβ-bradykinin interactions

As a follow up to studies of $A\beta_{1\text{-}40}$-LE interactions, presented here are CCS and K_d values for the interactions of $A\beta_{1\text{-}40}$ with galanin, and an additional peptide not in the initial screen but shown to bind with Aβ: bradykinin. Data was collected on the Waters Synapt HDMS with the instrument parameters given in chapter 3. In a mixture of 10 µM $A\beta_{1\text{-}40}$: 10 µM neuropeptide the 1:1 interaction is observed in the 6^+, 5^+ and 4^+ charge states for galanin. In contrast, at the same ratios of Aβ:bradykinin both the 1:1 and 2:1 complexes are observed with a greater intensity than that of the 1:1 Aβ:galanin. The K_d values were calculated using the equations and methodology provided in chapter 3. While only one ligand binding is observed in equimolar mixtures, when incubated in excess we see up to

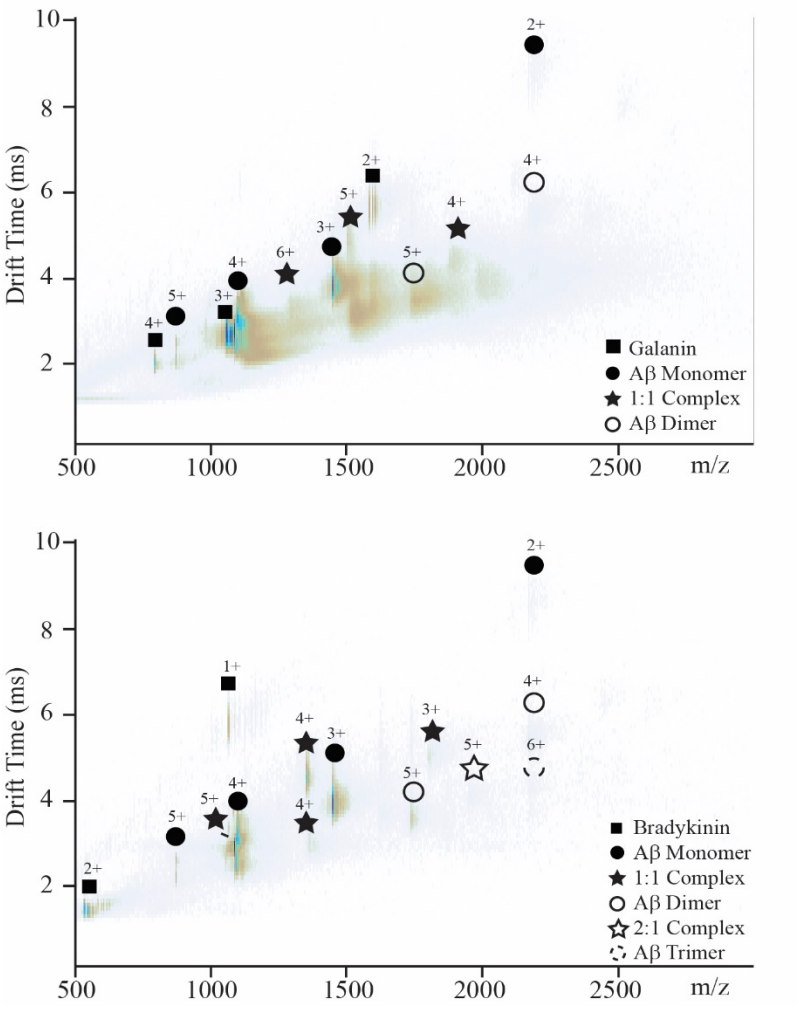

Figure I-1. Top) 10 µM Aβ incubated with 10 µM galanin. Dark stars represent the 1:1 complex at the labeled charge state. Bottom) 10 µM Aβ incubated with 10 µM bradykinin. Dark stars represent the 1:1 complex and the outlined star represents the Aβ dimer in complex with one bradykinin.

five bradykinin binding to one Aβ, and up to three binding to the dimer. Single ligand binding is observed on oligomers up to the Aβ pentamer (data not shown). Table I-1 highlights CCS data collected for both galanin and bradykinin incubations. Table I-2 provides measured K_d values taken over a concentration range up to an eight fold excess. K_d values are within magnitude of those measured for the Aβ:LE interactions (1:1 ~65-80 μM). This supports further detailed analysis of the interaction in the hopes of finding potential biotherapeutics.

Table I-1. CCS values of Aβ, Galanin, Bradykinin and their complexes. Std Dev is given on replicates and is not inclusive of the standard ±3% from instrumental error.

Aβ			
	Charge State	CCS (Å^2)	Std Dev (Å^2)*
$A\beta_{1-40}$	2^+	651.4	57.0
$A\beta_{1-40}$	3^+	628.2	14.2
$A\beta_{1-40}$	4^+	646.7	14.7
$A\beta_{1-40}$	4^+	721.6	47.7
$A\beta_{1-40}$	5^+	760.3	40.7
$A\beta_{1-40}$	5^+	824.3	13.3
$A\beta_{1-40}$ Dimer	3^+	835.6	
$A\beta_{1-40}$ Dimer	3^+	1065.0	4.66
$A\beta_{1-40}$ Dimer	4^+	1009.3	5.97
$A\beta_{1-40}$ Dimer	5^+	981.0	17.7
$A\beta_{1-40}$ Dimer	5^+	1218.5	44.5
$A\beta_{1-40}$ Dimer	6^+	1358.1	52.9
$A\beta_{1-40}$ Dimer	7^+	1321.5	24.1
$A\beta_{1-40}$ Dimer	7^+	1501.7	13.9
$A\beta_{1-40}$ Trimer	4^+	1409.9	5.17
$A\beta_{1-40}$ Trimer	5^+	1354.1	9.58
$A\beta_{1-40}$ Trimer	6^+	1314.4	53.1
$A\beta_{1-40}$ Trimer	7^+	1319.3	35.3
$A\beta_{1-40}$ Trimer	7^+	1499.6	22.1
$A\beta_{1-40}$ Trimer	7^+	1697.0	72.8
$A\beta_{1-40}$ Trimer	8^+	1788.3	
$A\beta_{1-40}$ Trimer	8^+	2084.5	
$A\beta_{1-40}$ Tetramer	6^+	1646.8	62.2
$A\beta_{1-40}$ Tetramer	7^+	1617.7	24.6
$A\beta_{1-40}$ Tetramer	8^+	1593.3	99.0
$A\beta_{1-40}$ Tetramer	9^+	1928.0	40.8
$A\beta_{1-40}$ Pentamer	8^+	1896.0	21.8
$A\beta_{1-40}$ Pentamer	9^+	1907.3	51.8
Bradykinin			
	Charge State	CCS (Å^2)	Std Dev (Å^2)*
Monomer	1^+	266.7	0.78
Monomer	2^+	248.7	45.5

Dimer	2^+	382.3	10.3
Dimer	3^+	389.1	27.3
Trimer	2^+	513.0	2.70
Trimer	3^+	949.7	10.3
Tetramer	4+	993.8	0.88
Galanin			
	Charge State	CCS ($Å^2$)	Std Dev ($Å^2$)*
Monomer	2^+	516.8	19.9
Monomer	3^+	512.8	4.21
Monomer	4^+	583.8	6.38
Dimer	3^+	820.4	6.77
Dimer	4^+	803.6	50.7
Trimer	5^+	1095.5	9.55
Tetramer	7+	1434.3	25.8
Aβ:Bradykinin			
	Charge State	CCS ($Å^2$)	Std Dev ($Å^2$)*
1:1	2^+	782.8	3.28
1:1	3^+	725.8	5.86
1:1	4^+	719.1	43.9
1:1	4^+	911.4	19.0
1:1	5^+	1000.9	37.0
1:2	3^+	835.9	2.63
1:2	4+	793.4	11.3
1:2	4^+	998.5	9.56
1:3	3^+	942.9	2.89
1:3	4^+	890.1	5.15
1:3	5^+	861.2	7.32
1:3	5^+	1201.4	8.44
1:4	4^+	977.8	0.00
1:4	5+	956.8	19.0
1:4	5^+	1214.5	61.6
1:5	4^+	1084.5	4.52
1:5	5^+	1040.2	0.00
2:1	4+	1104.6	5.29
2:1	5^+	1072.7	50.3
2:1	6^+	1416.8	40.8
2:2	4+	1205.8	0.51
2:2	5^+	1146.8	
2:3	5^+	1239.1	6.01
2:3	6^+	1239.3	3.99
3:1	5+	1212.2	328
3:1	6^+	1380.7	20.1
3:1	7^+	1393.9	17.9
3:2	6^+	1481.7	3.40
4:1	8+	1689.3	28.8
Aβ:Galanin			

	Charge State	CCS (Å^2)	Std Dev (Å^2)*
1:1	3^+	941.4	1.57
1:1	4^+	890.6	12.1
1:1	5^+	943.8	17.4
1:1	5^+	1189.5	38.4
1:1	6^+	1288.6	13.6
1:2	5^+	1131.8	30.1
1:2	6+	1208.4	22.0
2:1	4^+	1301.8	
2:1	5^+	1288.2	54.0
2:1	6^+	1252.1	29.5
2:1	7^+	1671.1	69.1
3:1	6^+	1558.5	
3:1	7^+	1513.2	31.4
3:1	8+	1669.0	21.4

Table I-2. Measured K_d values for the Aβ:neuropeptide complexes

Aβ:Galanin		
	K_d (μM)	Std Dev (σ)
$Aβ_{1-40}$ Dimer	45.0	50.1
$Aβ_{1-40}$ Trimer	46.8	26.4
1:1	64.5	55.7
1:2	71.2	34.6
2:1	31.8	9.14
3:1	21.9	13.7
Aβ:Galanin		
	K_d (μM)	Std Dev (σ)
$Aβ_{1-40}$ Dimer	32.0	25.5
$Aβ_{1-40}$ Trimer	16.5	18.8
$Aβ_{1-40}$ Tetramer	38.4	21.2
$Aβ_{1-40}$ Pentamer	43.3	30.8
$Aβ_{1-40}$ Hexamer	8.64	3.26
1:1	78.1	36.4
1:2	102.4	34.1
1:3	102.7	25.5
1:4	159.2	29.6
1:5	127.7	43.1
2:1	140.6	69.6
2:2	1124.5	994.9
2:3	18.3	24.9
3:1	137.7	116.2
4:1	416.7	208.8
5:1	95.4	35.5

Appendix II. Chapter 3 Supporting Information

II.I CD Spectroscopy

WT $A\beta_{1\text{-}40}$ and all its alanine variants were buffer exchanged from ammonium acetate stock solution in phosphate buffer using Nest Group G-10 columns and diluted to 25 µM. Measurements were performed using a Jasco CD-Spectropolarimeter operated between the wavelengths of 180 and 260nm and averaged over 10 scans. CD spectroscopy was used to characterize tertiary structure of synthesized alanine variants.

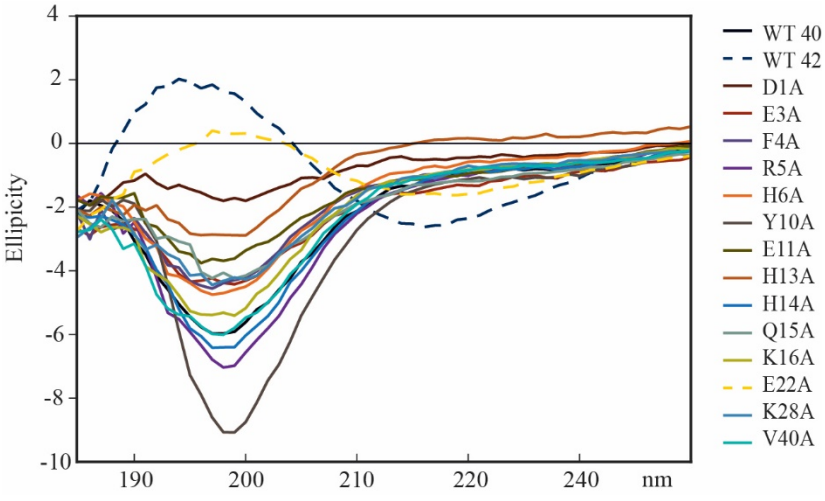

Figure II-1. CD spectra for alanine mutations of $A\beta_{1\text{-}40}$ analyzed. Spectra in solid lines have characteristic random coil structure. Those with the dashed lines ($A\beta_{1\text{-}42}$ and E22A) have β-sheet structure.

While the majority of alanine mutations did not result in a change to the tertiary structure, $A\beta_{1\text{-}40}$ E22A has characteristic β-sheet structure rather than random coil. We therefore are unable to conclusively determine if a change in binding affinity with FL is due to a structural change or because of side-chain specific interactions.

II.II $A\beta_{1\text{-}40}$ site directed amino acid substitution interaction with LE

Similarly to the experiments with FL, we performed binding experiments with alanine variants of Aβ and LE. Data is shown in figure II-2. D1A, E3A, H6A, Q15A, K16A and V40A have a K_d near that of the WT:LE 1:1 interaction (12.1 ± 8.5 µM). However only H6A and V40A have values which fall within one standard deviation (18.2 ± 9.65 and 10.3 ± 6.54 µM respectively). F4A, R5A, Y10A, H13A, H14A and K28A range in K_d from 55.6 ± 22.2 to 81.3 ± 9.08 µM. E11A deviates most significantly at 126 ± 23.6 µM, pointing to E11 as being the most critical residue for interaction with LE.

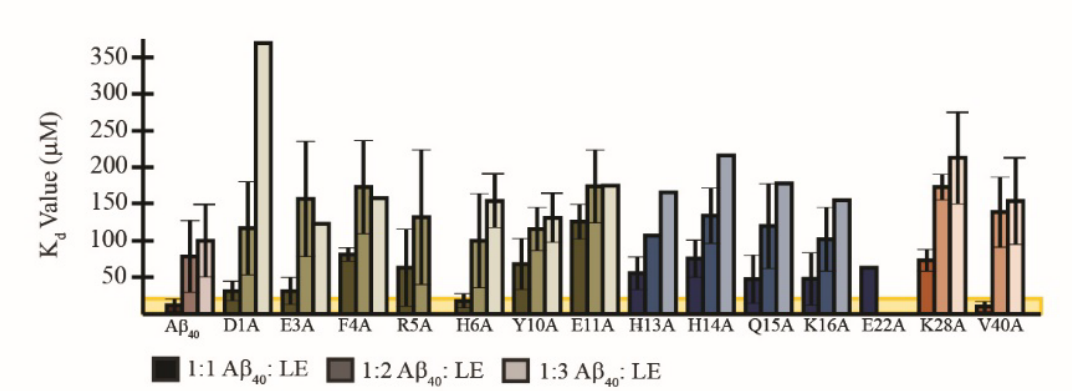

Figure II-2. K_d values for the interaction of Aβ:LE. The darkest box represents the 1:1 interaction of Aβ:LE, middle 1:2, and the lightest represents the 1:3 interaction. Only measurements with at least three replicates are shown with error bars. The yellow box represents the ±1 standard deviation of the $Aβ_{1-40}$:LE 1:1 interaction.

Appendix III. Aβ-Small Molecule Interactions

Aβ:Diphenylpropynone derivative interactions at high concentrations

Amit S. Pithadia, Akiko Kochi, **Molly T. Soper**, Michael W. Beck, Zuzhong Liu, Sanghyun Lee, Alaina S. DeToma, Brandon T. Ruotolo, and Mi Hee Lim (2012). Reactivity of Diphenylpropynone Derivatives Toward Metal-Associated Amyloid-β Species, *Inorg. Chem. 51*, 12959-12967

In Alzheimer's disease (AD), metal-associated amyloid-β (metal-β) species have been suggested to be involved in neurotoxicity; however, their role in disease development is still unclear. To elucidate this aspect, chemical reagents have been developed as valuable tools for targeting metal-Aβ species, modulating the interaction between the metal and Aβ and subsequently altering metal-Aβ reactivity. Diphenylpropynone derivatives (DPP1 and DPP2) were designed, prepared and characterized, with attention to reactivity. The derivatives are composed of structural moieties for metal chelation and Aβ interaction (bifunctionality). The interactions of these molecules with Aβ were confirmed by UV-vis, NMR, docking studies and IM-MS. The effects of these bifunctional molecules on the control of *in vitro* metal-free and metal induced Aβ aggregation were investigated and monitored by gel electrophoresis and TEM. Both DPP1 and DPP2 showed reactivity toward metal-Aβ species over metal-free Aβ species to different extents. In particular, DPP2, which contains a dimethylamino group, exhibited greater reactivity with metal-Aβ species than DPP1, suggesting a structure-reactivity relationship. In depth discussion of the interactions as observed with IM-MS is presented here.

III.I Materials and Methods

All reagents were purchased from commercial suppliers and used as received unless otherwise stated. The compound, 3-phenyl-1-(pyridine-2-yl)prop-2-yn-1-one (DPP1), was prepared following previously reported methods[1-3]. DPP2 was synthesized by slight modifications to a previously reported procedure[3]. $A\beta_{1-40}$ was purchased from AnaSpec (Fremont, CA).

The interaction of DPP1 or DPP2 with $A\beta_{1-40}$ was investigated by nESI-MS on a Waters Synapt G2 ion mobility- mass spectrometer (Milford, MA). Samples were prepared by mixing stock solutions of DPP1 or DPP2 (prepared in DMSO) and $A\beta_{1-40}$ (dissolved in 100 mM ammonium

acetate, pH 6.8) to generate desired final concentrations of the peptide and compound. Mixtures were incubated on ice or at room temperature for 2 or 4 h, respectively, and then analyzed. To produce protein complex ions, an aliquot of the sample (ca. 5 µL) was sprayed from the nESI emitter using a capillary voltage of 1.4 kV, with the source operating in positive ion mode and the sample cone operated at 50 V. To normalize nESI-MS data for nonspecific and electrospray artifact interactions that could occur at high concentrations, data were acquired for $A\beta_{1\text{-}40}$ samples containing thioflavin-T (ThT), a compound known to have no affinity for soluble forms of the $A\beta_{1\text{-}40}$ peptide[4], under identical concentration conditions as our DPP1 and DPP2 experiments. Any ThT binding observed was assumed to be due to either nonspecific binding or the electrospray process, and subtracted from the intensities of the DPP1 and DPP2 interactions observed[5]. This procedure was performed over a broad range of concentrations. The mass spectra were acquired with the following settings and tuned to avoid ion activation and to preserve noncovalent protein-ligand complexes[6]: backing pressure, 7.3 mbar; IMS pressure reading, 3.09 mbar; ToF analyzer pressure, 1.14×10^{-6} mbar.

III.II Aβ Interaction with DPP1 and DPP2 Studied by MS

The interaction of DPP1 and DPP2 with $A\beta_{1\text{-}40}$ in the absence of metal ions was probed by ESI-MS, tuned to preserve noncovalent protein-ligand interactions[6]. At low $A\beta_{1\text{-}40}$ concentrations (10 µM), a small signal corresponding to the interaction between DPP2 (30 µM) and the $A\beta_{1\text{-}40}$ monomer in the 3^+ charge state could be detected, whereas no interaction between DPP1 (60 µM) and the peptide was observed under these conditions (Figure III-1).

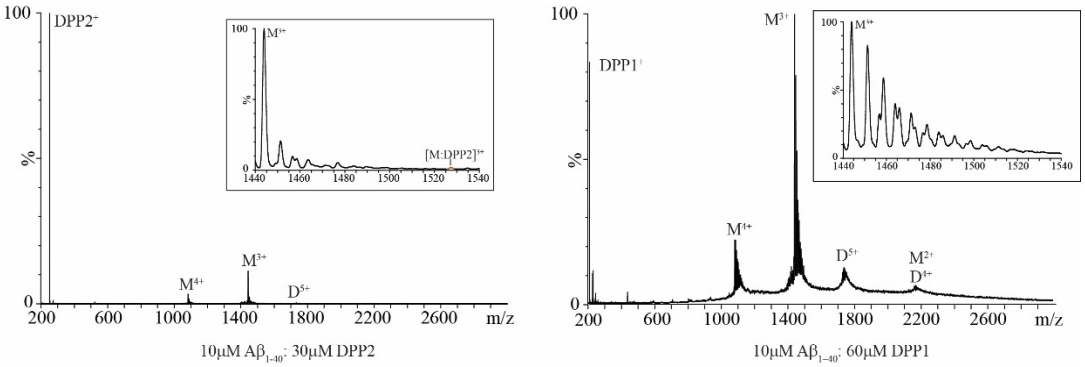

Figure III-1. Right) Interactions of DPP1 (60 µM) and Left) DPP2 (30 µM) with $A\beta_{1\text{-}40}$ (10 µM) determined by nESI-MS. Binding of DPP2 to Aβ monomer was observed at the 3^+ charge state. Incubation time = 2 h on ice.

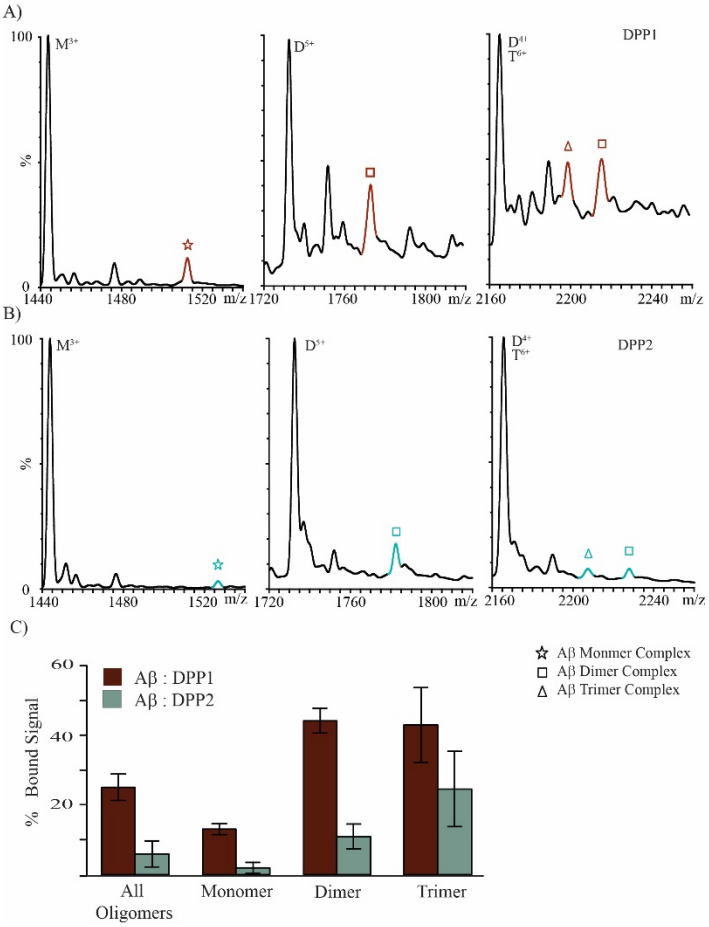

Figure III-2. Interactions of DPP1 and DPP2 with $A\beta_{1\text{-}40}$. MS data for the complexes of $A\beta_{1\text{-}40}$ and A) DPP1 and B) DPP2. ([Aβ] = 100 µM; [compound] = 600 µM; M= monomer, D = dimer, T = trimer). Many binding stoichiometries were detected, including 1:1 (star), 2:1 (square), and 3:1 (triangle). C) histogram showing the total bound MS signal intensity, normalized for nonspecific interactions and ESI-MS artifacts, for each binding stoichiometry observed in A) and B).

At high concentrations of the peptide (100 µM) and compounds (600 µM), both DPP1 and DPP2 interacted with $A\beta_{1\text{-}40}$ species to different extents (Figure III-2). Data for DPP1 indicated that the molecule interacted broadly with $A\beta_{1\text{-}40}$ monomers and oligomers in 1:1, 2:1, and 3:1 $A\beta_{1\text{-}40}$ to ligand ratios. In the case of DPP2, a stronger preference toward larger $A\beta_{1\text{-}40}$ oligomers was shown, but with similar stoichiometries as DPP1. The total bound intensities recorded from MS data, and those from individual oligomeric species are shown in Figure III-2 and Table III-1. The intensities shown were normalized for both nonspecific interactions and a artifactual complexes formed during the electrospray process using $A\beta_{1\text{-}40}$:ThT binding data as a control, and ion mobility separation was used to separate oligomers that overlapped in m/z[6-8]. From these data, it was clear that, at high concentrations, a higher proportion of DPP1 was bound to $A\beta_{1\text{-}40}$ species than DPP2, but that both could be classified as having a weak $A\beta_{1\text{-}40}$ affinity in solution (low mM K_d). Therefore, a weak $A\beta_{1\text{-}40}$/compound interaction was captured by MS. Normalized intensity data suggest that DPP2 binding was almost exclusively driven through $A\beta_{1\text{-}40}$ multimer interactions. Overall, our MS results suggest that although both compounds could interact with $A\beta_{1\text{-}40}$ species at high concentrations, DPP2 was able to bind $A\beta_{1\text{-}40}$ species at both low and high concentrations.

Table III-1. Raw MS signal intensity data for the interaction of DPP1 or DPP2 with $A\beta_{1-40}$ species.

DPP1						
	Avg Unbound Signal	Avg Bound Signal	Total Signal for Bound/Unbound	% Bound	% ThT Bound	Normalized % Bound
Monomer	20966.82	4336.01	25302.84	17.14	0.26	16.88
Dimer	2527.24	1386.40	3913.64	35.42	0.00	35.42
Trimer	444.05	450.33	894.38	50.35	5.71	44.64
All Oligomers	23938.12	6172.74	30110.86	20.50	0.43	20.07
DPP2						
	Avg Unbound Signal	Avg Bound Signal	Total Signal for Bound/Unbound	% Bound	% ThT Bound	Normalized % Bound
Monomer	4386.14	230.22	4616.37	4.89	0.26	4.63
Dimer	929.44	251.82	1181.26	20.37	0.00	20.37
Trimer	520.65	238.58	759.23	29.71	5.71	24.00
All Oligomers	5836.23	720.63	6556.86	10.60	0.43	10.18

III.III References

[1] Seregin, I. V., Schammel, A. W., and Gevorgyan, V. (2007) Base-and Ligand-free Room-Temperature Synthesis of N-Fused Heteroaromatic Compounds via the Transition Metal-Catalyzed Cycloisomerization Protocol, *Organic letters 9*, 3433-3436.

[2] Harkat, H., Blanc, A., Weibel, J.-M., and Pale, P. (2008) Versatile and expeditious synthesis of aurones via AuI-catalyzed cyclization, *The Journal of organic chemistry 73*, 1620-1623.

[3] Friel, D. K., Snapper, M. L., and Hoveyda, A. H. (2008) Aluminum-catalyzed asymmetric alkylations of pyridyl-substituted alkynyl ketones with dialkylzinc reagents, *Journal of the American Chemical Society 130*, 9942-9951.

[4] Reinke, A. A., and Gestwicki, J. E. (2011) Insight into amyloid structure using chemical probes, *Chemical biology & drug design 77*, 399-411.

[5] Sun, J., Kitova, E. N., Wang, W., and Klassen, J. S. (2006) Method for distinguishing specific from nonspecific protein-ligand complexes in nanoelectrospray ionization mass spectrometry, *Analytical chemistry 78*, 3010-3018.

[6] Hernández, H., and Robinson, C. V. (2007) Determining the stoichiometry and interactions of macromolecular assemblies from mass spectrometry, *Nature protocols 2*, 715-726.

[7] Teplow, D. B., Lazo, N. D., Bitan, G., Bernstein, S., Wyttenbach, T., Bowers, M. T., Baumketner, A., Shea, J.-E., Urbanc, B., and Cruz, L. (2006) Elucidating amyloid β-protein folding and assembly: a multidisciplinary approach, *Accounts of chemical research 39*, 635-645.

[8] Bernstein, S. L., Dupuis, N. F., Lazo, N. D., Wyttenbach, T., Condron, M. M., Bitan, G., Teplow, D. B., Shea, J.-E., Ruotolo, B. T., and Robinson, C. V. (2009) Amyloid-β protein oligomerization and the importance of tetramers and dodecamers in the aetiology of Alzheimer's disease, *Nature chemistry 1*, 326-331.

Appendix IV. Aβ preparation.

IV.I Steps for preparation.

These steps should result in consistent stocks, with a mostly monomeric starting species. Dimers and occasionally timers will be observed in low abundance. This preparation should be used for all WT and mutant Aβ stocks.

I) Dissolve 1 mg Aβ peptide in 200 μL 1% (v/v) Ammonium Hydroxide. Vortex if necessary.

II) Add 1300 μL 100 mM ammonium acetate, pH 6.9 (or pH 7.4 depending on requirements).

III) Inject sample into Slide-A-Lyzer Dialysis Cassete (2K MWCO, 3 mL volume, Thermo Scientific)

IV) Add 100 mM ammonium acetate to fill to volume of cassette capacity.

V) Dialyze in 100 mM ammonium acetate for 3.5 to 4 hours.

VI) Refresh buffer. Dialyze 3.5 to 4 hours.

VII) Refresh buffer. Continue dialysis overnight for a total of ~24 h.

VIII) Remove sample from dialysis cassette.

IX) Lyophilize (freeze dry) overnight.

X) Dissolve lyophilized stock in 200 μL 1% ammonium hydroxide. Vortex if necessary

XI) Add 1300 μL 100 mM ammonium acetate, pH 6.9 (or pH 7.4 depending on requirements).

XII) Measure absorbance at 280 nm in triplicate to determine concentration.
$\varepsilon = 1490\ M^{-1}cm^{-1}$ for WT Aβ

XIII) Aliquot and freeze in liquid nitrogen (store at -80 °C)